2018-11

Demonstration of a Novel 3-D Wind Sensor for Improved Wind Shear Detection for Aviation Operations

Anthony O'Connor
Technological University Dublin

School of Electrical & Electronic Engineering

TECHNOLOGICAL UNIVERSITY DUBLIN

Demonstration of a Novel 3-D Wind Sensor for Improved Wind Shear Detection for Aviation Operations

A THESIS SUBMITTED TO THE DUBLIN INSTITUTE OF TECHNOLOGY IN FULFILMENT FOR THE DEGREE OF MASTER OF PHILOSOPHY

COLLEGE OF ENGINEERING & BUILT ENVIRONMENT

BY

ANTHONY O' CONNOR BSc, CEng, MIET

Supervisors: Dr. Derek Kearney; Prof. Michael Conlon

November 2018

Abstract

Low level wind shear and turbulence present a serious safety risk to aircraft during the approach, landing and take-off phases. Low level wind shear has been identified as one of the primary factors for aircraft go-arounds and aborted landings. Aviation reports have concluded that pilots need to have improved information in relation to tailwinds, wind shear and wind variations on approach and during the landing phases. The ability for a pilot to land an aircraft safely without the need to go-around or abort a landing due to wind conditions is crucial. During any given year, wind shear occurs thousands of times at airports around the world, affecting the arrival and departure of aircraft. It is therefore vital that the most accurate information is recorded and relayed by the Air traffic controllers to the flight crew. At present wind is measured using anemometers and wind vanes in airport terminal areas. The design of this instrumentation has not changed greatly since its first use in 1846. These instruments are constructed and limited by their design to only measure wind as a two-dimensional entity. Wind blows freely in three dimensional space so three dimensional measurement is required.

This thesis will argue that a solution to the problem of forecasting low level wind shear and turbulence for the approach, landing and go-around flight phases for aircraft can be addressed by incorporating the Wind Urchin as part of the Low Level Wind Shear Alerting System in all airports. This thesis will show that wind data taken from the Wind Urchin at a test site at Baldonell Aerodrome measured the vertical wind component, when wind data from existing wind measurement instruments at Baldonell for the same time only recorded the horizontal wind. Initial research produced a wind profile providing greater resolution of the wind data showing when turbulence is high and when it is safe for aircraft to land.

DECLARATION

I certify that this thesis which I now submit for examination for the award of Master of Philosophy, is entirely my own work and has not been taken from the work of others, save and to the extent that such work has been cited and acknowledged within the text of my work.

This thesis was prepared according to the regulations for postgraduate study by research of Technological University Dublin and has not been submitted in whole or in part for another award in any other third level institution.

The work reported on in this thesis conforms to the principles and requirements of the TU Dublin guidelines for ethics in research.

Signature _____ Date _____

Candidate: Anthony O' Connor

Acknowledgements

I would like to express my sincere gratitude and thanks to my project supervisor Dr. Derek Kearney for his advice and guidance and friendship during the course of this project. I would like to thank all the staff at DIT for their help and support with this project. I would like to thank Dennis Hart, Graham Roberts and Marco Gibellini at EUROCONTROL for their support and the information provided. I would like to thank the various people in the FAA for their help and in particular Bob Stuckert for his support. I would like to thank David Bullock and Juhani Polvinen at Vaisala for the detailed information provided on their Low Level Wind Shear Alert Systems and their advice. I would like to thank Antonio Massidda and Christine Gerencher and all her staff and associates at the Aviation & Environment, Transportation Research Board for their assistance and help. I would like to thank David Hiscotte at Air New Zealand for the information provided. I would like to thank Michael Baiada at the ATH Group. I would like to thank Steve Neal at the Australian Civil Aviation Safety Authority for his assistance. I would like to thank Paul Sadler at the Australian Transport Safety Bureau for his assistance. I would like to thank Perry Flint at the IATA for his assistance.

I would also like to thank my wife Suzanne and family for their support during this project.

Abbreviations:

A	Swept Area
ACFT	Aircraft
AD	Aerodrome
ADC	Aerodrome chart
AEP	Annual Energy Production
AFS	Aeronautical fixed service
AIS	Aeronautical information services
ALERFA	Alert phase
ANSI	American National Standards Institute
ANSP	Air Navigational Service Provider
AP	Airport
APCH	Approach
API	Application Program Interface
ASTM	American Society For Testing And Materials
ATC	Air Traffic Control
ATS	Air Traffic Services
AVG	Average
AZM	Azimut
BIPM	Bureau International De Poids Et Mesures
BLO	Below Clouds
BMO	British Meteorological Office
BTL	Between Layers
C.	CIRCA
CAA	UK Civil Aviation Authority
CAB	Conformity Assessment Board
CAT	Clear Air Turbulence
CCGT	Combined Cycle Gas Turbine
CD	Compact Disc
CEN	European Committee For Standardisation
CENELEC	European Committee For Electrotechnical Standardisation
CF	Capacity Factor
CFD	Computational Fluid Dynamics
CIV	Civil
CM	Centimetre
CMB	Climb
COND	Condition
COOR	Coordinate or Co-Ordination
COORD	Coordinates
CRM	Collision Risk Model
DEG	Degrees
DEP	Depart or Departure
DEV	Deviation
DFW	Dry Friction Whip
DIST	Distance
DIT	Dublin Institute Of Technology
DVOR	Doppler VOR
EC	European Commission
ET	Extreme Turbulence
EASA	European Aviation Safety Agency

ESOS	European Standards Organisations
ETSI	European Telecommunications Standards Institute
EUROCONTROL	European Organisation for the Safety of Air Navigation
FAA	United States of America Federal Aviation Administration
FL	Flight Level
FNA	Final Approach
FPN	Feet Per Minute
GAIN	Airspeed or Headwind Gain
GE	General Electric
GEUM	Expression Of Uncertainty In Measurement
GRIB	Processed Meteorological Data
GS	Ground Speed
ICAO	International Civil Aviation Authority
IEC	International Electrotechnical Commission
IMC	Instrument Meteorological Conditions
IMO	International Meteorological Organisation
IP	Intellectual Property
ISO	International Standards Organisation
KG	Kilogram
KHZ	Kilohertz
KIAS	Knots Indicated Airspeed
KM	Kilometre
KMH	Kilometre per Hour
KT	Knots
KW	Kilowatts
LIDAR	Light Detection And Ranging
LOSS	Airspeed or Headwind Loss
MAG	Magnetic
MPS	Metres per Second
MRS	Minimum Radar Separation
MTH	Multi-Tube Head
MTP	Multi-Tube Probe
MBST	Microburst
METAR	Aerodrome Routine Meteorological Report
MHPS	Multi-Hole Pressure Probes
MCTOM	Maximum Certified Take-Off Mass
NI	National Instruments
NM	Nautical Mile
NATS	UK National Air Traffic Services
NREL	National Renewable Energy Laboratory
OIML	International Organisation Of Legal Metrology
PLC	Programmable Logic Controller
PCB	Printed Circuit Board
POD	Prediction of Detection
PVC	Poly-Vinyl Chloride
R&D	Research and Development
RPI	Radar Position Indicator
RWY	Runway
RECAT	Re-Categorisation
SD	Standard Deviation

SI	International System of Units
SEV	Severe (used to quantify icing and turbulence reports)
SMR	Surface Movement Radar
SARPS	Standards and Recommended Practices
SDOS	Standards Developing Organisations
SODAR	Sonic Detection And Ranging
SEAI	Sustainable Energy Authority Of Ireland
TAF	Aerodrome Forecast in Meteorological Code
TBS	Time Based Separation
TDZ	Touchdown Zone
TURB	Turbulence
. . . V . . .	Variations from the mean wind direction
VER	Vertical
VRB	Variable
VSP	Vertical Speed
VTOL	Vertical Take-off and Landing
WS	Wind Shear
WT	Wake Turbulence
WAC	World Aeronautical Chart
WDI	Wind Direction Indicator
WMO	World Meteorological Organisation
WSPD	Wind Speed

Nomenclature

A	Swept Area (M^2)
A	The Angle Between The Actual Wind At Anemometer Level And Geostrophic Wind
B	Constant Comprising Viscosity And Coriolis Parameters
C	Speed Of Sound
C_1	Coefficient
Cf	Capacity Factor
Cf	Flow Distortion Correction Factor
C_p	Power Coefficient Or Rotor Efficiency
C_t	Topographic Correction Factor
D	Drag
F	Coriolis Parameter
G	Acceleration Due To Gravity ($M\ S^{-2}$)
H	Height (M)
K	Von Karmans Constant Approximately 0.38
Ks/S	Kilo-Samples Per Second
L	Lift
L	Distance Between Two Transducers
N	Sample Size
N	Total Number Of Wind Samples
P	Fluid Pressure (Nm^{-2})
P	Power In The Wind (W)
$P_{1,2}$	Pressure (Pa)
P_a	Atmospheric Pressure (Nm^{-2})
P_x	Magnitude Of The Pressure Gradient ($Nm^2\ Kg^{-1}$)
R	Gas Constant (J/Mol·K)
Re	Reynolds Number
T	Time (S)
T	Temperature On The Absolute Scale (K)
Ta	Taylor Number
Tf	Transit Time In The Forward Direction
Ti	Turbulence Intensity
Tr	Transit Time In The Reverse Direction
T1	Transit Time Of Ultrasound
T2	Transit Time Of Ultrasound
U	Velocity Of The Largest Eddy ($M\ S^{-1}$)
U	Velocity ($M\ S^{-1}$)
U	Characteristic Velocity ($M\ S^{-1}$)
$U(Z)$	Wind Speed At Height Z ($M\ S^{-1}$)
$U*$	Friction Velocity ($M\ S^{-1}$)
U_c	Corrected Wind Speed ($M\ S^{-1}$)
U_o	Anemometer Threshold ($M\ S^{-1}$)
$U\&V$	Horizontal Components Of The Wind At Height Z
$U,U1$	Wind Speeds At Heights Z, Z1, Respectively
V	Velocity
V	Kinetic Viscosity Of The Fluid ($M\ S^{-1}$)
V	Velocity Of The Smallest Eddy ($M\ S^{-1}$)
V	Critical Velocity ($M\ S^{-1}$)

V	Upstream Wind Velocity At The Entrance To The Rotor Blades (M S^{-1})
V	Mean Wind Speed (M S^{-1})
Vg	The Geostrophic Wind
Vw	Wind Velocity
V_{rio}	Voltage Measured By Compactrio
V_0	Downstream Wind Velocity At The Exit Of The Rotor Blades (M S^{-1})
V_1	Known Wind Speed At The Measurement Height Z_1 (M S^{-1})
V_1	Initial Velocity (M S^{-1})
V_2	Unknown Speed At Height Z_2 (M S^{-1})
V_2	Final Velocity (M S^{-1})
V_{ge}	Output Voltage From Ge Novasensor (V)
	Mg (Mass Of Aircraft X Acceleration Due To Gravity)
W	Set Of One Second Wind Samples
Xi	A Parameter That Depends On The Stability, Surface Roughness And
Y	Height With A Value Between 0 And +1 Determined Empirically
Z	Height Above Earth's Surface (M)
Z_0	Earth's Surface Roughness Height (M)
Z_0	Terrain Roughness
Z_{0u}	Effective Roughness Length Of The Terrain Upstream Of The Measurement Station (M)
Z_1	Height Of Static Pressure Port (M)
Z_2	Height Of Total Pressure Port (M)
A	Wind Shear Exponent
H	Length Of The Smallest Eddies (M)
M	Fluid Dynamic Viscosity (N S/M^2)
P	Air Density (Kg/M^3)
Σ	Standard Deviation Of Wind Speed (M S^{-1})
Φ	Latitude (°)

Table of Contents

Abstract i

DECLARATION ii

Abbreviations: iv

Nomenclature vii

Table of Contents ix

List of Figures xi

List of Tables xiv

List of Equations xv

1. Introduction 1

1.1 Aims and Objectives 4

2. Literature Review of Difficulties with Aircraft during Landing and Take-off Phases 6

2.1 Overview of Disruption to Aircraft Due to Low Level Wind Shear 6

2.2 Adverse Effects on Flight Safety on Approach and Landing from Turbulence 7

2.3 Flight Go-around Procedures as a Result of Low Level Wind Shear 12

2.4 Aircraft Accidents Attributed to Low Level Wind Shear and Turbulence 16

2.5 Recommendations on Wind Shear from Air Crash Investigation 17

2.6 Effect of Wake Turbulence on Aircraft During Take-off and Landing 20

3. Standards and Regulations for the Aviation Industry 26

3.1 Meteorological Standards and Regulations for Aviation 26

3.2 Conclusion on Aviation Standards 32

4. Measurement of Wind Shear and Turbulence at Airports 33

4.1 The Complex Nature of Turbulence and Wind Shear 33

4.2 Low Level Turbulence Types as Defined by ICAO 35

4.2.1 Convective Turbulence 35

4.2.2 Mechanical Low Level Turbulence 37

4.2.3 Orographic Induced Turbulence 39

4.2.4 Low Level Jets 41

4.2.5 Clear Air Turbulence 43

4.2.6 Wake Turbulence 44

4.2.7 Low Level Wind Shear 45

4.3 Current Procedures and Methods for Recording Low Level Wind Shear 51
4.3.1 A Brief History of How LLWS Systems Came About 51
4.3.2 Systems and Methods to Record Low Level Wind Shear at Airports 53
4.3.3 Instruments Currently used in LLWAS in the Terminal Area 76
5. Flight Go-arounds 84
5.1 Go-Around Research Data Obtained From Aviation Industry 84
5.2 Cost to the Aviation Industry due to Go-arounds 86
6. Brief Overview of Wind Urchin 93
6.1 Detailed Description of Wind Urchin Technology 94
6.2 Computer Programme to Analyse and Recorded Wind Data 101
6.3 Compare Wind Urchin Data Against On site Wind Instruments 106
7. Potential For Improved Safety In Landing And Cost Saving To The Aviation Industry 116
8. Conclusion 117
8.1 Further Research 122
Bibliography 124
Appendices 131
Appendix 1: Software Programme and Urchin Baseline file 131
Publish Papers with Recommendations and Results 148

List of Figures

Figure 2.1 Forces acting on an aircraft in flight (ICAO, 2005) 9
Figure 2.2: Resultant flight path following decrease in airspeed due to Horizontal wind shear (ICAO, 2005) 10
Figure 2.3: Resultant flight path following increase in airspeed due to Horizontal wind shear (ICAO, 2005) 10
Figure 2.4: Wind Shear Effect for Approaching Aircraft (ICAO, 2005) 11
Figure 2.5: Wind Shear Effect for Aircraft Taking Off (ICAO, 2005) 11
Figure 2.6: Percentage of NAS Delays 12
Figure 2.7: Environmental Conditions of Percentage of Weather Related Delays 13
Figure 2.8: Environmental Wind Conditions 14
Figure 2.9: Flight Crew Go-around Action 14
Figure 2.10: Potential Hazardous Go-arounds 15
Figure 2.11: Aircraft Accident Incidents 17
Figure 2.12: Trailing Wake Vortices (ICAO, 2005) 21
Figure 2.13 Wake Vortex Distance (ICAO, 2005) 22
Figure 4.1: Effect of Convective Currents on Flight Path (FAA, 2016) 36
Figure 4.2: Aircraft is subject to bumpiness from Convective Currents below Clouds (FAA, 2016) 37
Figure 4.3: Mechanical Turbulence (FAA, 2016) 38
Figure 4.4: Effect of Head/Tail Mechanical shear on Aircraft (WMO 2007) 39
Figure 4.5: Mountain Wave Turbulence (FAA, 2016) 40
Figure 4.6 Mountain Terrain Induced Airflow Pattern (ICAO, 2005) 41
Figure 4.7: Low-level jet forward of a Cold Front (WMO, 2007) 42
Figure 4.8: Wind shear effect on an Aircraft brought by Low-level Jet Stream (ICAO, 2005) 43
Figure 4.9: Wake Vortex Turbulence from Aircraft Wings (IATA, 2015) 44
Figure 4.10: Wind Shear Microburst Effects on Aircraft Taking Off (FAA, 2016) 46
Figure 4.11: Wind Shear Effect on Landing Aircraft from a Microburst ((FAA, 2016) 47
Figure 4.13: Wind Profiles from Atmospheric Boundary Layer Effects (Ellis, 1978) 50
Figure 4.13: LLWAS (Allweatherinc, 2018) 55
Figure 4.14: LLWAS ATC Monitor Display (CAWCR, 2010) 57
Figure 4.15: Gust Observed with Anemometer Data Sydney Airport 15 January 2001 (CAWCR, 2010) 58
Figure 4.16: Concept of Uplink to the Cockpit (Hong Kong Observatory, 2018) 59
Figure 4.17: Doppler Radar Operation Principle (Hong Kong Observatory, 2018) 62
Figure 4.18: Microburst and Shear Line Detected ((Office of Aviation Weather Observations, 2010) 63
Figure 4.19: TDWR Image Map of Doppler Velocity Warning of a Tornado (Observatory, 2018) 64
Figure 4.20: TDWR Image Map of Doppler Reflectivity Warning of a Tornado (Observatory, 2018) 65

Table 4.4: Accuracy of low level wind shear detection 65
Figure 4.21: Doppler Lidar Principle of Operation (Hong Kong Observatory, 2018) 66
Figure 4.22: Doppler Lidar Systems Scanning Runways at Hong Kong (Hong Kong Observatory, 2018)..... 67
Figure 4.23: Lidar Map of Mountain Turbulence (Hong Kong Observatory, 2018) 69
Figure 4.24: TDWR/Lidar Detection Parameters Japan (Office of Aviation Weather Observations, 2010) 70
Figure 4.25: TDWR & LIDAR Integration (Office of Aviation Weather Observations, 2010) 71
Figure 4.26: VCP Elevations Plotted on Range/Height Grid (NOAA, 2010) 74
Figure 4.27: RPG Graphic User Interface for the WSR–88D (OFCM, 2006)..... 75
Figure 4.28: Microburst Detected by WSR-88D (NOAA, 2018) 76
Figure 4:29 Belford Cup and Vane Anemometer 77
Figure 4:30: Vaisala Sensor (Vaisala, 2018) Figure 4.31: Gill WindObserve Sensor (Gill , 2018) 78
Figure 4.32: Measurement Path of Vaisala WMT700 (Vaisala, 2018)..... 79
Figure 4:33: ASCII UV Format (Gill , 2018) 80
Figure 4:34: ASCII Polar Format (Gill , 2018)..... 80
Figure 4:35: Averaging ASCII Format Output (Gill , 2018) 81
Figure 4:36: Logged Data of Averaging ASCII format from the sensor (Gill , 2018) 81
Figure 4:37: Gill Sensor Principle of Operation (Gill , 2018) 82
Figure 5.1: FedEx Crash Nariata Airport (Aviation Safety Network, 2009)..... 87
Figure 6.1: Wind Urchin (ERG, 2018) 93
Figure 6.2: Pitot Tube on Airbus (Monniaux, 2007) Figure 6.3: (FAA, 2018) 95
Figure 6.4 : Conversion of air pressure to wind velocity (Kearney, 2014)..... 97
Figure 6.5: NPH Pressure Sensor (Amphenol, 2018) Figure 6.6: NPH Schematic Diagram 98
Figure 6.7: Gage 3000 General Purpose Transducer Interface Board (A.A.Lab Systems, 2018) 99
Figure 6.8: CompactRIO Single-Board Controller (National Instruments, 2017) 100
Figure 6.9: LabVIEW Screenshot for Data Logging of the Wind Urchin (Kearney, 2014) 101
Figure 6.10: Signal Sampling for TDMS File Input 102
Figure 6.11: TDMS Convert to CSV file 103
Figure 6.12: Pitot Tube Grid Map..... 104
Figure 6.13: R-Code Output Vertical Wind direction Graph..... 105
Figure 6.14: R-Code Output Horizontal Wind direction Graph 106
Figure 6.15: R-Code Output Wind Speed Graph 106
Figure 6.16 : Baldonnell runway and Urchin Location (sensor, 2018)..... 107
Figure 6.17 : Urchin Position Baldonnell (ERG, 2018)..... 107

Figure 6.18: Performance Characteristics of A Cup Anemometer (J.-Å. Dahlberg, 2006) 108
Figure 6.19: Wind Urchin Pitot Tube Grid Layout 109
Figure 6.20: Wind Urchin Principle of Operation 109
Figure 6.21: Cup Anemometer - Wind Urchin Comparison 110
Figure 6.22: Wind Urchin - Cup Anemometer Speed Comparison for One Month / 10 Minute Averages 111
Figure 6.23: Negative From Below Tilt Angle Test (J.-Å. Dahlberg, 2006) 111
Figure 6.24: Horizontal Wind Speed Comparison for Wind Urchin - Cup Anemometer / 10 Min Avr 112
Figure 6.25: Urchin-cup Average of Fig 6 24 113
Figure 6.26: Vertical Wind Speed Comparison for Wind Urchin - Cup Anemometer / 10 Min Avr 113
Figure 8.1: Concept of a Future LLWAS Incorporating the Wind Urchin 120
Figure 8.2: 3-D Image of Wind Intensity on the Surface of Wind Urchin (ERG, 2018) 121

List of Tables

Table 2.1: Wind shear Related Accidents 18
Table 2.2: Aircraft Categories (ICAO, 2018) 24
Table 2.3: Aircraft Separation Criteria (ICAO, 2018) 24
Table 2.4: Wake Turbulence Attributed Accident (SKYbrary, 2018) 25
Table 3.1: Table A6-3 Wind shear Warning Alert (WMO, 2016) 29
Table 3.2: A6-4 Ranges and Resolutions for Wind Shear Warning (WMO, 2016) 30
Table 3.3: Measurement and Instrument Performance (WMO, 2010) 31
Table 4.1: Turbulence Intensity Category (WMO, 2007) 35
Table 4.2: Guide to intensity of Turbulence for Wind Speeds and Terrain (WMO, 2007) 38
Table 4.3: Guide relating CAT to Horizontal and Vertical Wind Shear (WMO, 2007) 44
Table 4.5: Comparison of Vaisala and Gill Ultrasonic Sensors 83
Table 5.1 (Airlines for America, 2016) 88
Table 5.2 Go-around Calculated Costs 89
Table 5.3 Comparison of Go-around figures for Sampled Aircraft 90

List of Equations

Eq: 2.1 8
Eq: 2.2 8
Eq: 2.3 8
Eq: 2.4 8
Eq: 4.1 49
Eq: 4.2 50
Eq: 4.3 50
Eq: 4.4 51
Eq: 4.5 54
Eq: 4.6 79
Eq: 4.7 82
Eq: 4.8 82
Eq: 6.1 96
Eq: 6.2 97
Eq: 6.3 97
Eq: 6.4 97
Eq: 6.5 97
Eq: 6.6 99
Eq: 6.7 99

1. Introduction

The Aviation industry supports $2.7 trillion of the world Gross Domestic Product (GDP) which accounts for 3.5% of the world GDP. This is more than double that of the automotive industry and greater that the chemical and automotive industries combined. The commercial aviation is second only to the global financial services industry. Just to put this into perspective, if the commercial aviation industry were a country, its GDP would rank 21st in the world. The aviation industry carries over 4 billion passengers a year. When aircraft crash, are unable to land or forced to go-around due to wind conditions, this has a substantial human and monetary cost. The ability for a pilot to land an aircraft safely without the need to go-around or abort a landing due to wind conditions is crucial.

Low level Wind shear can affect aircraft performance and has potentially adverse effects on flight safety during landing and take-off phases. Providing immediate and accurate data relating to all prevailing wind conditions including low level wind shear on the runway is crucial for approaching aircraft. Providing the pilot with a complete and comprehensive analysis of wind conditions will facilitate the pilot's decision to land or to go-around. The problem for the commercial aviation industry can be broken into two areas. Human safety which can result in the loss of life or injury to passengers and crew from a plane crash or plane landing related accident. The second area is the monetary cost associated with resulting loss or damage to an aircraft, knock on delays to other aircraft, additional fuel used in the go-around procedure, baggage handling delays and the additional cost of man power resources.

The problem caused by low level wind shear on aircraft is well documented and recognised in the literature. The aviation industry concluded that the majority of

accidents that occurred over the past 10 years have occurred during the approach, landing and go-around flight phases. At the Go-Around Safety Forum in Brussels in 2013, it was concluded that due to rapid changing weather and runway conditions, a pilot does not always have the latest information on which to make a landing or go-around decision. Air accident reports have stated that between 2000 and 2012 there were 10 fatal accidents attributed to flight go-arounds in which 614 people died. Six go-around safety issues were identified with 57% of risk bearing go-arounds being attributed to the crew failing to initiate the go-around procedure. At the Brussels forum it was established that out of 44 risk bearing go-around decisions taken by crew that 45% of the go-arounds were because of an un-stabilised approach on landing. The weather conditions were responsible for 34.7% of all go-around procedures. A further conclusion of the Brussels forum was that improved information should be provided to crews in relation to tailwinds, wind shear and wind variations. In several air accident reports some involving fatalities, it has been concluded that the lack of real time adverse wind shear information can be attributed to the cause of the accident. A report in 2002 by the Australian Transport Safety Bureau into an accident caused by a microburst involving a Boeing 737-400 recommended that that the Bureau of Meteorology expedite the research and development program to examine wind shifts and wind shear, with the objective to improve the detection and forecasting of wind shifts and the detection of wind shear in the vicinity of high risk airport terminal areas and that the Civil Aviation Safety Authority place greater emphasis on the effect of wind shear.

This thesis will argue that a solution to the problem of forecasting low level wind shear and turbulence for the approach, landing and go-around flight phases for aircraft could

be addressed by incorporating the Wind Urchin as part of the Low Level Wind Shear Alerting System (LLWAS) in all airports.

This requires a change of approach and thinking on the characteristics of wind measurement when quantifying and analysing wind shear, turbulence and microburst for the approach, landing and go-around phases for aircraft. The science of wind measurement, has remained largely unchanged. It is relies on cup and or sonic anemometer to determine wind speed and on wind vanes to determine wind direction. These instruments are constructed and limited by their design to only measure wind as a two-dimensional entity. The data obtained from these instruments is then used to provide the information to the air traffic controller who then relays this to the aircraft crew concerning the presence of low level wind shear. Equipped with this limited data and analysis of the prevailing wind shear conditions, the crew must decide on what course of action to take when coming in to land. Wind shear can be summarised as a change in wind speed and/or direction in space including updrafts and downdrafts. Wind blows freely in three dimensional space but is only measured in two dimensions. It must be noted that wind shear is a vector and hence the speed and direction of the two winds must be factored into the equation. Because of the complexity of wind shear, it cannot be calculated by simple scalar calculation of wind speeds. Current methods of wind shear calculations involve data from an aircraft on descent and recording data from different anemometers spaced at different levels along a runway on masts. The limitation in this approach is that the calculation of wind shear from two winds separated by a distance gives the overall wind shear between those two points. The information does not indicate if the rate of shear is linear or not or where most of the shear occurs between the points sampled. It is wholly inadequate and does not give the maximum shear.

This would indicate that traditional meteorological instrumentation used in the aviation industry are not adequately providing all the necessary data required by the air traffic controllers and flight crew with the information that is critically on approach and landing, leading to greater safety of passengers and crew.

1.1 Aims and Objectives

The aims of the research is to mine data from the beta test urchin in Baldonell Aerodrome capturing wind shear wind flow inclination and wind turbulence characteristics. To analyse the data and results and compare with World Meteorological Organization (WMO) standard. To quantify the safety and monetary cost of flight go-arounds to the aviation industry from wind shear occurrences.

Description and analysis of results from using a three dimensional instrument to measure wind shear. Discussion of cost savings to the commercial aviation industry globally.

This research project aims to demonstrate that the Wind Urchin can improve the forecasting and recording of wind shear and low level turbulence at airports leading to increased safety for passengers and crew and greater cost savings to the aviation industry. The thesis will show that despite greater technological advances in the aviation industry there is still disruption caused to aircraft landing and taking off caused by low level wind shear and turbulence. The thesis will demonstrate that the current methods and instruments used to measure wind shear and turbulence at airport runways are not complete and does not give the most up to date and accurate information to the pilot and crew on approach, landing or take off phases of an aircraft. The methodology utilised both a qualitative and quantitive research approach to obtain the main objective of the thesis which is to show that incorporating the Urchin as part of the Low Level Wind Shear Alerting System (LLWAS) at airports could reduce the

number of flight go-around manoeuvres performed as a result of wind conditions on landing. The thesis will argue that the potential for improved safety in landing and cost saving to the aviation industry by reducing go-around manoeuvres can be achieved with accurate three dimensional wind data from the Urchin. The qualitative research involved investigating and researching reports, manuals and forum information as well as direct contact with the relevant sectors of aviation to help gain an in-depth understanding of subject matter necessary to conduct the quantitative research. The quantitative research analysed data to quantify the problem of air accidents as a result of Low Level wind shear, to quantify the cost to aviation as a result of go-arounds as a result of wind conditions. This enabled numerical data to be transformed into statistical information and tables to meet the aims and objectives of the thesis.

2. Literature Review of Difficulties with Aircraft during Landing and Take-off Phases

2.1 Overview of Disruption to Aircraft Due to Low Level Wind Shear

Low level wind shear can effect aircraft performance and has potentially adverse effects on flight safety during landing and take-off phases. It cannot be underestimated how serious the effect of low level wind shear can be on an approaching aircraft (Daidzic, 2016). The disruption cause by wind shear and low level turbulence can range from severe, resulting in an aircraft accident and fatalities to minor resulting in delays at airports and additional resulting monetary costs. Wind shear can occur at any level but low level wind shear can cause problems of such magnitude that it can affect the air crew's ability to control the plane during take-off or on approach to landing (Civil Aviation Authority, 2013). Airline companies, civil aviation authorities and the Flight Safety Foundation have produced reports and manuals for Air Traffic Controllers and flight crews in stipulated procedures to be followed when a low level wind shear warning has been issued (Flight Safety Foundation, 2009). Increased pilot training in dealing with the problems caused as a result of low level wind shear and turbulence has been adapted by all major airlines (ICAO, 2005). Despite all the advances in wind shear and turbulence warning systems at airports, the conclusion from many reports have stated that the best course of action for a pilot to take is to avoid wind shear completely (Albright, 2015). The concluding summary issued to airlines by the ICAO in their manual on low level wind shear was to avoid wind shear and if in doubt, delay take off and on approach, hold until conditions improve or divert to an alternative airport.

2.2 Adverse Effects on Flight Safety on Approach and Landing from Turbulence

Wind shear can be defined as the sudden, drastic change of wind velocity and/or direction over a very small area (FAA, 2016) . The ICAO expand further and define the term wind shear as a change in wind speed and/or direction in space including updrafts and downdrafts. Changes in the wind speed and/or direction concern changes in the prevailing wind from one reference point in space to another. From this, it can be concluded that any atmospheric phenomenon or any physical obstacle to the prevailing wind flow that produces a change in wind speed and/or direction, in effect, causes wind shear. Short term fluctuations in speed and/or direction are referred to as variations from the prevailing wind and are usually temporary and result in bumpiness to an aircraft. However the scale in which wind shear occurs in relation to the size of an aircraft is of fundamental importance (ICAO, 2005). In order to understand the effect that wind shear and turbulence can have on an aircraft, it is important to understand the four main forces that act on an aircraft while in flight. The thrust is provided by the engines, the lift is provided by the wings, the third and fourth force acting on the aircraft is the weight of the aircraft and the drag from the aircraft. In non-accelerating flight the thrust has to balance the drag and the lift has to balance the weight. When the forces on the aircraft are in equilibrium there are no resultant forces and in accordance of Newton's first law of motion, this will continue whether the aircraft is climbing, descending or in level flight until the balance is disturbed. In a normal level flight the thrust has to balance the drag and the lift has to balance the weight. In a flight that is climbing the thrust also has to balance a portion of the weight ($W \sin \gamma$), hence more thrust is needed that in normal level flight and the thrust is proportional to the angle of climb. The four main forces acting on an aircraft are effected by wind shear. Fig 2.1 shows the forces acting on an aircraft in flight. The

Thrust (T) of the aircraft is the force produced by the aircraft engines; the Weigh (W) is defined as the Mass (m) of the aircraft x acceleration due to gravity (g) where W = mg. The Lift (L) and Drag (D). From Eq 2.1 and Eq 2.2, the angles of climb of the aircraft can be derived.

Eq: 2.1 $$T = D + W\gamma$$

Eq: 2.2 $$\gamma = \frac{T-D}{W}$$

Where

W = mg (Mass of aircraft x acceleration due to gravity)

L = Lift

D = Drag

The Lift (L) and Drag (D) are proportional to the density of the air (ρ), the area of the wing (S) and the square of the velocity of the air passing over the wings. (V) L&D α ρ, S & V^2. The lift and drag coefficients CL and CD are constants of proportionality as shown in Eq 2.3 and Eq 2.4 such that,...

Eq: 2.3 $$L = ½\ C_L\ \rho S\ V^2$$

Eq: 2.4 $$D = ½\ C_D\ \rho S\ V^2$$

These equations demonstrate that the lift and drag depend on the angle of attack on the wing and the square of the airspeed. Wind shear can affect both the angle of attack and the airspeed which in turn can affect lift and drag. This in turn disturbs the equilibrium of the aircraft.

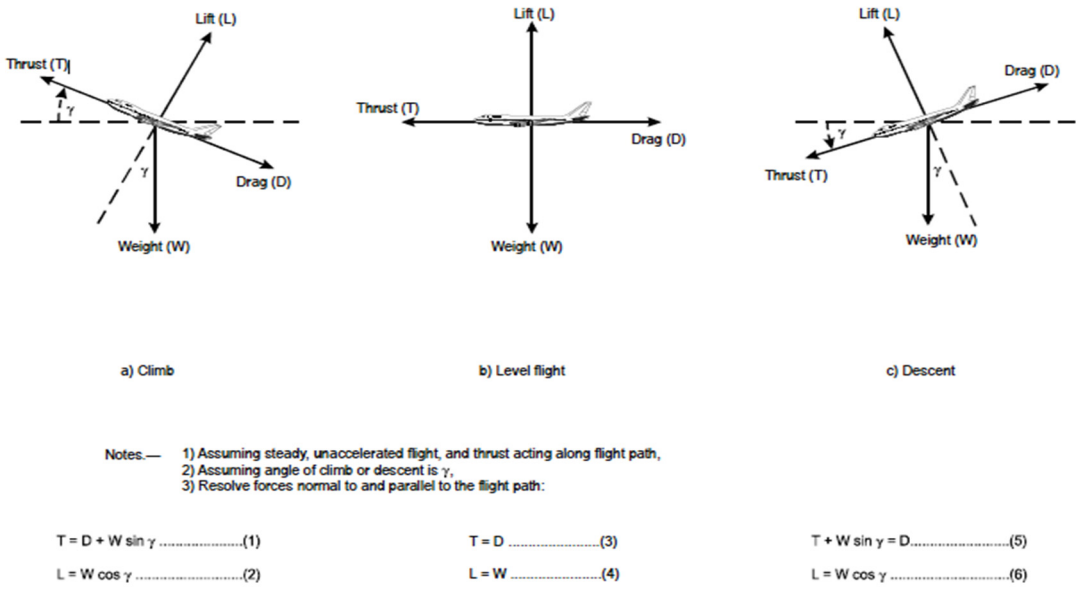

Figure 2.1 Forces acting on an aircraft in flight (ICAO, 2005)

Vertical wind shear causes variations of the horizontal component of the wind which can affect the aircraft speed on approach to landing or on take-off. Horizontal variations of the wind can result in an increase or decrease in head and tail wind affecting the landing and take-off of aircraft. Fig 2.2 and Fig 2.3 illustrate the effect of wind shear on aircraft.

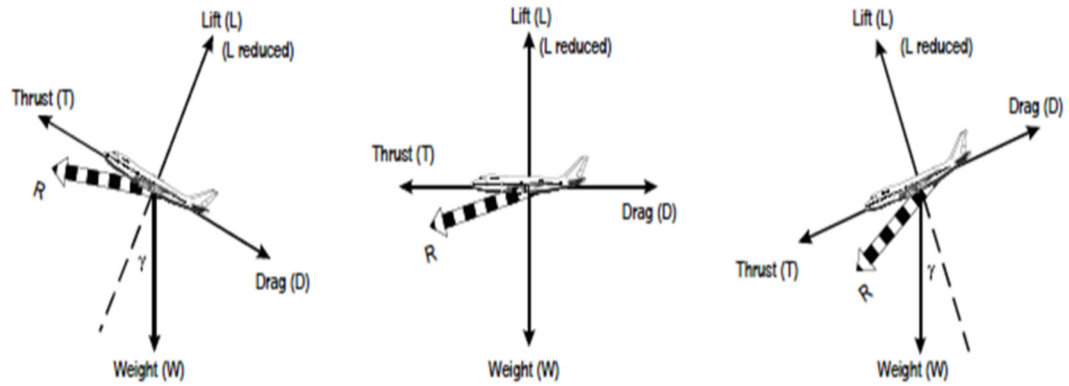

Figure 2.2: Resultant flight path following decrease in airspeed due to Horizontal wind shear (ICAO, 2005)

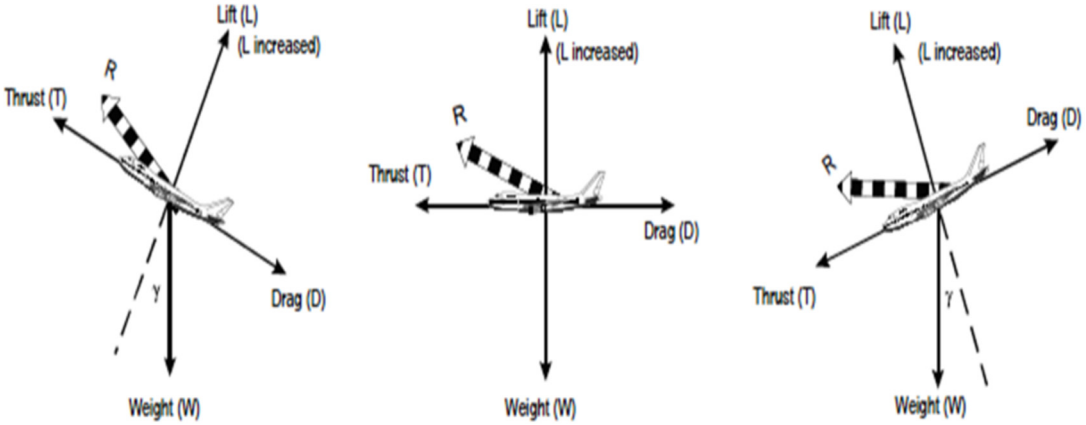

Figure 2.3: Resultant flight path following increase in airspeed due to Horizontal wind shear (ICAO, 2005)

Extreme low level wind shear and turbulence can at its worst cause and aircraft to crash resulting in fatalities and injuries to passengers and crew and destruction or damage to an aircraft. At the lower end of the scale, wind shear and turbulence will result in delays to take offs and landings, aborted landings resulting in flight go-around manoeuvres or flights being diverted to another airport. Fig 2.4 illustrates the effect on wind shear on approaching aircraft coming in to land. It can be seen that the speed of the aircraft is increased by the wind resulting in a greater stopping distance being needed to halt the aircraft. Fig 2.5 illustrates the effect of wind shear on aircraft taking-off.

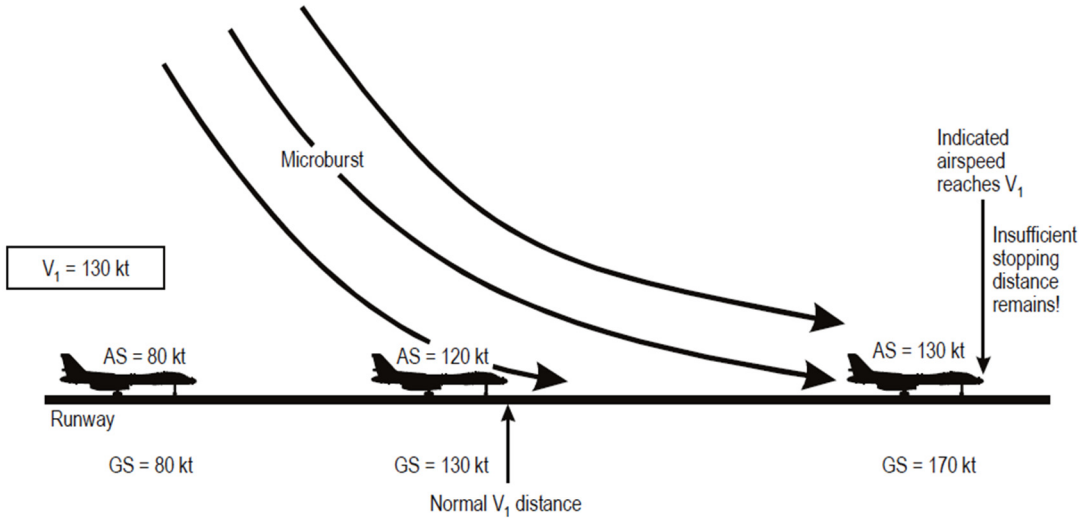

Figure 2.4: Wind Shear Effect for Approaching Aircraft (ICAO, 2005)

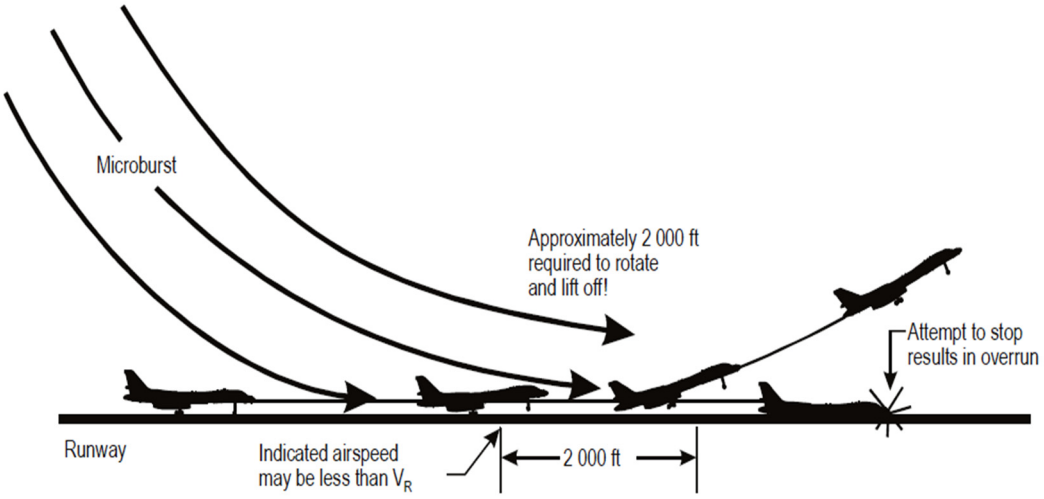

Figure 2.5: Wind Shear Effect for Aircraft Taking Off (ICAO, 2005)

According to the U.S. Department of Transport records from the National Aviation System (NAS) 33% of all delayed flights in 2016 were delayed due to weather conditions. The figure for 2017 to date is over 50% due to weather conditions (Bureau of Transportation Statistics, 2017). Figure 2.6 illustrates how weather is still the primary cause of delays to aircraft. Despite many advances in on-board aircraft wind warning systems and ground based warning systems, wind shear is a formidable force that coupled with a microburst can overpower any aircraft (Albright, 2015).

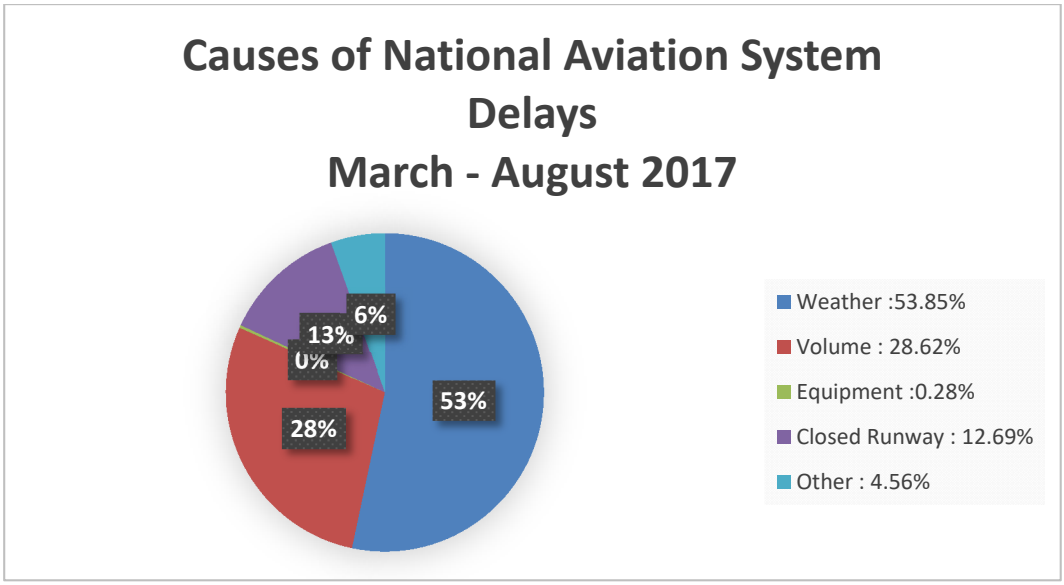

Figure 2.6: Percentage of NAS Delays

2.3 Flight Go-around Procedures as a Result of Low Level Wind Shear

A flight go-around is an aborted landing on final approach of an aircraft. A go-around procedure is performed by the pilot if it is believed that the correct conditions are not suitable to make a safe landing. In a report by the International Air Transport Association (IATA) for the Go-Around Safety Forum (IATA, 2013), it was found that out of 1050 random data samples of Aircraft Safety Reports (ASR) on go-arounds that over 39% listed environmental conditions as the reason for a go-around. 42% of those reports noted wind as the reason for a go-around. Fig 2.5, illustrates how the environmental conditions break down to the number of go-around manoeuvres.

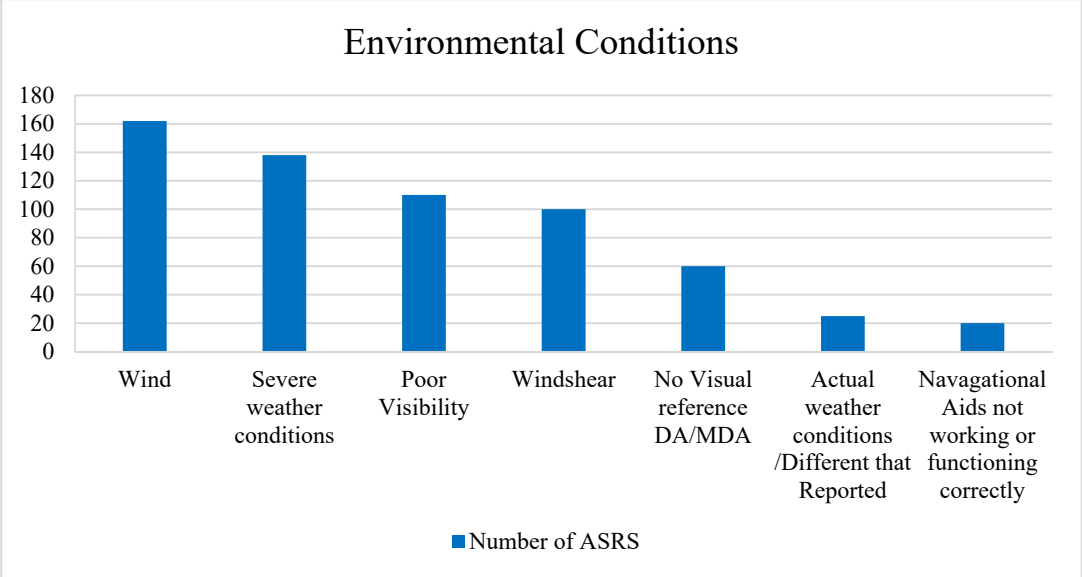

Figure 2.7: Environmental Conditions of Percentage of Weather Related Delays

From the graph in Fig 2.7, it can be seen that wind and wind shear combined represent the overwhelming majority of go-arounds due to environmental conditions. The components of wind conditions can be further analysed as shown in Fig 2.8 to show the number of Aviation Safety Reports for go-arounds attributed to each documented wind condition. In the survey conducted by the IATA it was found that over 78% of all go-arounds were initiated by the flight crew and 22% were initiated by the Air Traffic Control (ATC). This would seem to indicate the wind shear and turbulence data recorded by the ATC was not accurate or up to date for the approaching aircraft and it was the flight crew who deemed it necessary to abort the landing based on the conditions that they encountered on approach.

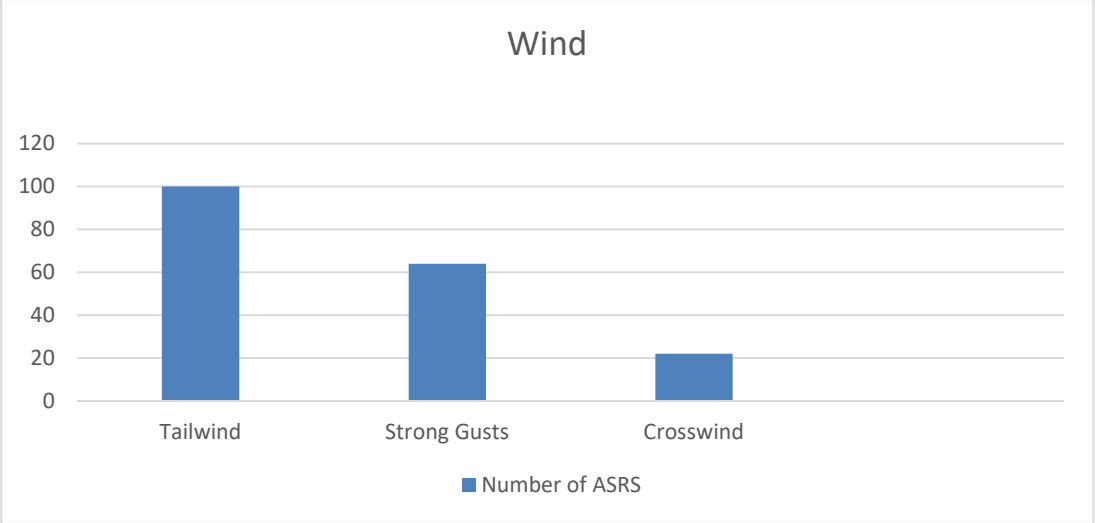

Figure 2.8: Environmental Wind Conditions

Fig 2.9 can further illustrate the flight crews recorded statistics from the ASRs as to the reason for initiating a go-around.

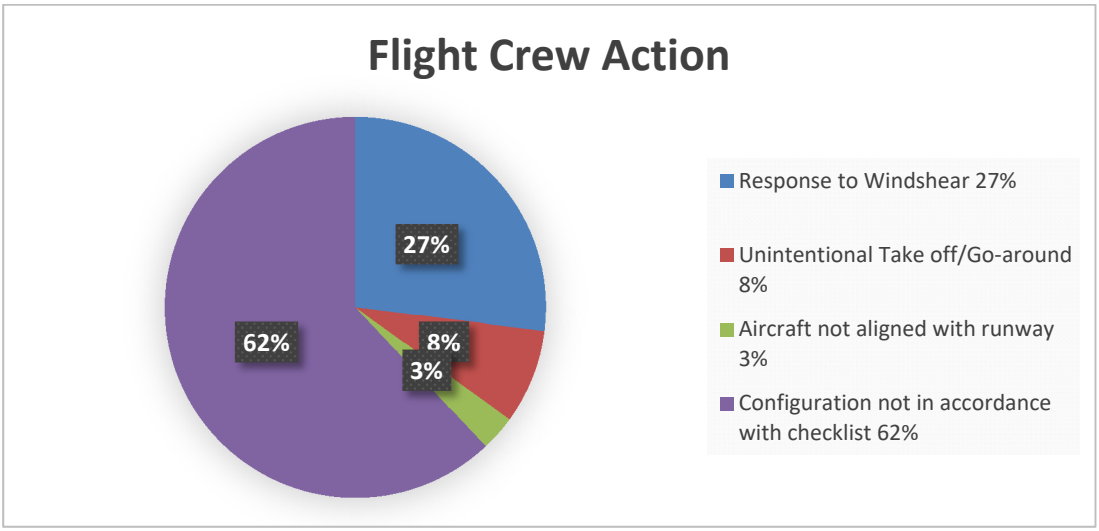

Figure 2.9: Flight Crew Go-around Action

In the data set analysed for the Go-Around Forum Report, it was noted that over 9% of the go-arounds recorded a potential hazardous outcome. In Fig 2.10 it can be seen how on 30 go-arounds that the aircraft exceeded its performance limits.

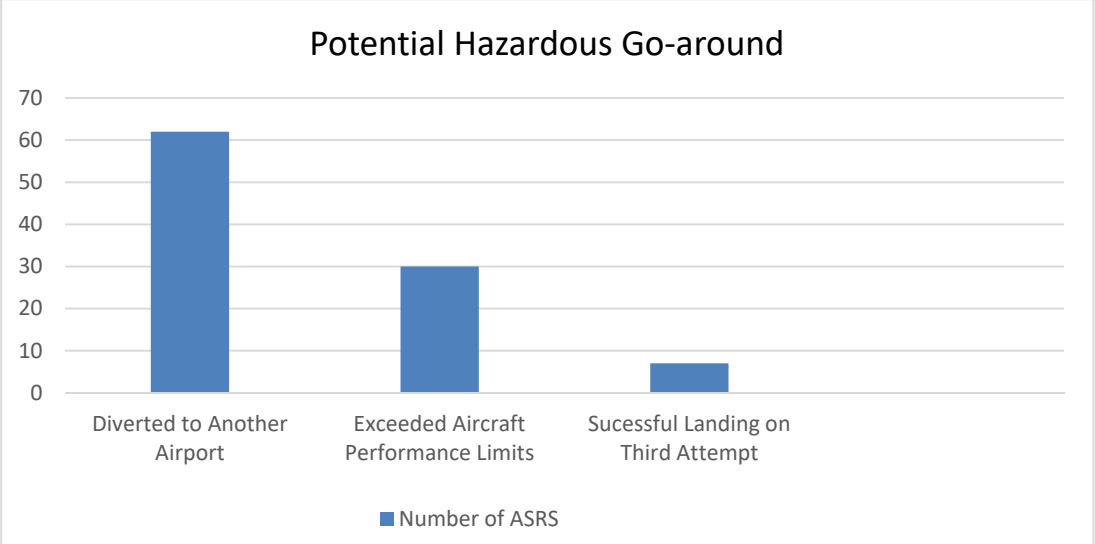

Figure 2.10: Potential Hazardous Go-arounds

The majority of accidents in the past 10 years have occurred during this go-around procedure (EUROCONTROL, 2013). The Federal Aviation Authority (FAA) with the Boeing Company has produced documents and training videos for pilots in how best to prepare and cope with adverse wind shear conditions (FAA, 1990). The FAA and the ICAO recommendations to flight crew regarding wind shear is that avoidance is the best precaution. They further state that taking precautions and coupled with the best recovery piloting skills cannot guarantee a successful escape from microburst wind shear. (ICAO, 2005). In 2011 over 68% of commercial aviation accidents were attributed to this procedure. One of the finding of the conference on Go-Around Safety Forum was that due to rapid changing weather conditions, the pilot doesn't always have the latest information on which to base a landing/go-around decision. The forum also recommended that more relevant quicker updated and improved information should be provided to flight crews on wind shear, tailwinds and wind variation on approach to landing. In the IATA report to the Go-Around Forum they concluded that the actual wind conditions versus the recorded and reported wind conditions given to the flight crew on final approach were an area of concern. They most worryingly noted

that 31% of all aircraft exceeded aircraft performance limits during the go-around manoeuvre.

2.4 Aircraft Accidents Attributed to Low Level Wind Shear and Turbulence

Accidents attributed to wind shear and turbulence have reduced over the past twenty years. This can be attributed to improved equipment, better education and better awareness of the hazardous outcomes that have resulted from past air accidents. The aviation industry has published several reports on wind shear and turbulence. Air crew training now incorporates, training specific to wind shear related events such as go-around manoeuvres. Air traffic controllers, pilots, airline bodies and aircraft manufacturers have all contributed to forums in which guidelines (Civil Aviation Authority, 2013) and safety rules have been stipulated in relation to wind shear and turbulence events (EUROCONTROL, 2013). Despite all of the improvements in training, equipment and aircraft over the past number of years, wind shear and low level turbulence still presents a significant risk to aircraft on take-off and approach to landing. The present advice given to pilots and aircrew is to avoid and delay take-off when a wind Shear alert has been issued. It can be seen from Fig 2.11 that almost 50% of all recorded commercial accidents since 1990 were as a result of wind shear or severe low level wind gusts. Table 2.1 details the accidents and incidents of commercial airlines as a result of wind shear.

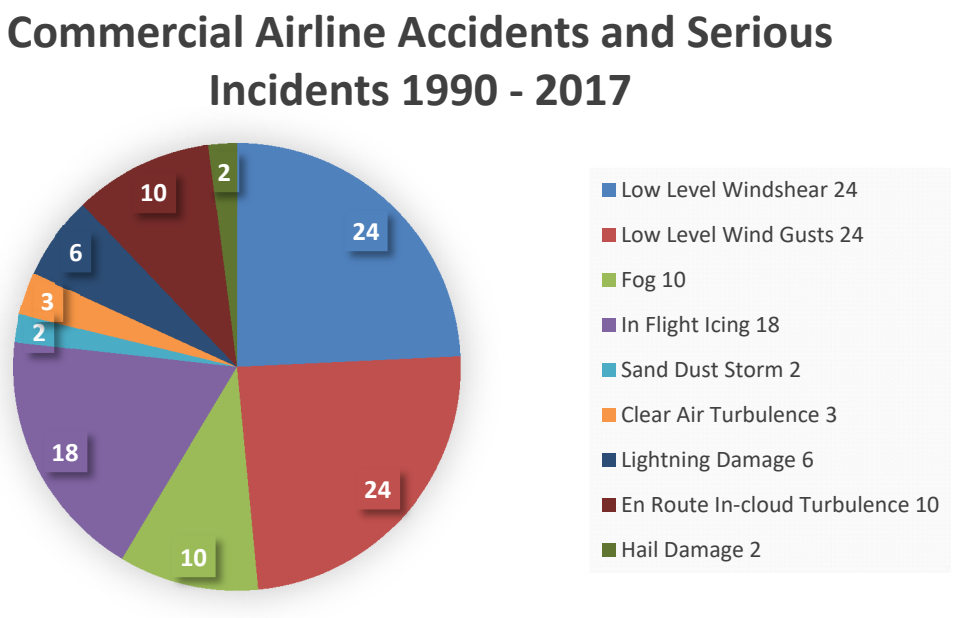

Figure 2.11: Aircraft Accident Incidents

2.5 Recommendations on Wind Shear from Air Crash Investigation

Despite increased safety structures and better warning systems in the commercial aviation industry, there continues to be air accidents attributed to low level wind shear and turbulence at international airports. Only as recent as 2016, a devastating crash occurred killing all 62 occupants of a modern Boeing 737 aircraft reroute from Dubai to Russia operated by Fly Dubai Airlines (SKYbary, 2017). As with most air crash investigation reports, there is a series of events which lead to the final outcome. The Air crash Investigation Report (Interstate Aviation Committe, 2016) stated that the air crew initiated a go-around procedure after the on-board wind shear warning had activated. The crew aborted the landing and initiated a go-around at a height of 220 m after a sudden 20-knot increase in speed to 176 knots in less than 3 seconds. This indicated the presence of wind shear to the crew. As with most commercial airline pilots, they did not have sufficient experience or training in how to handle an aircraft during a go-around caused by a wind shear event. Deficient crew handling there after resulted in the aircraft crashing with the loss of all lives on board. Table 2.1 details the

accidents and incidents of commercial airlines as a result of wind shear from 1994 to 2016. In all of the accidents which resulted in fatalities, it can be shown that wind shear initiated a go-around procedure by air crew who were deficient in experience and knowledge of the aircrafts handling capabilities during a go-around manoeuvre while encountering low level wind shear and turbulence. In two incidents involving Qantas Airline aircraft, it was concluded by aviation investigation that the Air Traffic Control failed to communicate accurate up to date wind shear information to the air crews. The first incident occurred in 2001 involved a Boeing 737 (Australian Transport Safety Bureau, 2002) which initiated a go-around after encountering a microburst and wind shear. The aircraft diverted to another airport and landed safely. The second incident involved a Boeing 747-400 (Australian Transport Safety Bureau, 2009) which experienced a hard touchdown on landing resulting in minor damage to the aircraft. If more accurate wind shear recording and warning devices were available to the ATC, this may have resulted in more accurate and up to date information being relayed to air crews sooner enabling them to make a more informed decision of whether to initiate a flight go-around and at what stage to initiate a go-around.

Table 2.1: Wind shear Related Accidents

AIR ACCIDENTS ATTRIBUTED TO WINDSHEAR						
YEAR	**AIRCRAFT MODEL**	**AIRLINE COMPANY**	**COUNTRY OF ACCIDENT**	**INJURIES & DAMAGE**	**OUTCOME**	**ACCIDENT REPORT CONCLUSIONS**
19-Mar-2016	Boeing B737	Fly Dubai	Rostov-on-Don,Russia	55 Passengers and 7 Crew Killed. Aircraft Destroyed	Crashed into Runway	Failed to complete a go-around initiated after encountering Wind shear
7-Oct-2014	Airbus A321	Air Canada	Montreal, Canada	Damage to Aircraft lights and Runway edge lights	Veered off Runway onto grass verge	Lateral Wind shear suddenly increased Aircrafts drift to the left of runway

2-Jan-2014	ATR-72-212A	Not Listed	Cork, Ireland	No injuries, No Damage	Landed after two go-around manoeuvres	Severe wind shear and Turbulence forced the aircraft to go-around twice
25-Oct-2013	Bombardier CRJ 900	Air Nostrum	San Sebastian, Spain	Damage to Aircraft landing gear and wheels	Hard and Bounced landing on Runway	Low level wind shear sped up the approach. Deficient Crew handling
20-Apr-2012	Boeing 737-200	Bhoja Air	Islamabad, Pakistan	127 passengers and Crew Killed. Aircraft Destroyed	Crashed into Ground 4nm from Runway	Inappropriate crew response to severe wind shear- skills deficiency of Crew
21-Dec-2011	Airbus A321	Austrian Airlines	Manchester, UK	Damage to Tail of Aircraft	Tail of Aircraft struck Runway	Low-level Wind shear forced a go-around. Deficient crew handling
4-Apr-2011	Bombardier CRJ 100	Georgian Airways	Kinshasa, DR of Congo	32 Passengers and Crew Killed	Crashed into the Runway	Inadequate weather information given to crew. Aircraft encountered severe Wind shear during go-around
1-Dec-2010	De Havillands DHC8-100	Wideroe Flyvesselskap	Svolvaer, Norway	Temporary Loss of Control of Aircraft	Aerodynamic Stall, Temporary Control loss. Landed Safely	Low level Wind shear and Strong Gusts caused Rapid descent & drop of speed avoiding Sea collision
14-Sep-2010	Airbus A319	Sichuan Airlines	Wuxi, China	Temporary Loss of Control of Aircraft	Aerodynamic Stall, Temporary Control loss. Landed Safely	Low level Wind shear. Flight crews inappropriate decisions and handling under adverse weather conditions
20-Dec-2008	Boeing 737-500	Continental Airlines	Denver, USA	47 Passengers injured seriously injured. Aircraft Fuselage Broke in two	Aircraft Blown off Runway on take-off	Pilot Error & inadequate training for Low level Wind shear conditions. Wind information from ATC not provided
15-Apr-2007	Boeing 747-400	Qantas Airways	Sydney, Australia	Ceiling panels dislodged and Fell Down. No serious injury or damage	Hard Touchdown on Runway, followed by Go-around.	Low level Wind shear. ATC failed to communicate accurate Wind shear information to Flight Crew
29-Oct-2006	Boeing 737-200	ADC Airlines	Abuja, Nigeria	96 of the 105 Occupants Killed 9 injured. Aircraft Destroyed	Crashed 76 Seconds after Take-off into End of Runway	Crew should not have attempted Take-off in known Adverse Wind shear Conditions. Aircraft Stalled & Crashed
10-Dec-2005	Douglas DC 9-32	Sosoliso Airlines	Port Harcourt, Nigeria	108 of the 110 Occupants Killed. Two injured. Aircraft Destroyed in Fire	Crashed into the Ground during Attempted Go-around	Low level Wind shear conditions caused the pilot to Go-around. Improper Go-around Procedure by Pilot
23-Sep-2005	AS 350 Helicopter	Heli USA Airways	Hawaii, USA	3 of 6 Occupants Killed Injured. Aircraft Destroyed	Aircraft Crashed into the Ground. Airspeed Dropped to Zero	Pilots Decision to continue to Fly in Adverse Weather Conditions. Loss of Control in Severe Wind shear Conditions

1-Sep-2005	De Havillands DHC-2	Nordplus	Quebec, Canada	Pilot and Passenger Killed. Aircraft Destroyed	Crashed into Lake after Encountering Server Turbulence	Severe wind shear and Turbulence Contributed to an Aerodynamic Stall from which Recovery was not Possible
21-Jan-2002	A321-100	Nippon Airways	Hakeodate, Japan	3 Crew injured. Severe Damage to Aircraft Aft Fuselage	Aft Fuselage impacted Runway on Touchdown. Landed after Go-around	Delay in Response to Wind shear Conditions by Crew caused Tail of Aircraft to Strike the Runway
7-Feb-2001	Airbus A320-200	Iberia Airlines	Bilbao, Spain	25 Passengers Injured. Severe Structural Damage to Aircraft. Hull Loss	Aircraft Hit Runway while attempting Go-around	Wind shear Prompted Crew to initiate Go-around. Automatic AOA protection Opposed Crew input Pitch Input. Aircraft Software Error
18-Jan-2001	Boeing 737 - 400	Qantas Airways	Brisbane, Australia	No injuries, No Damage	Go-around initiated. Full Engine Thrust Needed. Diverted to another Airport	Aircraft Encountered Wind shear during Go-around. ATC Require Upto date Wind shear Training. More Accurate Wind shear Recording Required
3-Dec-1999	Boeing 737 - 500	Maersk Airlines	Copenhagen, Denmark	No injuries, No Damage	Diverted after Go-around at two different Airports. Aircraft landed with No Reserve Fuel	Significant delays by ATC in providing Crew with up to date Information on Adverse Weather and Wind shear Conditions
1-Jun-1999	Douglas DC 9-82	American Airlines	Little Rock, USA	11 Killed. 105 Seriously injured. Aircraft Destroyed in Post-Crash Fire	Overran the End of Runway. Crashed into Fence & Metal Structures	Crew Failed to Discontinue Approach when Severe Thunderstorms & Turbulence had moved into Airport Landing Area
2-Jul-1994	Douglas DC 9-30	US AIR	Charlotte,USA	37 of the 57 Occupants Killed. 16 Seriously injured Minor injuries. Aircraft Destroyed	Aircraft Crashed into Trees and House after Go-around initiated	Crews Failure to Recognise Wind shear Situation. Lack of Real Time Wind shear information from ATC.

2.6 Effect of Wake Turbulence on Aircraft During Take-off and Landing

Wake Turbulence is generated behind an aircraft as it passes through the air. It is often referred to as Wake Vortex Turbulence as it is principally caused by wing tip vortices. It is generated from the moment the nose of the aircraft leaves the ground and will continue while the aircraft is airborne until the nose of the aircraft touches down on landing. Wing tip vortices are formed any time an aerofoil is producing lift. Lift is generated by the aircraft wings caused by a pressure differential over the wing surfaces. The lowest pressure is formed on the upper side of the wind while the highest pressure is formed under the wing surface. The air will flow to the wing tips as this is

the area of lowest pressure. The pressure differential causes the roll up of the air flow at the wing tips which results in swirling air cones trailing downstream of the wing tips as can be seen in Fig 2.12. Viewed from the rear of the plane the left vortex rotates clockwise while the right rotates anticlockwise.

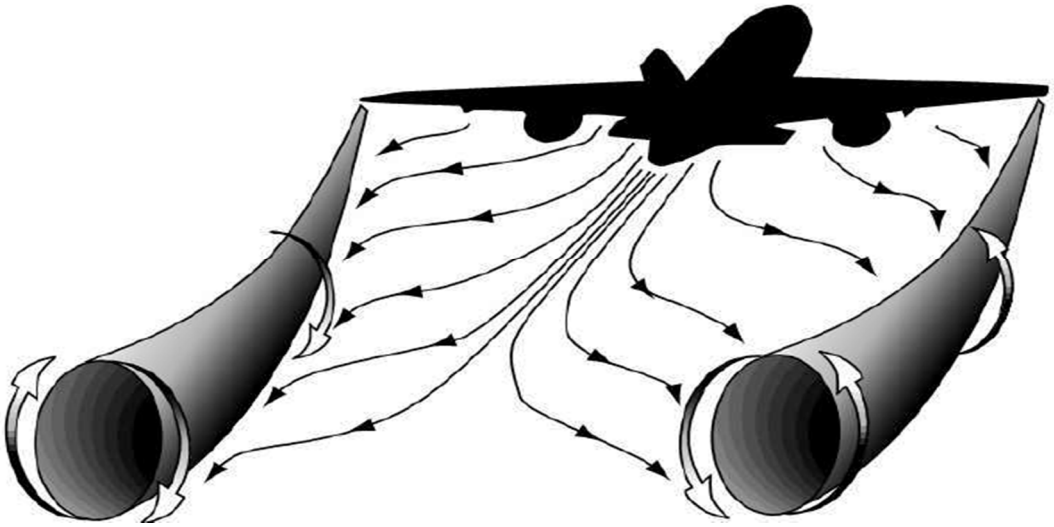

Figure 2.12: Trailing Wake Vortices (ICAO, 2005)

The vortex develops a circular motion around a core. This core can vary from a few centimetres to several metres depending on the size and weight of the aircraft. The air speed inside the core can vary up to 100 metres per second. The core is surrounded by an outer vortex which can be as large as 30 metres (CAA New Zealand, 2008). The wake vortex can last for as long as 4 minutes in the case of the Airbus A380-800 aircraft. Wake vortices spread laterally away from the aircraft and descend at between 500 to 900 feet at distances of up to 5 miles. Fig 2.13 illustrates the descend and distance of a wake vortex.

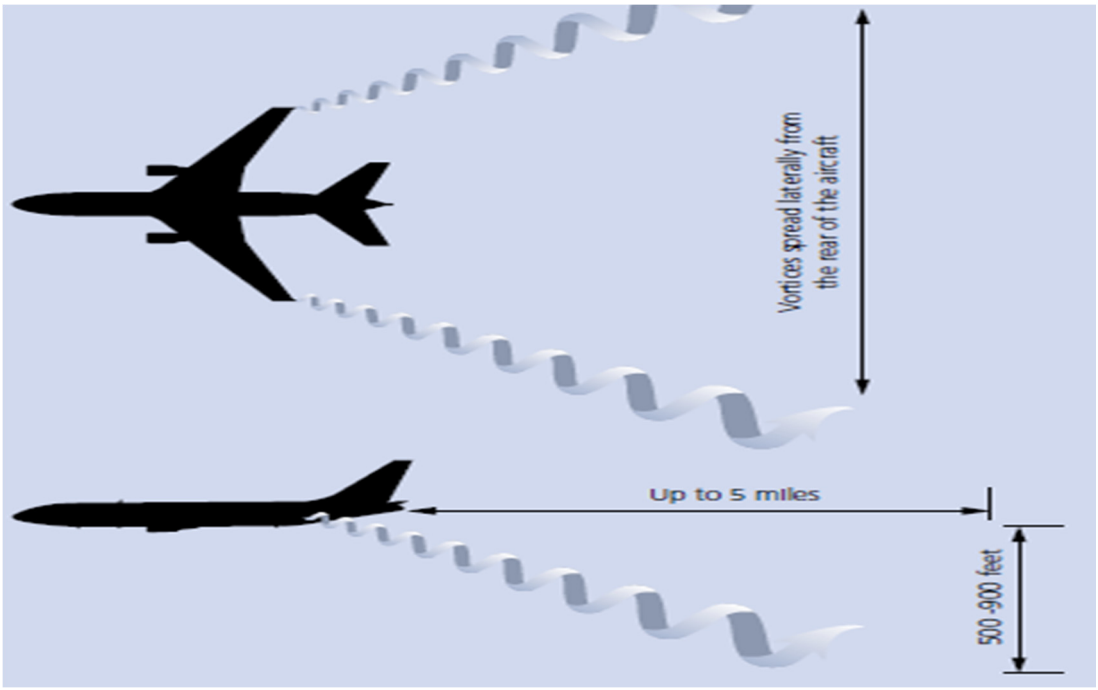

Figure 2.13 Wake Vortex Distance (ICAO, 2005)

Wake turbulence can have a potentially hazardous effect on aircraft during the take-off and landing phases, because of the aircraft's close proximity to the ground making any change in normal procedure due to wake turbulence can be difficult and potentially fatal. The effect and severity of wake turbulence on an aircraft is predominantly dependent on the size and weight of the aircraft producing the turbulence and the size and weight of the aircraft behind coupled with the distance between the two aircraft. The ICAO, FAA and EUROCONTROL after years of research have now categorised aircraft types in accordance with their weight and size which is illustrated in Table 2.2. Mild wake turbulence will have a similar effect as shaking an aircraft similar to mid-air turbulence. Severe wake turbulence will induce roll and yaw, which can result in a complete loss of control of the aircraft. The ICAO, FAA and EUROCONTROL have issued separation guidelines in relation to time and distance for take-off and landing phases as well as for in flight aircraft (Eurocontrol, 2015). These guidelines state the minimum distance and time that an aircraft must maintain when following an aircraft of a stated specific category to avoid the wake

vortex turbulence generated from the leading aircraft. Table 2.3 depicts the separation criteria for aircraft as stipulated by the ICAO. The first RECAT separation standards were implemented in the USA in 2012. The FAA has reported greater airport efficiency as a result of these implementations. This can be attributed to the fact that ATC now have specific guidelines and tables for all aircraft types which eliminates blanket times and distances for leading and following aircraft. The first European implementation of the RECAT separation standards was in April 2015. EUROCONTROL's re-categorisation of the ICAO wake turbulence separation minima on approach and departure for all aircraft was revised due mainly to the arrival of the Airbus A380 Super passenger jet. The A380 became the largest passenger aircraft in the world generating wake vortices greater than any previously recorded by other aircraft. The RECAT-EU guidelines were formulated from wake data gathered over a two year period at London Heathrow and Frankfurt airports. The study monitored and recorded aircraft wake turbulence based on aircraft geometry and final approach speeds, the formulation of the severity metric was developed by experts independent of all aircraft manufacturers. They confirmed the non-linear influence of individual vortex spacing on wake decay properties. These studies have increased the knowledge of wake turbulence in the aviation operational environment with a greater understanding of the vortices generated and how they impact on other aircraft, leading to greater safety for passengers and aircraft and enabling the construction of new technologies to analyse and record wake vortex turbulence.

Table 2.2: Aircraft Categories (ICAO, 2018)

AIRCRAFT TYPES AND CATEGORIES					
Super Heavy CAT-A	**Upper Heavy CAT- B**	**Lower Heavy CAT-C**	**Upper Medium CAT-D**	**Lower Medium CAT-E**	**Light CAT-F**
AIRBUS A-380-800	AIRBUS A-330-200	AIRBUS A-300-600	AIRBUS A-318	ATR ATR-42-300/320	DASSAULT Falcon 10
ANTONOV An-124 Ruslan	AIRBUS A-330-300	AIRBUS A-300	AIRBUS A-319	ATR ATR-42-500	DASSAULT Falcon 20
ANTONOV An-225 Mriya	AIRBUS A-340-300	AIRBUS A-310	AIRBUS A-320	ATR ATR-72-201	FAIRCHILD DORNIER 328
	AIRBUS A-340-500	BOEING 707-300	AIRBUS A-321	BOEING 717-200	EMBRAER Brasilia
	AIRBUS A-340-600	BOEING 757-200	ANTONOV An-12	BOEING 737-200	BEECH 400 Beechjet
	AIRBUS A350-900	BOEING 757-300	BOEING 737-600	BOEING 737-300	RAYTHEON BAe-125-700/800
	BOEING 747-400 (international, winglets)	BOEING 767-200ER	BOEING 737-700	BOEING 737-400	BRITISH AEROSPACE Jetstream 32
	BOEING 747-8	BOEING 767-300ER	BOEING 737-800	BOEING 737-500	BRITISH AEROSPACE Jetstream 41
	BOEING 777-200 / 777-200ER	BOEING 767-400	BOEING 737-900	BOMBARDIER Challenger 600	GATES LEARJET Learjet 35
	BOEING 777-300	BOEING C-135 Stratolifter	LOCKHEED AC-130 Spectre	BOMBARDIER Regional Jet CRJ-100	LEARJET Learjet 60
	BOEING 777-200LR and 777-F	MCDONNELL DOUGLAS DC-10	MCDONNELL DOUGLAS MD-81	BOMBARDIER Regional Jet CRJ-700	SAAB 340
	BOEING 787-8 Dreamliner	MCDONNELL DOUGLAS MD-11	MCDONNELL DOUGLAS MD-90	BOMBARDIER Dash 8 Q400	PIAGGIO P-180 Avanti
	ILYUSHIN Il-96	ILYUSHIN Il-76	TUPOLEV Tu-204	EMBRAER ERJ-135/145/170 Gulfstream 4	CESSNA 650/525/152 Citation 3/6/7

Table 2.3: Aircraft Separation Criteria (ICAO, 2018)

SEPERATION DISTANCE FOR ARRIVAL / DEPARTURE. TIME SEPERATION DEPARTURE							
Leader /Follower		**Super Heavy CAT-A**	**Upper Heavy CAT-B**	**Lower Heavy CAT-C**	**Upper Medium CAT-D**	**Lower Medium CAT-E**	**Light CAT-F**
Super Heavy	**CAT-A**	**3NM**	**4NM 100s**	**5NM 120s**	**5NM 140s**	**6NM 160s**	**8NM 180s**
Upper Heavy	**CAT- B**	**2.5NM**	**3NM**	**4NM**	**4NM 100s**	**5NM 120s**	**7NM 140s**
Lower Heavy	**CAT-C**	**2.5NM**	**2.5NM**	**3NM**	**3NM 80s**	**4NM 100s**	**6NM 120s**
Upper Medium	**CAT-D**	**2.5NM**	**2.5NM**	**2.5NM**	**2.5NM**	**2.5NM**	**5NM 120s**
Lower Medium	**CAT-E**	**2.5NM**	**2.5NM**	**2.5NM**	**2.5NM**	**2.5NM**	**4NM 100s**
Light	**CAT-F**	**2.5NM**	**2.5NM**	**2.5NM**	**2.5NM**	**2.5NM**	**3NM 80s**

Despite advances in aviation technology and new guidelines, there have been several accidents attributed to wake turbulence encounters over the past ten years, with a serious wake turbulence encounter as recent as this year. Table 2.4 illustrates accidents attributed to wake turbulence over the past 10 years.

Table 2.4: Wake Turbulence Attributed Accident (SKYbrary, 2018)

AIR ACCIDENTS ATTRIBUTED TO WAKE TURBULENCE						
YEAR	**AIRCRAFT MODEL**	**AIRLINE**	**COUNTRY**	**INJURIES & DAMAGE**	**OUTCOME**	**ACCIDENT REPORT CONCLUSIONS**
7-Jan-2017	Bombardier CL604	Private	Muscat	6 passengers and two crew injured. Two seriously Hull Loss	Loss of power. Emergency landing ok. Aircraft hull loss	Loss of power and loss of control caused aircraft to roll due to wake turbulence from A380 passing 1000ft above aircraft
29-Apr-2014	Embraer 170	Japan Air Lines	Tokyo, Japan	2 crew sustained injuries, one serious	Aircraft rolled to the left after encountering wake turbulence on descent	Wake turbulence encountered from proceeding Airbus A340 10NM and 2 minutes ahead on the same track.
13-Dec-2011	A32-200	Aeroflot	Frankfurt, Germany	No injuries, No Damage	Wake vortex separation minima of 7NM, 1000ft was breached. Near Miss	ICAO, Wake vortex separation minima was not met. ATC clearance error. ATC ineffective monitoring.
26-Sep-2009	Piper PA28-140	Private	Humberside, UK	Pilot seriously injured. Aircraft destroyed	On approach aircraft rolled uncontrollably to the right and struck the ground. Hull loss	On approach the aircraft encountered wake turbulence from a S76 Helicopter one mile ahead. Ineffective regulation oversight.
3-Nov-2008	Saab 340B	Regional Express AL	Sydney, Australia	1 Passenger sustained injury	On approach encountered wake turbulence, temporary loss of control.	Strong crosswind caused wake turbulence generated from A380 to drift across on adjacent runway into descending path
10-Jan-2008	Airbus A319-100	Air Canada	Toronto, Canada	11 passenger's injured, 3 seriously. Slight internal damage to aircraft	Serious of rolls and unintended descent. Dining carts struck ceiling	Unexpected encounter from wake turbulence from B747-400 11NM ahead. Pilots responded with inappropriate measures
28-May-2006	Airbus A320-200	Vueling Airlines	Barcelona, Spain	7 passengers and three crew injured. Superficial internal aircraft damage	Temporary control loss due to encounter from wake turbulence from A340-300	Encountered significant turbulence caused by wake vortices from A340 10NM ahead. Incorrect handling decisions by crew

3. Standards and Regulations for the Aviation Industry

3.1 Meteorological Standards and Regulations for Aviation

The International Civil Aviation Organization (ICAO), International Standards and Recommended Practices, Annex 3 to the Convention of Civil Aviation, Meteorological Service for International Air Navigation (ICAO, 2007) stipulates and outlines the requirements for the monitoring, recording and forecasting of aeronautical meteorological information. Part, Chapter 4 of Annex 3 provides recommendations for the Aeronautical Observation and reporting of surface wind conditions at aerodromes. This Chapter 4 of the ICAO Guide outlines how runway sensors should be automated to analyse, record and provide data to the ATC. It sets out how the mean direction and speed of surface wind should be measured as well as well as significant variations in the wind direction and speed. In ICAO Guide section 4.6.1.2, it recommends that for departing aircraft the surface wind reports should be representative of conditions along the runway and that for landing aircraft the surface wind recorded data should be representative of the touchdown zone. This requires wind sensors to be mounted on masts 10 m above the runway surface. The exact location of wind monitoring sensors along an airport runway is subject to a site survey of the location. The United States, Department of Transport, Federal Aviation Administration Order 6560.21A provides detailed recommendations for the siting of wind monitoring sensors along airport runways for the purpose of providing a Low Level Wind shear Alert System (LLWAS). Figure 3 depicts a layout recommendation for the ideal positioning of wind sensors to monitor and record wind speed and direction along an airport runway (FAA, 1989). FAA Order 6560.21A stipulates that a minimum of six recording stations be positioned along a single runway. ICAO Document 9817 AN/449 manual on Low Level Wind Shear (ICAO, 2005) recommends extending system coverage to an area of 5.5 km around critical areas

such as runway approaches and take-off corridors to provide increase detection capabilities for low level wind shear and microbursts. Increasing the perimeter area to be monitored, increases the number of sensors required to cover the increased area. Up to 35 or more sensors have been sited in airports to improve the detection of wind shear and turbulence. Chapter 7 of Annex 3, ICAO advises that guidance on the subject of low level wind shear at airports is contained in ICAO Document 9817.

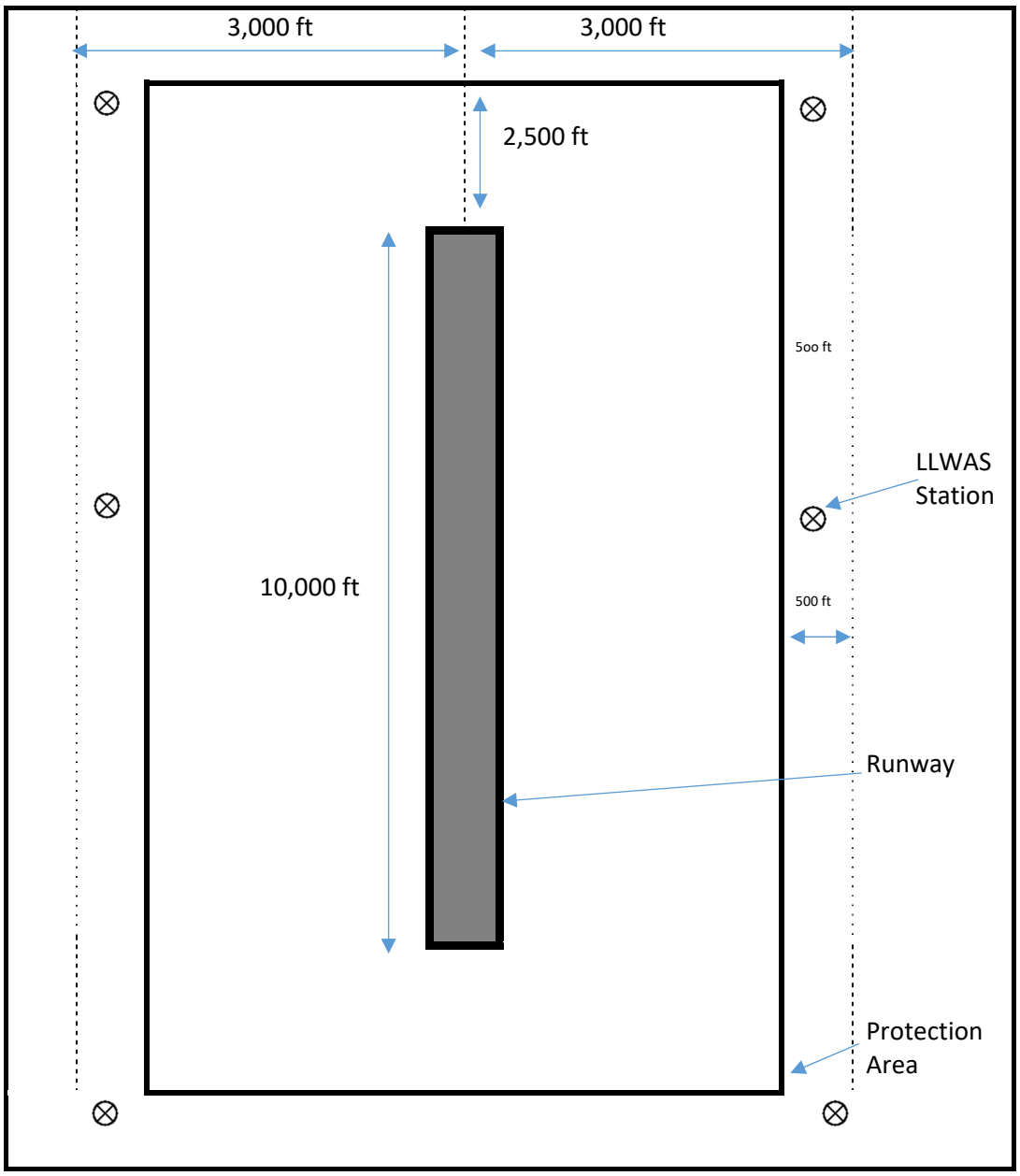

Figure 3.1: LLWS Sensor Location on Runway (FAA, 1989)

Standards and recommendations for sensors and instruments to monitor, detect and record wind speed, direction, wind gusts and fluctuations are stipulated in the World Meteorological Organisation document WMO-No-8 Guide to Instruments and Methods of Observation (WMO, 2010). Chapter 5 specifically details and specifies the criteria for the measurement of surface wind. The WMO notes that there are important differences for the measurement and reporting of wind at aerodromes for aeronautical purposes than measurements at meteorological stations. At meteorological stations wind direction should be measured namely from the azimuth setting with respect to true north and have an averaging time of 10 minutes. At aerodromes wind direction must be measured with respect to magnetic north with an averaging time of 2 minutes. The WMO states that surface wind measurement is usually measured and recorded by a wind vane and cup or propeller anemometer. Section 5.1.4 notes that cup-rotor and propeller anemometers, and direction vanes as well as cup and vane, propeller and vane, and propellers alone are common combinations for the measurement of surface wind. The WMO states in Chapter 2 that the measurement of vertical wind shear may be determined by anemometers on 10 m masts around the runway, as depicted in Fig 3.1 and recommended by the FAA. The siting recommendations for wind measuring is identical to ICAO, Annex 3, Section 4.1.1. Vertical measurements can also be recorded with the assistance of remote-sensing systems such as Doppler Radar, Lidar, Sodar and the Wind Profiler. The Lidar uses laser light, the Sodar is based on acoustic radiation, and the Wind Profiler Radar employs electromagnetic radiation at a frequency of around 50 MHz, 400 MHz or 1,000 MHz. Horizontal wind shear is recorded over the entire airport using a system of anemometers. The NCAR Phase III Algorithm (Sharman, 2013) developed in conjunction with the FAA and University Corporation for Atmospheric Research

(UCAR) enables a wind shear alert to be issued. Table 3.1 and Table 3.2 are WMO and ICAO templates used to issue a low level wind shear warning.

Table 3.1: Table A6-3 Wind shear Warning Alert (WMO, 2016)

Element	Detailed content	Template(s)	Example
Location indicator of the aerodrome (M)	Location indicator of the aerodrome	nnnn	YUCC1
Identification of the type of message (M)	Type of message and sequence number	WS WRNG [n]n	WS WRNG 1
Time of origin and validity period (M)	Day and time of issue and, where applicable, validity period in UTC	nnnnnn [VALID TL nnnnnn] or [VALID nnnnnn/nnnnnn]	211230 VALID TL 211330 221200 VALID
IF THE WIND SHEAR WARNING IS TO BE CANCELLED, SEE DETAILS AT THE END OF THE TEMPLATE			
Phenomenon (M)	Identification of the phenomenon and its location	MOD] or [SEV] WS IN APCH or [MOD] or [SEV] WS [APCH] RWYnnn or [MOD] or [SEV] WS IN CLIMB-OUT or [MOD] or [SEV] WS CLIMB-OUT RWYnnn or MBST IN APCH or MBST [APCH] RWYnnn or MBST IN CLIMB-OUT or MBST CLIMB-OUT RWYnnn	WS APCH RWY12 MOD WS RWY34 WS IN CLIMB-OUT MBST APCH RWY26 MBST IN CLIMB-OUT
Observed, reported or forecast phenomenon (M)	Identification whether the phenomenon is observed or reported and expected to continue, or forecast	REP AT nnnn nnnnnnnn or OBS [AT nnnn] or FCST	REP AT 1510 B747 OBS AT 1205 FCST
Details of the phenomenon (C)2	Description of phenomenon causing the issuance of the wind shear warning	SFC WIND: nnn/nnMPS (or nnn/nnKT) nnnM (nnnFT)-WIND: nnn/nnMPS (or nnn/nnKT) or nnKMH (or nnKT) LOSS nnKM (or nnNM) FNA RWYnn or nnKMH (or nnKT) GAIN nnKM (or nnNM) FNA RWYnn	SFC WIND: 320/5MPS 60M-WIND: 360/13MPS (SFC WIND: 320/10KT 200FT-WIND: 360/26KT) 60KMH LOSS 4KM FNA RWY13 (30KT LOSS 2NM FNA RWY13)
OR			
Cancellation of wind shear warning3	Cancellation of wind shear warning referring to its identification	CNL WS WRNG [n]n nnnnnn/nnnnnn	CNL WS WRNG 1 211230/2113303

Table 3.2: A6-4 Ranges and Resolutions for Wind Shear Warning (WMO, 2016)

Elements as Specified in Appendices 2 and		Range	Resolution
Advisory Number	for VA (index)* for TC (index)*	000 – 2000 00 - 99	1 1
Maximum Surface Wind	MPS KT	00 – 99 00 – 99	1 1
Central Pressure	hPa	850 – 1050	1
Surface Wind Speed	MPS KT	15 – 49 30 - 99	1 1
Surface Visibility	M M	0000 – 0750 0800 - 5000	50 100
Cloud Height of Base	M FT	000 – 300 000 - 1000	30 100
Cloud Height of Top	M M FT FT	000 – 2970 3000 – 20000 000 – 9900 10000 - 60000	30 300 100 1000
Latitudes	*(degrees) *(minutes)	000 – 180 00 - 60	1 1
Longitudes	*(degrees) *(minutes)	000 – 180 00 - 60	1 1
Flight Levels		000 – 650	10
Movement	KMH KT	0 -300 0 -150	10 5

The guide is also as stated by Annex 3, ICAO. Annex 3 of the ICAO and WMO-No-8 are identical in their recommendations and guides for Aeronautical instruments and forecasting in respect to the recording of wind data. Table 3.3 illustrates the recommendations for the operational measurement and instrument performance as set out by WMO, Chapter 1, Annex 1.D.

Table 3.3: Measurement and Instrument Performance (WMO, 2010)

Variable	Range	Reported Resolution	Mode of Measurement Observation	Required Measurement Uncertainty	Sensor Time Constant	Output Averaging Time	Achievable Measurement Uncertainty	Remarks
Wind Speed	– 75 m s–1	0.5 m s–1	A	0.5 m s–1 or ≤ 5 m s–1 10% for > 5 m s–1	Distance Constant 2-5 m	2 and/or 10 min	0.5 m s–1 for ≤ 5 m s–1 10% for > 5 m s–1	Average over 2 and/or 10 min Non-linear devices. Care needed in design of averaging process Distance constant is usually expressed as response length Averages computed over Cartesian components (see Part III, Chapter 3, section 3.6 of this Guide) When using ultrasonic anemometers, no distance constant or time constant is needed. For moving mobile stations, the movement of the station needs to be taken into account, inclusive of its uncertainty.
Wind Direction	0 – 360°	1°	A	5°	Damping Ratio > 0.3	2 and/or 10 min	5°	
Wind Gusts	0.1 – 150 m s–1	0.1 m s–1	A	10%		3 s	0.5 m s–1 for ≤ 5 m s–1 10% for >5 m s–1	
					Remarks			
					Highest 3 s average should be recorded			

The WMO recommends that in aerodromes with high levels of traffic that an integrated automatic systems for acquisition, processing and dissemination/display in real time of the meteorological parameters affecting landing and take-off operations should be in operation. These automatic systems should be capable of accepting the manual insertion of meteorological data that cannot be measured by automatic means. This is to enable data and warnings regarding turbulence and wind shear from approaching and departing aircraft observations to be entered into the system. The ICAO, Section 5.6 states " Note.— Icing, turbulence and, to a large extent, wind shear are elements which, for the time being, cannot be satisfactorily observed from the

ground and for which in most cases aircraft observations represent the only available evidence."

ICAO, Annex 3,7.4.3 recommends that Wind shear alerts shall give concise, up-to-date information related to the observed existence of wind shear involving a headwind/tailwind change of 30 km/h (15 kt) or more which could adversely affect aircraft on the final approach path or initial take-off path and aircraft on the runway during the landing roll or take-off run. The wind shear alerts should be updated at least every minute.

3.2 Conclusion on Aviation Standards

The WMO guides to Meteorological Instruments and Methods of Observation together with ICAO, Annex 3 and FAA order documents provide an authoritative set of recommendations, standards and guides for measuring and recording of surface wind and wind shear at aerodromes globally. These bodies stipulate the instruments approved for wind measurement and the criteria to which they must comply for the measurement of aeronautical meteorological data. It be must however noted that despite the recent advances in wind measuring techniques using Lidar, Sodar, Doppler and LLWS systems there is no satisfactory way of measuring turbulence or wind shear to date from the ground as noted in ICAO, Annex 3.5.6. Based on the foregoing and the evidence presented in Table 2.1 of continuing aircraft accidents to date, there is a requirement for a new instrument, capable of recording high-frequency variations in wind speed, direction, and turbulence. This thesis will argue that a solution to the problem of forecasting low level wind shear and turbulence for the approach, landing and take-off of aircraft can be addressed by incorporating the wind Urchin as part of the Low Level Wind Shear Alerting System (LLWAS) in all airports.

4. Measurement of Wind Shear and Turbulence at Airports

The aim of Chapter 4 is to present an overview of the complexity of wind shear and turbulence as an unpredictable force and how such an entity is measured and recorded at airports and ground monitoring stations.

4.1 The Complex Nature of Turbulence and Wind Shear

Wind blows freely as a three-dimensional entity in space. It can be defined simply as air motion relative to the earth's surface. This means that relative to the surface of the earth, it has components in the north/south, east/west and the up/down directions. In the case of wind with respect to aircraft, this means that the headwind/tailwind constitutes the longitudinal components of the wind, the left/right crosswind constitutes the lateral component and the updraft/downdraft makes up the vertical component of the wind. At ground level or runway level the vertical component of the wind is usually small when compared to the horizontal components. Because at ground level the horizontal components predominate, it is assumed that the wind blows parallel to the earth's surface neglecting the vertical component. In certain circumstances where phenomena such as thunderstorms, microbursts, frontal surfaces or convective clouds and thermals occur the vertical component of the wind predominates resulting in low level turbulence and wind shear.

Low level turbulence and wind shear is defined by the WMO as layers or columns of air, flowing with different velocities (speed and/or direction) to adjacent layers or columns (WMO, 2007). Despite all the advances in new technology, wind shear is still a serious concern and hazard to aviation. Wind shear can occur in the horizontal or vertical direction or could be a combination of both. The ICAO defines horizontal wind shear as a change in horizontal wind direction and/or speed with horizontal distance as would be determined by two or more anemometers mounted at the same

height along a runway. The mounting height as previously stated is 10 m. Vertical wind shear is defined by the ICAO as a change in horizontal wind direction and/or speed with height, as would be determined by two or more anemometers mounted at different heights on a single mast (ICAO, 2005). The main effects of wind shear on an aircraft can be turbulence, resulting in the shaking of the aircraft. Wind shear can cause violent up- or down-draughts resulting in a sudden drop in aircraft height. An aircraft on a seeming less smooth flight can cross between laminar streams resulting in turbulent effects on the aircraft. As the aircraft is on approach to land or after take-off, wind shear can cause a sudden increase or decrease in airspeed causing the pilot to lose control. The tail or head wind will be determined by the flight direction on the runway relative to velocity changes. While the aircraft has touched down or is accelerating for take-off, a sudden occurrence of wind shear will cause an increase or decrease in ground speed which could cause the aircraft to lose control and crash. The effect or damage to an aircraft will depend on the type, size and weight of the aircraft. Smaller aircraft being much more susceptible to the effects of wind shear and turbulence and as the intensity of the turbulences increases the effects on the aircraft will increase as shown in Table 4.1

Table 4.1: Turbulence Intensity Category (WMO, 2007)

CLASSIFICATION	DESCRIPTION	EFFECT
Light	Slight changes in altitude (pitch, roll, yaw) Occupants may feel an Altitude and/or attitude (pitch, roll, or yaw).	Passengers may feel a slight strain on seat belts. Unsecured object may move
Moderate	Moderate changes in aircraft altitude and/or height. Aircraft in positive control at all times. Airspeed variations small. Changes in accelerometer readings 0.5-1.0g at aircrafts centre of gravity.	Passengers feel the strain of seat belts. Difficulty in walking. Loose objects move about.
Severe	Abrupt changes in aircraft altitude and/or height. Aircraft may experience loss of control for short periods. Air speed variations can be large. Changes in accelerometer readings greater than 1.0g at aircrafts centre of gravity.	Passengers are shaken and pressed hard against seat belts. Loose objects are tossed about.
Extreme	Effects are more pronounced than severe. Causes the aircraft to be violently tossed about. Aircraft may be totally out of control	Passengers are violently shaken and injuries can occur.

The types of turbulence encountered by aircraft has been categorised by the ICAO for aviation purposes. It must be noted that as the intensity of the turbulence increases, the effect of each type of turbulence on aircraft will vary in accordance with the ICAO turbulence category as illustrated in table 4.1

4.2 Low Level Turbulence Types as Defined by ICAO

There are five main types of Low level turbulence that are of concern to aircraft during approach to landing or during the take-off phase of the flight.

4.2.1 Convective Turbulence

Convective turbulence also known as thermals is caused by vertical currents of air rising from differential surface heating producing updrafts and downdrafts. These localized currents of ascending and descending vertical air movements tend to be most active during warm summer afternoons when winds are light. The strength of the currents will vary over short distances due to uneven heating of the surface. The heated air creates an unstable layer as the warm air is forced upwards. Cold air comes into

contact with the warmer ground surface causing the air currents to rise up to several hundred metres which will cause turbulence to aircraft. Low level turbulence can cause abrupt changes in aircraft airspeed which is potentially hazardous to aircraft on approach to land. Fig 4.1 illustrates the effect that convective air currents can have on the intended flight path of an aircraft.

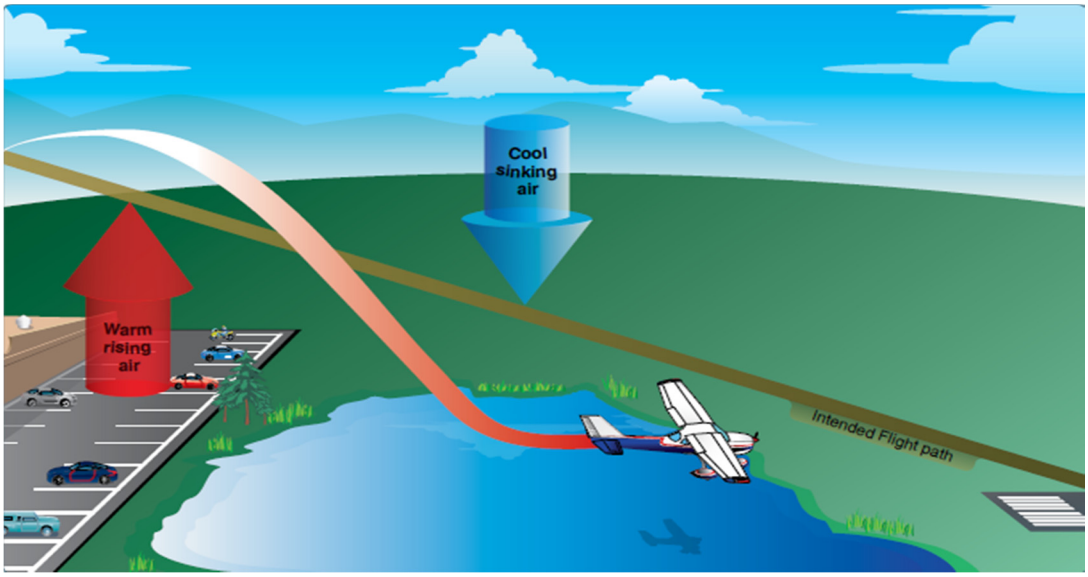

Figure 4.1: Effect of Convective Currents on Flight Path (FAA, 2016)

The effect of convective turbulence on an aircraft will be dependent on the severity of the turbulence as stated in Table 4.1. At its simplest it will cause bumpiness in flight. The convective air currents will produce varying vertical wind speeds where sudden headwind will lift the aircraft followed by sudden downdraught and tailwind causing substantial loss in height which could result in a fatal accident.

Fig 4.2 illustrates the effect of a convective currents on the flight path of an aircraft if the pilot failed to take corrective action to correct for the gain or loss of lift. Here there is wind shear between ascending and descending columns of air and across the boundary.

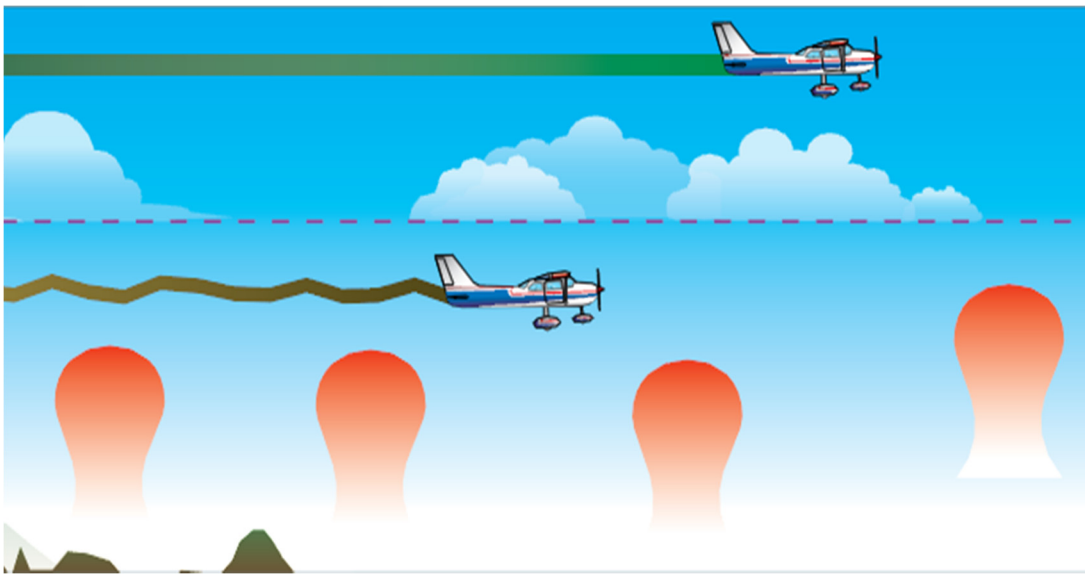

Figure 4.2: Aircraft is subject to bumpiness from Convective Currents below Clouds (FAA, 2016)

4.2.2 Mechanical Low Level Turbulence

Mechanical turbulence occurs close to the ground and is also referred to as low level turbulence. It occurs solely from shear where surface friction is the main cause of vanishing wind at the surface. The intensity of the turbulence depends on the wind strength, terrain roughness and atmospheric stability near the surface. Mechanical turbulence will form where surface winds exceed 20 knots on uneven terrain. Where the air is being heated from the surface and rising, the vertical motion causes eddies to grow in the unstable air causing extensive choppiness. Where surface wind speed exceed 20 knots, the airport terminal buildings, hangers and outbuildings can contribute to strong eddies which can fluctuate erratically with sudden increases in speed that can be carried downwind for several kms. These eddies can cause severe turbulence lasting several minutes. Fig 4.3 illustrates how buildings and terrain contribute to produce low level mechanical turbulence.

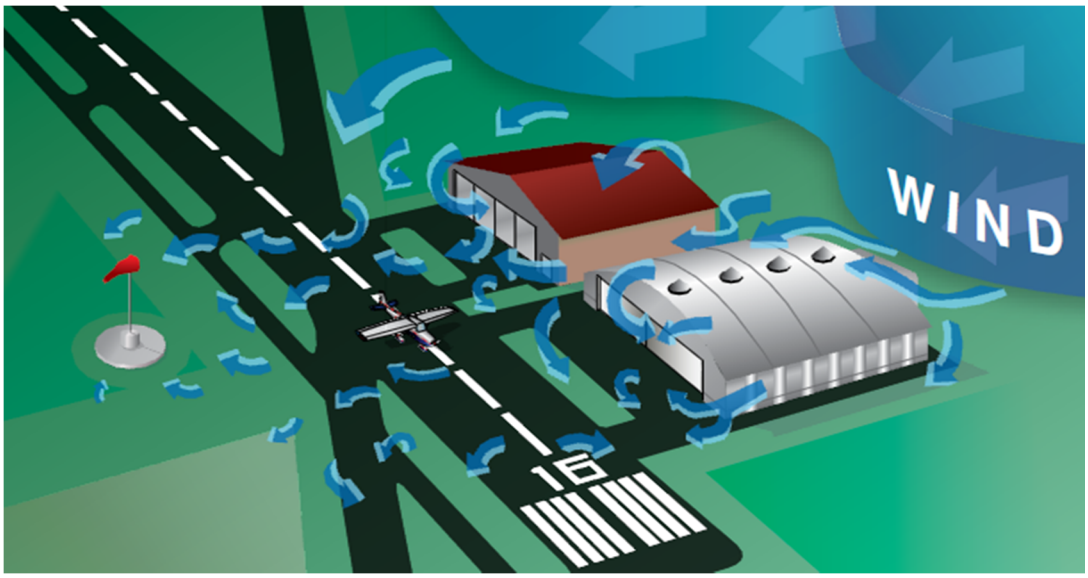

Figure 4.3: Mechanical Turbulence (FAA, 2016)

Light to moderate mechanical turbulence will cause bumpiness in flight. For any given intensity of turbulence, the faster the aircraft flies, the more it will be accelerated. When the aircraft is closer to the ground, there is less time to react. Severe mechanical turbulence may cause structural damage to the hull.

An estimation for the likely intensity mechanical turbulence possible for different wind speeds and terrain types can be seen in table 4.2 below as set out by the WMO.

Table 4.2: Guide to intensity of Turbulence for Wind Speeds and Terrain (WMO, 2007)

Surface Wind (Kt)	Sea	Flat Terrain	Hilly Terrain
15 to 35	Light to moderate	Moderate	Severe
Over 35	Moderate to Severe	Severe	Extreme

The WMO states that where a gale force surface wind warning is in operation that the default for low level mechanical turbulence warning should be severe.

Fig 4.4 illustrates the effect on an aircraft from head and tail winds as a result of mechanical turbulence.

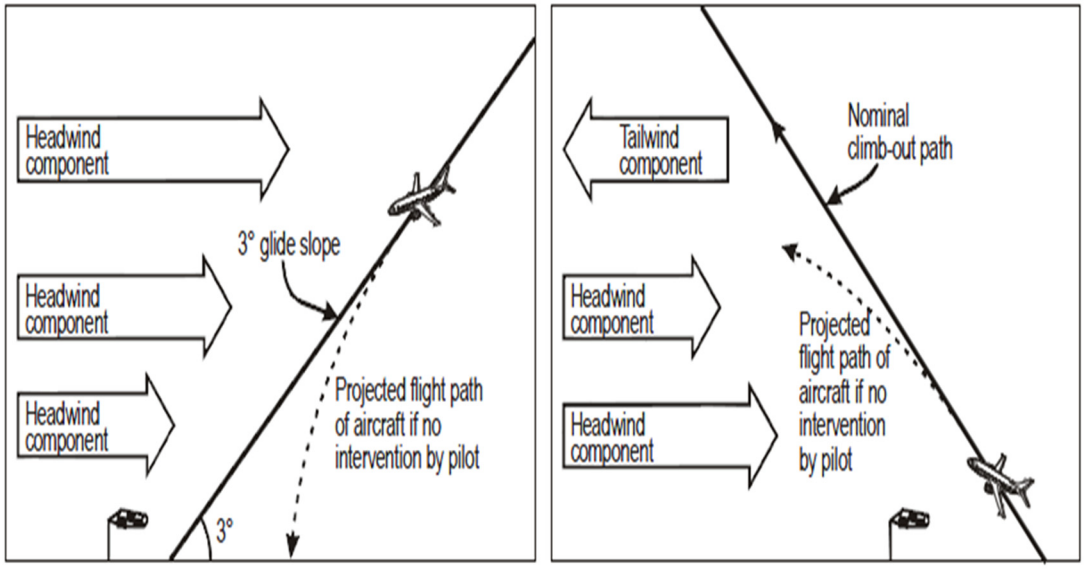

Figure 4.4: Effect of Head/Tail Mechanical shear on Aircraft (WMO 2007)

4.2.3 Orographic Induced Turbulence

This occurs where surface wind encounters cities, forests, hills and mountains. While the air flows smoothly up the windward side of the mountain, the upward currents provide lift to an aircraft helping fly over the mountains. As the air flows down the leeward side of mountains, the air follows the contours of the terrain which also produces mechanical turbulence causing the aircraft to be pushed towards the side of the mountain. The severity of the turbulence is again dependent on the strength of the wind. Large displacements of air from its original level generates gravity waves also known as mountain waves. These wave motions may persist for hundreds of miles downstream. Airflows can be funnelled along valleys which can cause severe turbulence close to ridges. Pilots must be aware not to be caught out by a calm scenario. It is recommended by the FAA that pilots unfamiliar with a mountainous area be accompanied by a mountain qualified flight pilot as mountain waves can break suddenly causing severe turbulence. The WMO state that the indication for the presence or occurrence of mountain turbulence would be strong winds exceeding 20

to 25 knots at the top of the boundary layer just below a sharp inversion. A wind blowing within 30 degrees of normal to the ridge axis. A low level neutral layer capped by a marked inversion of 1.5 to 2 times the height of the hills.

Turbulent rotors are usually associated with high amplitude lee waves or mountain waves and are classified as trapped or untrapped. Two types of rotors have been observed. The first type appears as harmless looking cumulus paralleling the mountain range. This type of rotor appears near mountain top inversion and contains moderate to severe turbulence. The second less common rotor contains severe to extreme turbulence and extends much higher than the upstream inversion. These rotors can cause severe to extreme turbulence presenting a hazard to aviation. Fig 4.5 illustrates orographic turbulence in a mountainous area.

Figure 4.5: Mountain Wave Turbulence (FAA, 2016)

Wind Rotor streaming from mountain waves can cause an unstable approach of aircraft. Wind direction can change abruptly affecting aircraft lift and drift. Strong updraughts and downdraughts can occur. Turbulent flow can quickly be replaced by strong air on the leeside often well outside the cross wind limits of the aircraft. It is possible for windsocks at different locations in an airport to indicate different wind

directions and strengths. Fig 4.5 illustrates orographic induced turbulence for an approaching aircraft. Mountain turbulence can be extremely hazardous if a pilot is caught unaware with the rapid change in height. If an aircraft is caught in a sudden downdraught, this could eliminate any terrain clearance margins and cause the aircraft to crash into the ground.

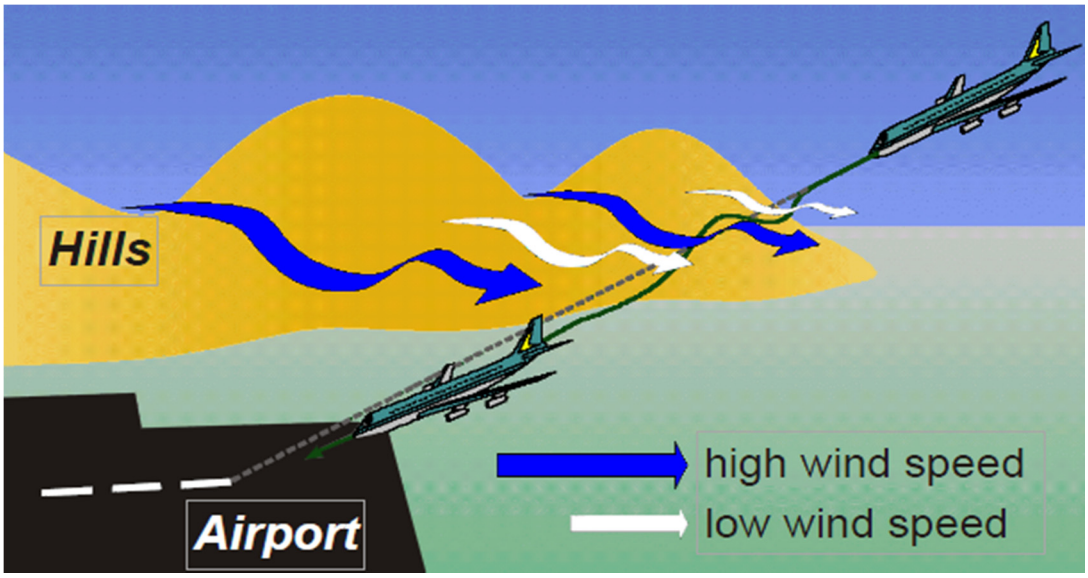

Figure 4.6 Mountain Terrain Induced Airflow Pattern (ICAO, 2005)

Fig 4.6 illustrates a mountain terrain induced airflow occurrence with low speed airspeed downwind of the peaks and high speed airstreams downwind of the peaks.

4.2.4 Low Level Jets

There are several types of low level jets. One form of low level jet has been described as a tube of enhanced low level wind flow along and ahead of a cold front and will move with the front. Another form of low level jet is known as sting jet which can form around low centres during explosive cyclogenesis. These jets like low level winds are regions of enhanced airflow, caused by descending air accelerating as it is cooled. These jets frequently occur over the Northern central plains of Europe, the

Great Plains of North America and over the lower plains of Australia. Under certain circumstances the airstream is deflected across these plains where the wind speed maximum is concentrated into a narrow band resembling a jet-stream. The wind speeds can exceed 120 km/h or 60 kt and are commonly referred to as low-level jet streams. Low-level jets are normally found below 500 m but can rise steadily to 1000 m after its formation. The formation of the jet streams occur after sunset and reaches a maximum around sunrise. Fig 4.7 shows the concept of a low-level jet formation forward of a surface cold front.

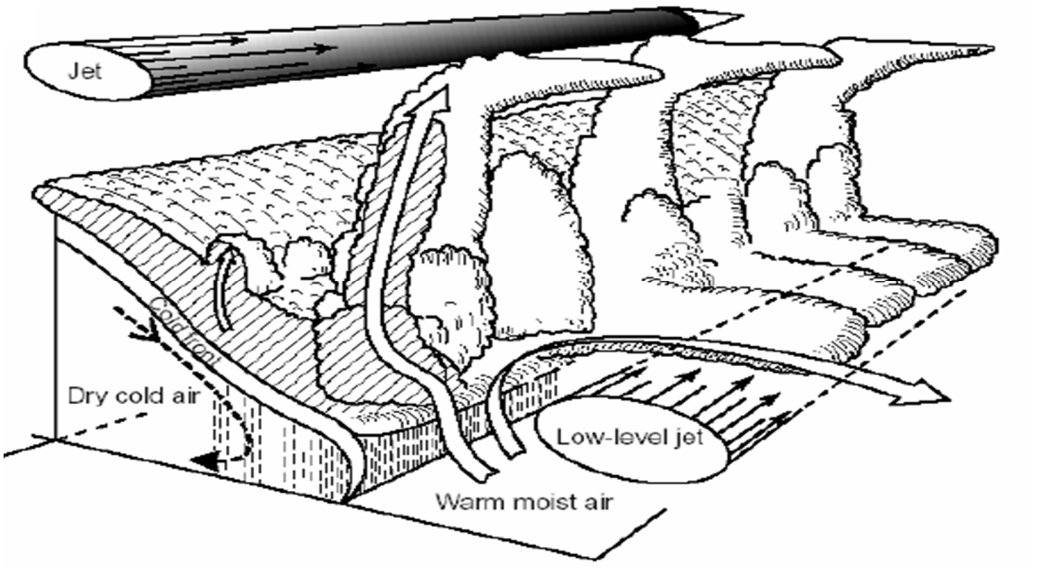

Figure 4.7: Low-level jet forward of a Cold Front (WMO, 2007)

The turbulence effects of the low-level jets can be sudden and unexpected for an aircraft. Wind shear will prevail across all the boundaries of the jet which may require corrective action by the pilot. Terrain clearance may become a problem to the aircraft because of the jets close proximity to the surface and could cause difficulties to the aircraft during the approach and landing phases. Changes in airflow across the wings while the aircraft is crossing a boundary may adversely affect lift during both landing

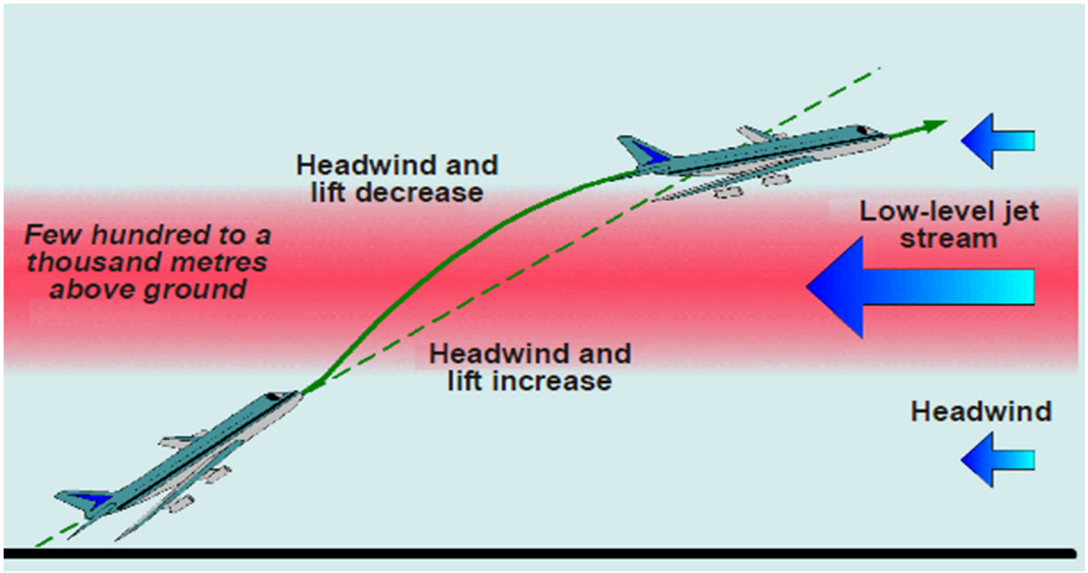

Figure 4.8: Wind shear effect on an Aircraft brought by Low-level Jet Stream (ICAO, 2005)

and take-off phases. The effect of the wind shear will depend on the width of the frontal surface. Fig 4.8 illustrates the effect of wind shear brought by a low-level jet stream on an aircraft. Vertical wind shear occurs at and behind the cold front with the maximum wind shear rises above the airport from ground level following the passage of the front.

4.2.5 Clear Air Turbulence

Clear Air Turbulence (CAT) is defined as the severe movement of air in regions where no clouds are present. It is a term to describe moderate to severe high-level turbulence in areas of marked wind shear (Skybary, 2017). It usually occurs in the high troposphere at the higher altitudes of around 7,000 to 12,000 metres and can be difficult to detect. At this altitude CAT is most frequently encountered in the region of jet streams. CAT occurs more often over land than sea and 60% of reports of CAT are near jet streams. The severity of CAT may be forecast if the vertical and horizontal wind shear values are known. Table 4.2 shows the estimated severity of CAT as stated by WMO-Aviation Hazards, Table 2.

Table 4.3: Guide relating CAT to Horizontal and Vertical Wind Shear (WMO, 2007)

	Moderate	Severe
Horizontal Wind Shear	20 kt per Degree of Latitude	30 kt per Degree of Latitude
Vertical Wind Shear	6 kt per 1000 ft	9 kt per 1000 ft

The degree of turbulence is categorised by ICAO and illustrated in Table 4.1 When encountered it will shake the aircraft making it uncomfortable for passengers, causing injuries to unrestrained passengers or from falling objects.

4.2.6 Wake Turbulence

Wake Turbulence is generated behind an aircraft as it passes through the air. It is often referred to as Wake Vortex Turbulence as it is principally caused by wing tip vortices. The wing tip vortices form two counter rotating cylindrical vortex funnels trailing behind the aircraft wing tips. Fig 4.9 depicts the wake vortices trailing behind the aircraft.

Figure 4.9: Wake Vortex Turbulence from Aircraft Wings (IATA, 2015)

It is generated when the aircraft leaves the ground and will continue while the aircraft is airborne until the aircraft touches down. They are not meteorological in origin and

are a function of the weight, size and aerodynamic properties of the aircraft. Wake turbulence occurring at a low level where two aircraft are taking off could create the conditions for a potential hazard. If the first aircraft was full, it would generate a more intense wake turbulence because of its weight. The following aircraft would be subject to wake turbulence which could affect its responsiveness to rudder control, depending on prevailing wind conditions. Wake turbulence is a mechanically generated wind shear and does not fall into the same category as the previous turbulences described because their effect on aircraft landing and taking off can be avoided by the ATC enforcement of the separation minima guidelines. Aircraft must adhere to separation distances recommended by the ICAO and as illustrated in Table 2.3 not only from instructions from the ATC but also in flight to avoid mid-air wake turbulence from the preceding aircraft in front or above the following aircraft. Due to increasing air passenger numbers and more airport congestion, calls have been made to reduce the minimum separation distances for aircraft taking off. However, it must be noted that only as recently as January 2017, a serious incident occurred in flight where a lighter aircraft 1000 ft. below an Airbus A380 was violently shaken and rolled out of control before making an emergency landing. The incident resulted in 6 passengers and two crew being seriously injured and with the aircraft hull being damaged beyond repair (Aviation Week, 2017).

4.2.7 Low Level Wind Shear

Wind shear is the sudden change in velocity and/or direction of wind speed over a small area, where layers or colums of air with different velocities flow to adject layers or coloums. Wind shear of itself is not categorised as turbulence but when it occurs the turbulence categories described above may become applicable. Low level wind shear is associated with thunderstorms, frontal systems, temperature inversions and

strong upper level winds exceeding 25 knots. Wind shear can occur at any level but it is the occurance of low level wind shear below 500 m that is especially hazardous to aircraft during landing and take-off phases. During the take-off and approach phases of the flight the aircrafts speed and height are near critical values and because of the aircrafts close proximity to the ground the pilot has to react immediately to initiate counter measures to maintain control of the aircraft.

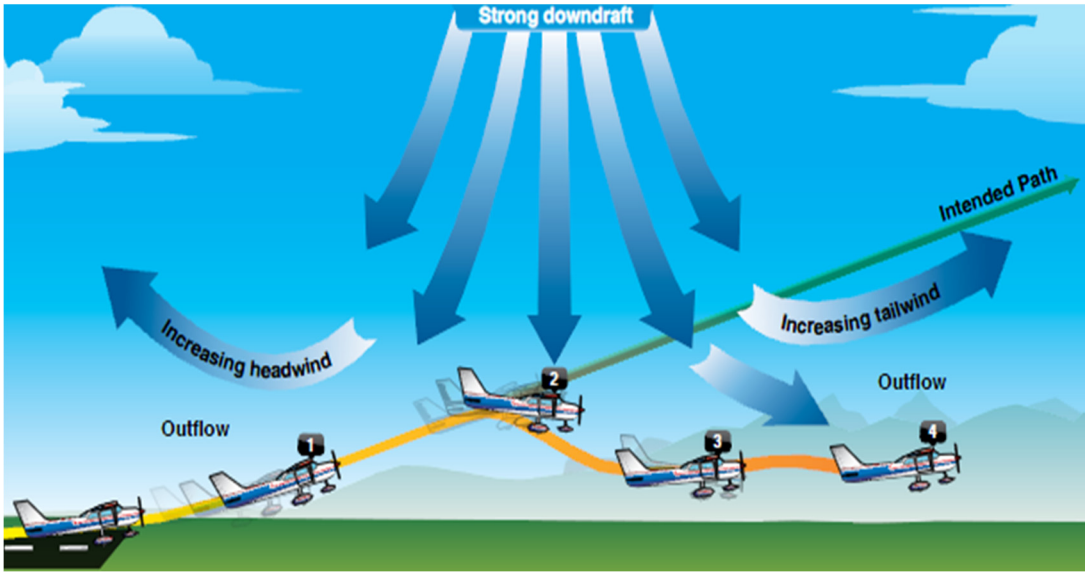

Figure 4.10: Wind Shear Microburst Effects on Aircraft Taking Off (FAA, 2016)

An aircraft taking off could experience a headwind producing lift for the aircraft then this can suddenly change to a downdraught followed by a tailwind which could lead to a loss of height if not countered causing the aircraft to crash into the ground. Fig 4.10 illustrates the effect of a microburst on an aircraft taking off.

In the FAA Pilots handbook, it states that wind only affects ground speed and drift. However in the case of wind shear where there is sudden changes in velocity and direction. It can be stated that wind has a transient effect on airspeed in which the aircraft will seek to restore its original trimmed airspeed. The most severe type of wind shear is a microburst. A microburst is defined as a downdraught that induces a sudden

outflow of damaging horizontal winds at the surface which can extend between 0.4 and 4 km in distance and has a nominal depth of 300 m (1000 ft).

The lifespan of a microburst is around 5-15 minutes and can produce downdraughts of 2000 m (6000 ft) per minute with headwind losses of between 30-90 kt. Microburst are associated with rain, convective cloud and thunderstorms. The small scale of the microburst in both space and time makes it extremely difficult to predict. Fig 4.11 illustrates the effect of a microburst on approaching aircraft. In this scenairo the aircraft may first encounter headwinds which produce additional lift to the aircraft, followed by downdraughts which could cause the aircraft to land short of the runway.

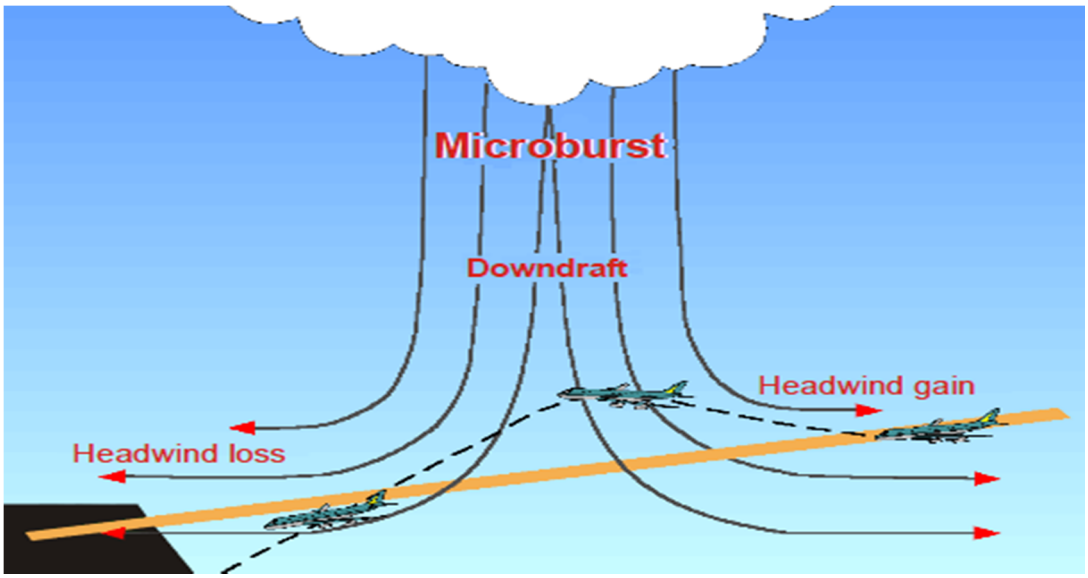

Figure 4.11: Wind Shear Effect on Landing Aircraft from a Microburst ((FAA, 2016)

The FAA, ICAO and other aviation bodies have invested signifigant resoursces into microburst detection systems. The main systems currently installed at all major airports in the US are the Low Level Wind Shear Alert System(LLWAS), Terminal Dopler Weather Radar (TDWR), ASR-9,Weather System Processor (WSP) and Light Detection and Ranging (LIDAR). These detection systems will be discussed in more detail in the following chapters. Since 1943, there have been over 1500 fatalities attributed to wind shear (Aviation Safety Network, 2018). There has been a marked

reduction in the number of aviation accidents attributed to wind shear over the past decade as a result of the measures and resouces invested in wind shear detection systems and also better pilot training in the area of identifying and countering wind shear occurances. However only as recent as 2016, a modern Boeing 737 aircraft crashed with the loss of all souls on board after encountering wind shear while attempting to land in Russia (Interstate Aviation Committee of Russia, 2016). Wind shear and low level turbulence will always be a serious hazard for aviation and a potential killer, and there must be continued vigilance, continued research and improvements in new systems to detect these occurances providing real time information to pilots. Continued pilot training on wind shear counter measures and go-around procedures should involve ongoing and refresher courses for all pilots.

4.2.7.1 Conditions that Cause Low Level Wind Shear

Outside of the meteorological phenomena which cause wind shear, it must be noted that wind shear is always present in the atmosphere and under normal circumstances does not present a difficulty to a pilot or adversely affect an aircraft. It is particularly noticeable below 600 m where the air closest to the surface of the earth changes in speed and direction, with height due to frictional drag. This layer is generally referred to as the “friction layer" and can be divided in two further sublayers. The lower layer is referred to as the “surface boundary layer” which extends up to 100 m from the earth’s surface. In this layer air motion is predominantly affected by friction with the earth’s surface. This layer is the lowest layer of the atmosphere, where wind direction is approximately constant with height and wind speed increases with height. To derive a mathematical relationship between wind speed and height under all possible stability conditions presents difficulties. However a more straightforward relationship can be

derived for a special condition of neutral stability (i.e. neither stable nor unstable). Assuming that the atmosphere in the surface boundary layer is neutrally stable, the theoretical variation of wind speed with height is given by Eq 4.1

Eq: 4.1 $$u = \frac{u*}{k} |n \frac{z}{z_\circ}$$

This equation is known as the “logarithmic wind law” or the “Prandtl equation” and it is from this equation that the logarithmic speed profile is derived (ICAO, 2005). This fits the observer wind speed profile in the surface boundary layer for neutral stability. Where the surface boundary layer is unstable, the shear in wind speed and height will be less than that calculated by the equation. Where the surface boundary layer conditions are stable, the shear in the wind will be greater than that calculated by the equation. The logarithmic wind law provides the wind shear model for use in flight simulators to train pilots. In the logarithmic profile the wind shear is strongest below 30 m and decreases with height.

The layer above the surface boundary layer is referred to as the “Ekman layer". This extends from a height of 100 m to 600 m. Friction is still a factor in this layer but decreases with increasing height as the horizontal pressure gradient and Coriolis forces become dominant as the wind speed increases with height, due to the decrease in friction with the earth’s surface. The wind direction does not remain constant with height as in the surface boundary layer but veers back with height. Fig 4.13 illustrates wind profiles from the atmospheric boundary layer effects.

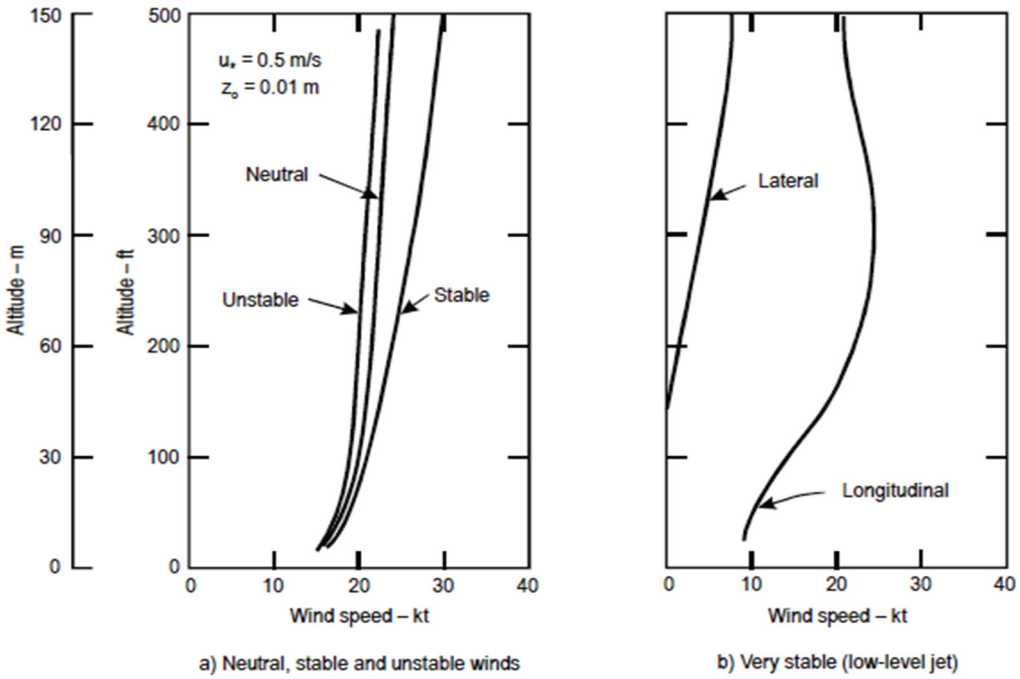

Figure 4.13: Wind Profiles from Atmospheric Boundary Layer Effects (Ellis, 1978)

The mathematical theory to explain these effects was first developed by Vagn Walfrid Ekman a Swedish Oceanographer while on an expedition to the North Pole. While observing icebergs, he noticed that they did not drift in the direction of the prevailing wind but at an angle of 20° to 40° to the right. The equation that Ekman derived was applied to the atmosphere and is applicable between 100 m and 600 m in a layer which is now known as Ekman's layer. The Ekman equation is written as shown in Eq:4.2 and Eq:4.3

Eq: 4.2
$$u = Vg - Vg\sqrt{2\sin a\, e^{-BZ}\, \cos\, (B2 + \frac{\pi}{4} - a)}$$

And

Eq: 4.3
$$v = Vg\sqrt{2\sin a\, e^{-BZ}\, \sin\, (B2 + \frac{\pi}{4} - a)}$$

Through-out the Ekman layer the horizontal pressure gradient and Coriolis forces are balanced with the friction forces. At the bottom of the layer a balanced flow is

achieved by the wind blowing across the isobars towards lower pressure. The level at which the wind blows along the isobars is referred to as the geostrophic wind level. At this level the winds computed using Ekman's theory are very close to geostrophic winds. However in practice the winds in Ekman layer increase speed with height while the wind blows at an angle across the isobars where the angle decreases with height and the wind veers back with height. A combination of the logarithmic and Ekman wind profiles provides an accurate representation of the normal wind shear from the surface of the earth up to 600 m. This has facilitated the research and development of improving algorithms for the detection of LLWS (ICAO, 2005).

Other wind profile models have been derived for atmospheric conditions where conditions are not stable. The "power law" being the most known links wind speeds at two levels of the atmosphere through a stability parameter as shown in Eq: 4.4.

Eq: 4.4 $$U = U1\,[\frac{z}{z1}]^{\gamma}$$

The power law is generally used under adiabatic conditions with strong wind speeds for the layer from 10 m to 200 m (Warit Werapuna, 2017).

4.3 Current Procedures and Methods for Recording Low Level Wind Shear

4.3.1 A Brief History of How LLWS Systems Came About

Between 1964 and 1983 there were over 28 commercial aviation accidents where the cause of the accidents were attributed to Low Level Wind Shear. The accidents claimed the lives of over 500 people and left hundreds with serious injuries. The crash of Eastern Airlines Flight 66, a Boeing 727 aircraft at JFK Airport, New York on 24 June 1975 (Flight Safety Foundation, 1975) with the loss of 113 souls and then just

six week later a Boeing 727 crashed at Denver International Airport shocked the public and aviation industry. The cause of both accidents were attributed to the aircraft losing control after encountering Wind Shear caused by a Microburst. The crash at New York occurred while the aircraft was on approach to land while the accident at Denver occurred during take-off, when the aircraft was 100 ft. off the ground. Both of these accidents occurring within weeks of each other was a major catalyst in accelerating research into observation, reporting and forecasting of Wind Shear. The in-depth reports on both of these crashes left no doubt that the cause was Wind Shear. The ICAO stated at that time that Wind Shear was one of the major problems facing the aviation industry (ICAO, 1987).The ICAO, a Low-Level Wind Shear and Turbulence Group (WISTSG) was formed. They issued guidance on the observation and reporting of Wind Shear and turbulence in 1979 (ICAO, 2005). Following further research Amendment 64 to Annex 3 - Meteorological Service for International Air Navigation was developed to include provisions for the monitoring and recording of Low Level Wind Shear. Following the crash at New York and Denver a Joint Airport Weather Studies (JAWS) project was formed at Denver, Colorado. The research from this project considerably increased our knowledge about the observation, monitoring and detection of Wind Shear and Turbulence and in particular Wind Shear associated with Microbursts. Over the past 20 years, advances in technology have significantly reduced the number of air accidents as a result of Wind Shear. Advances have been made in both ground based and airborne based wind Shear detection systems. However, despite the advanced systems installed presently at airports, there are still accidents as a result of Low Level Wind Shear and it must be noted that it will always be a serious hazard and potential killer to the aviation industry. Continued vigilance,

more research into better Wind Shear detection systems and continued pilot training must be ongoing into the future.

4.3.2 Systems and Methods to Record Low Level Wind Shear at Airports

Wind Shear detection systems have now become a common feature in most international and big commercial airports around the globe. There are many components that are integrated to provide forecasting and warnings for the hazards of Low Level wind Shear and Microbursts. The systems to be installed are tailored to give the best protection and warnings for that particular airport based on its location to the sea, its proximity to mountains, its proximity to ground clutter such as high rise buildings or forests, its altitude and the environmental susceptibility to thunderstorms and other weather events. A detailed site survey must be carried out by specialist engineers to determine the best and most cost effective system for a particular airport for its given position and environment. The site survey must be carried out in accordance with FAA order 6560.21-A. (Allweatherinc, 2018)

4.3.2.1 Low Level Wind Shear Alert System

One of the main way to measure LLWS around the airport runway is to install a series of wind sensors either side of the runway path and extended boundary to around 3 nm from the ends of the runway. This system is known as a Low Level Wind Shear Alert System (LLWAS). A typical LLWAS system uses a network of anemometers mounted on masts which are strategically located around the airfield with one centre field sensor that are connected to a digital processor with visual and audible warnings indicators. An airport may have from 6 to 32 sensors depending on the environmental conditions present and requirements. There are currently three LLWAS system fielded, LLWAS–Network Expansion, NE, (FA10387), LLWAS-2 (FA-10239 and

FA-10240) and the LLWAS-Relocation/Sustainment, RS, (14100). (FAA, 2001) The LLWAS-NE^{++} has superseded the LLWAS-NE and is the current system which allows for up to 32 remote sensing station. The remote sensing stations comprise of anemometers mounted on poles at a height of between 10 – 15 m which are connected to a master station which is interfaced to the Airports Weather Observation System (AWOS) (Gill Instruments, 2018). Here the data from the remote stations is processed using wind shear, microburst and gust algorithms to provide the ATC with wind speed, wind direction and type and severity of wind occurrences as they relate to specific areas along the runway. The wind data from the remote stations is processed every 10 seconds to measure any wind differences between stations along the runway. The system works by calculating headwind difference between adjacent anemometers or divergence/convergence within areas bounded by the anemometers. The system then calculates loss or gains in wind speed and generates Wind Shear or Microburst warnings based on the data recorded. The system will also identify the location along the runway or airfield where the event is forecast.

The Linear Averaged wind measurements shall be calculated using a predefined parameter number of 1 second independent wind sensor samples. Calculation of these measurements SHALL be based on equation, Eq: 4.5.

Eq: 4.5 $$X = (1/n)*\sum x_i$$

for all i from 1 to n

These linear measurements are used as inputs into the Gust Algorithm. They are also used for the threshold wind and Centre field wind calculations. This method assume a very short (less than one second) time constant for the wind sensor and electronics to acquire and digitize the wind sensor signals. The LLWAS system utilises the FAA

certified phase 3 algorithm which provides a probability of microburst detection of greater than 90% with a false alarm rate of less than 10%. (Allweatherinc, 2018). In an ICAO Wind Shear workshop report for the Centre for Australian Weather and Climate Research, the LLWAS system prediction of detection (POD) was stated to be 95% to 97% for microburst events within the network (CAWCR, 2010).

Current data and warnings are displayed for approach controllers in the Terminal Radar Approach Control Facility (TRACON) and for ground controllers in the Air Traffic Control Tower (ATCT) (UCAR, 2012). Fig 4.13 illustrates an example of a LLWAS.

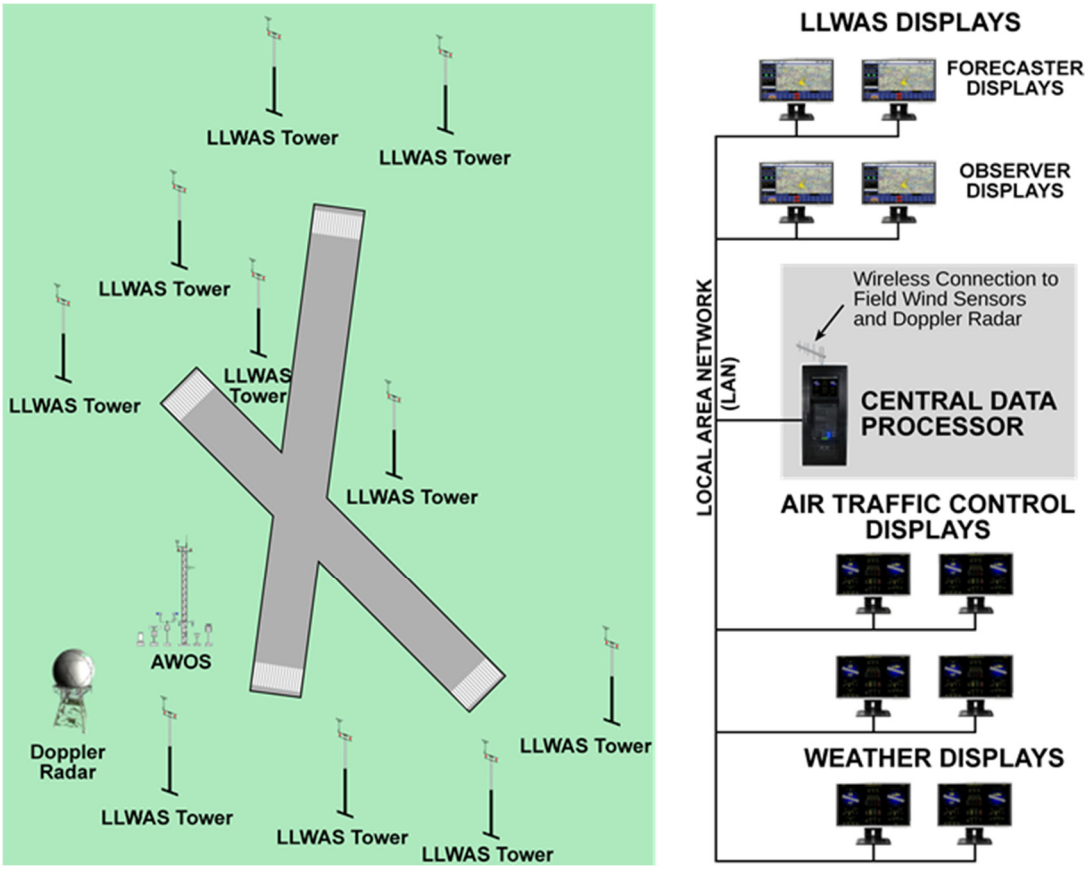

Figure 4.13: LLWAS (Allweatherinc, 2018)

Wind Shear alerts are issued via radio to approaching and departing aircraft by the final air traffic controllers. The wind shear warning issued by the ATC must identify the aircraft, describe the event, give details of the height of the wind shear, the time it

was recorded, the phase of the flight, runway on which the wind shear is present and operation information (ICAO, 2016). An example of such a report is as follows:

"WIND SHEAR B747 REPORTED STRONG WIND SHEAR AT 300 FT ON APPROACH RWY27 AT 0937 MAX THRUST REQUIRED".

Where a wind shear alert has been detected (>30 km/h (15-kt) vector difference) between a perimeter anemometer and centre field anemometer the ATC will issue a warning to the pilot as to where on the airfield the occurrence has been detected. An example of the warning is as follows:

"WIND SHEAR (ALERT) CENTRE FIELD WIND 270 DEGREES 20 KNOTS WEST BOUNDARY WIND 180 DEGREES 25 KNOTS"; or

"WIND SHEAR (ALERT) ALL QUADRANTS CENTRE FIELD WIND 210 DEGREES 14 KNOTS WEST BOUNDARY WIND 140 DEGREES 22 KNOTS".

The wind shear warning will continue to be issued by the ATC until cancelled by the MET office or by subsequent aircraft reports. An example of the monitor display from the LLWAS in the ATC at Sydney International Airport can be seen in Fig 4.14.

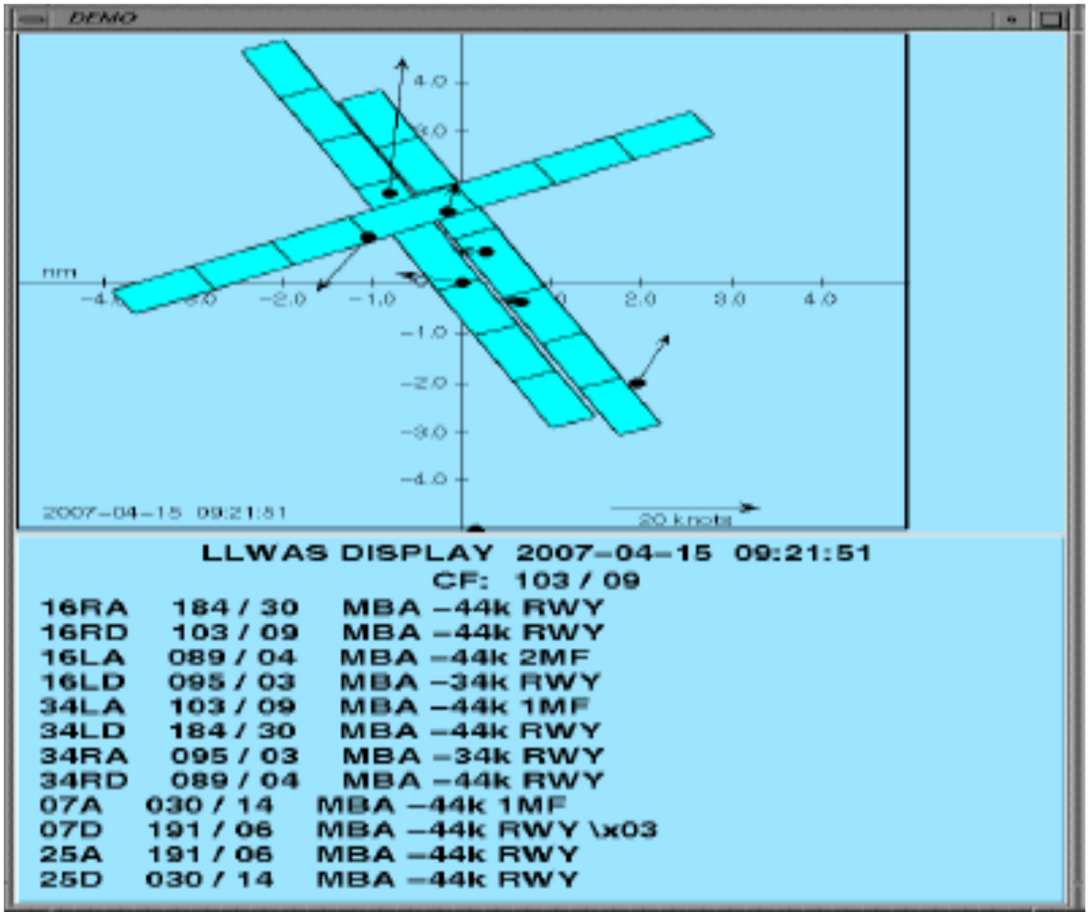

Figure 4.14: LLWAS ATC Monitor Display (CAWCR, 2010)

In Fig 4.15, it can be seen how a southerly gust was observed and recorded by the anemometers at Sydney international airport.

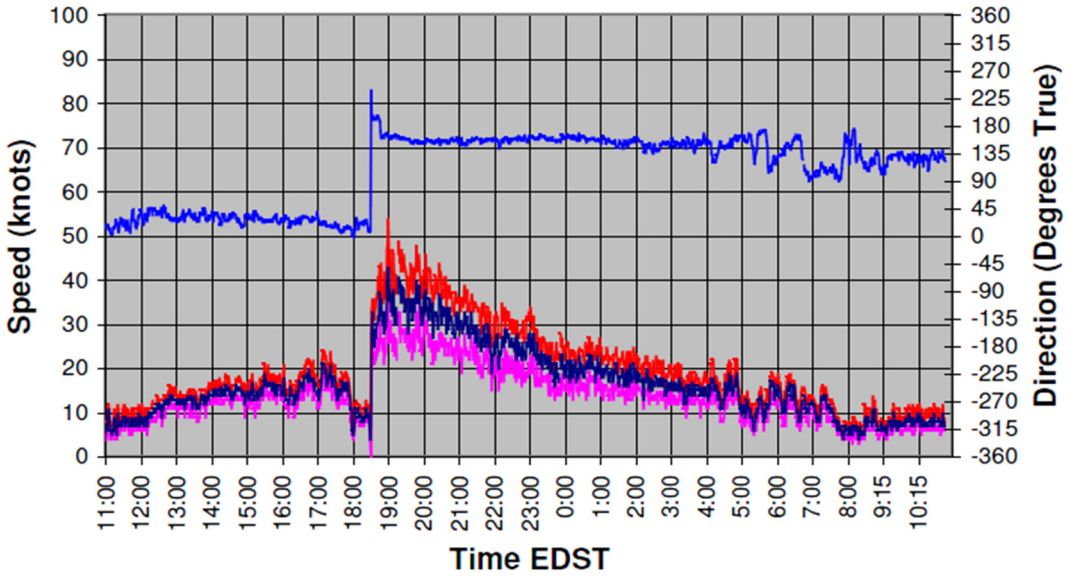

Figure 4.15: Gust Observed with Anemometer Data Sydney Airport 15 January 2001 (CAWCR, 2010)

Low Level wind shear detection research is ongoing with improved algorithms and better communication methods being devised. At Hong Kong Observatory, research is currently looking at a system that can Uplink textual and graphical wind shear alert warning data directly to the cockpit for pilots. This would then give the pilot first-hand forecasted wind shear warning data and allow him to make a more informed decision as to what measures to take in advance of take-off or landing. Fig 4.16 illustrates a concept of this future development.

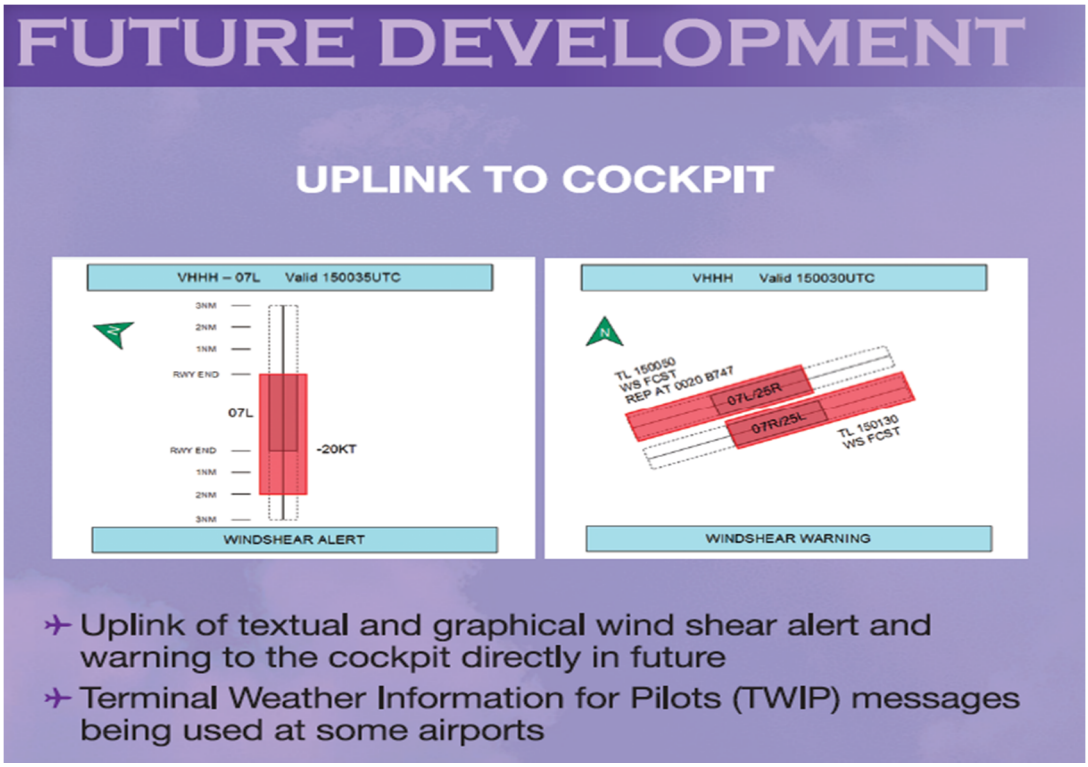

Figure 4.16: Concept of Uplink to the Cockpit (Hong Kong Observatory, 2018)

LLWAS works best for Low Level wind shear and microburst detection around the immediate area covered by the network of wind sensors. It has direct wind measurement and can sense and detect all type of wind shears. Its limitation is that many remote stations are needed to cover a limited area of 3 nautical miles or 6 km out from the runways.

4.3.2.2 Terminal Doppler Weather Radar

Following a series of air accidents as described in section 4.3.1 a specialised research group was formed at Lincoln Laboratory's known as the Lincoln Laboratory's Weather Sensing Group. Research conducted by the group led to development and operational deployment of the Terminal Doppler Weather Radar (TDWR) at 46 airports during the 1990's. The Doppler Effect explained simply is where one is on the street when a fire engine approaches with its siren on. As the fire engine gets closer

the pitch of the siren gets louder and as it travel away from you it get lower. The faster the fire engine approaches the higher the pitch.

As the name suggests the Terminal Doppler Weather Radars purpose is to protect the runways and terminal area of the airport and need careful siting relative to the airport and runways. Doppler radars are installed at most large commercial airports around the world. The radar scans the approach and departure corridors for incoming and outgoing flights. They provide coverage of microburst detection out to 20 km from the radar every 1 minute with wind shear detection out to 60 km every 6 minutes (Office of Aviation Weather Observations, 2010). The TDWR uses low elevation scans for the lowest 100 – 300 m from the surface. TDWR has the ability to measure the approach or departing speed of rain drops. TDWR is designed to detect wind shear and microbursts associated with convective storms. Precipitation intensity or rain drop intensity is measured by a ground based radar that emits a very short pulse of electromagnetic wave at approximately at the speed of light. As the wave encounters precipitation, part of the wave is bounced or reflected back to the radar. This is known as the echo. The strength of the returning signal or echo intensity is directly proportional to the size and quantity of the target in a given area. The echo intensity also known as the reflectivity and is measured in decibels (dBZ). Reflectivity is the amount of power bounced back to a radar from a target compared to a set point target power density at a distance of 1 metre from the radar. The reflective signal is received by the radar during its listening period. The software analyses the strength of reflected signal, the time it took to return and the frequency shift of the pulse. The ability to detect the shift in frequency of the pulse is what makes this a Doppler radar. The TDWR computer then measure the frequency change of the reflected pulse, the velocity of the target either away or towards the radar can be calculated from analysing

this frequency change. This data is then used to calculate the speed of the wind. The computer software is then able to generate a reflectivity image map of each of the three different tilt angles of the radar. The reflective image map results are displayed on a monitor in the ATC within 30 seconds after detection. Fig 4.17 illustrates the simple operation of the Doppler radar where a wave is emitted from the radar which is then reflected back and where the frequency of the reflective wave changes with the speed of the rain. By measuring the frequency change, the speed and movement of the rain can be calculated. TDWR operates at a 5 cm wavelength or frequency of 5600-5650 MHz on an angular resolution 0.55º x 0.55º (azimuth x elevation) antenna beam and transmits Unicode, 1 μs, 250-kW pulses (Weber, 2010).

The TDWR issues a microburst detection alert, when the maximum velocity differential is more than 8 m/s or 15 kt, when the area of the microburst is more than 3 km² and where the maximum rate of change of the Doppler velocity is more than 5.6 m/s/km.

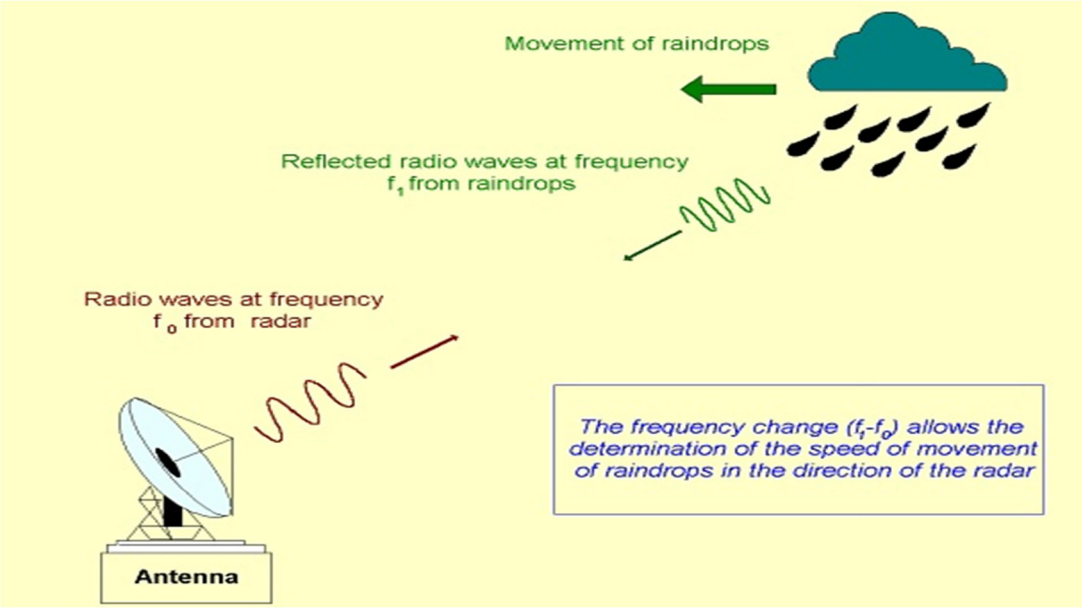

Figure 4.17: Doppler Radar Operation Principle (Hong Kong Observatory, 2018)

A wind shear alert is issued when the wind velocity difference of both sides of the shear line is more than 5 m/s or 9 kt, the length of the shear line is more than 10 km and the maximum radial of the shear line is more than 2 m/s/km. Fig 4.18 illustrates how a microburst detected by TDWR at Tokyo international Airport is depicted on a reflective image map or Echo intensity map.

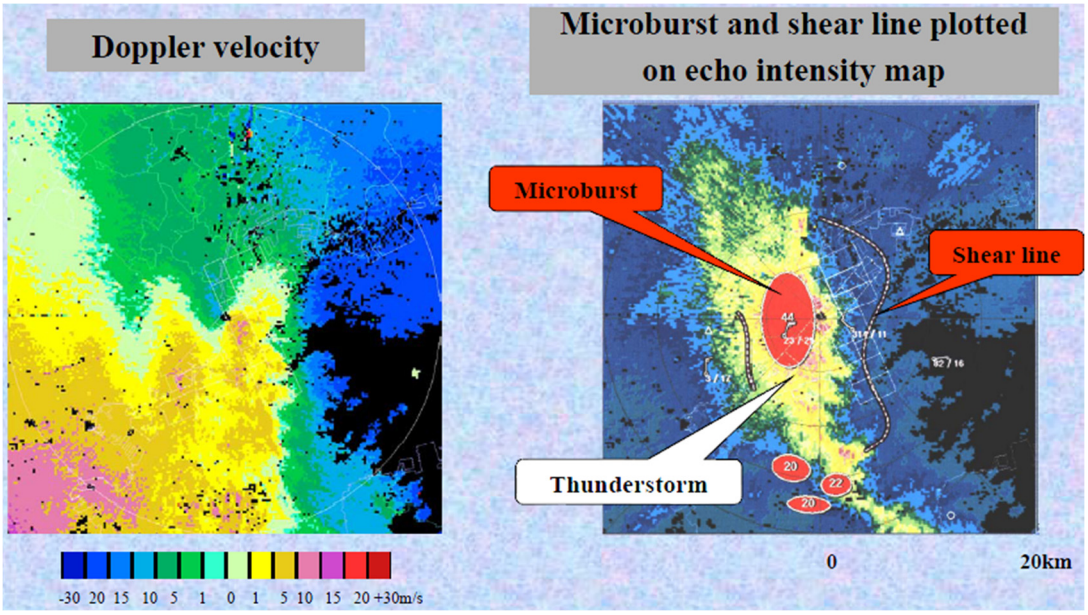

Figure 4.18: Microburst and Shear Line Detected ((Office of Aviation Weather Observations, 2010)

In May 2002 shortly after the TDWR was commissioned at Hong Kong International Airport, it detected its first Tornado. In Fig 4.19 the image of Doppler velocity indicates opposing winds of 90 kmh covering an area of one kilometre across as shown in the circled area of the image. The purple and blue coloured echoes represent winds blowing towards the northeast while orange and yellow echoes indicate winds blowing towards the southwest. The two bubbles of opposing wind as shown below is a typical pattern indication of a tornado.

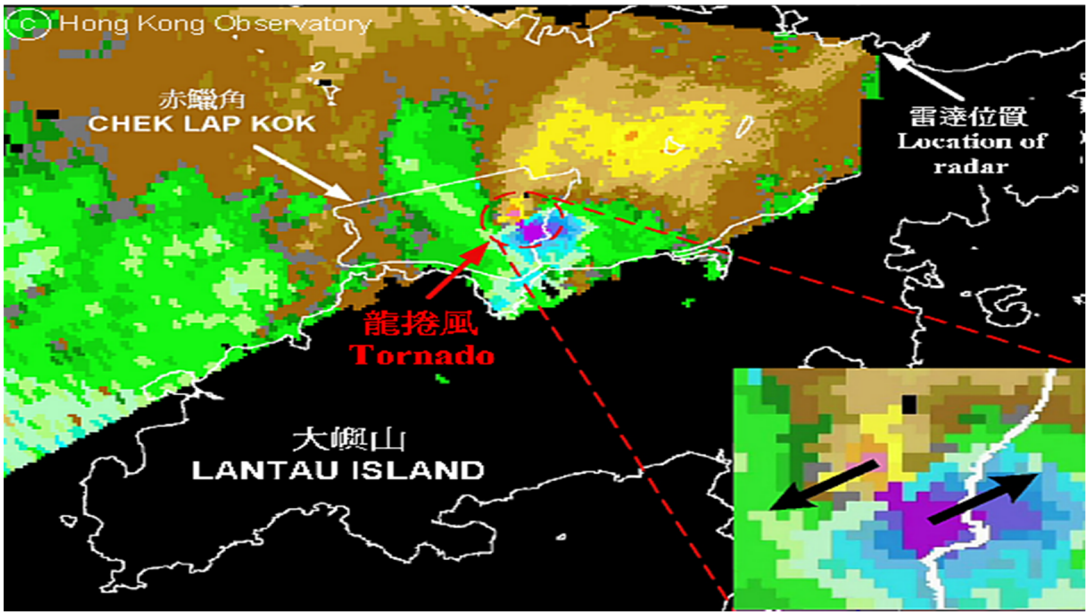

Figure 4.19: TDWR Image Map of Doppler Velocity Warning of a Tornado (Observatory, 2018)

In Fig 4.20 the TDWR Image of Reflectivity depicts the hook shaped characteristic of the approaching storm. This is another indication of the presence of a tornado. The Doppler radar's capability of measuring rain intensity and speed of rain has enabled the more accurate forecasting of wind strengths and cyclones within range of the radar. Since the development and deployment of LLWAS and TDWR there has been a significant reduction in wind shear related accidents at airports where these systems are installed. In a report carried out at Lincoln Laboratory's (Cho, 2010), it was found that in a comparison to other airport weather radars the TDWR had the best performance characteristics for terminal wind-shear detection. The TDRW was found to have the highest weather sensitivity and the narrowest antenna beam for clutter avoidance. TDWR have a POD of between 0.90 and 0.93 (John Y. N. Cho, 2008) in forecasting low level wind shear at precipitation or a microburst generated in connection with a convective storm.

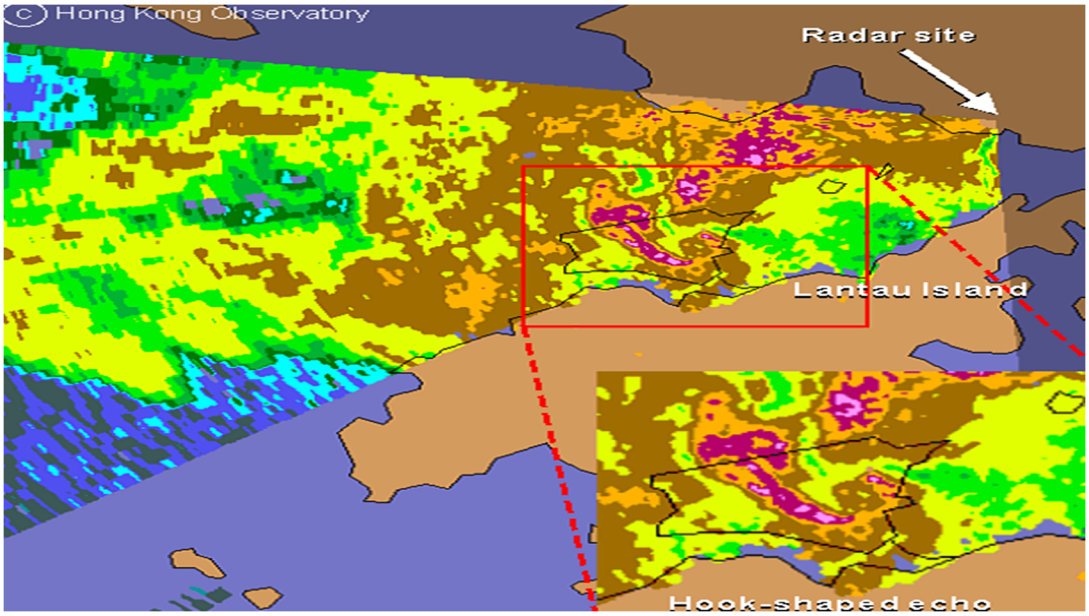

Figure 4.20: TDWR Image Map of Doppler Reflectivity Warning of a Tornado (Observatory, 2018)

A study carried out at Kansai International Airport in Japan (Office of Aviation Weather Observations, 2010) into the accuracy of low level wind shear detection by TDRW found that the POD was very much in line with the findings of a survey comparing wind shear detection systems carried out at MIT Lincoln Laboratory (John Y. N. Cho, 2008). Table 4.4 illustrates the findings from the low level detection survey at Kansai International Airport.

Table 4.4: Accuracy of low level wind shear detection

	⊿Vt (m/s)	Number Detected	Number Observed	POD (%)
Shear Line	5	71	83	86
	10	53	56	95
	15	19	20	95
Microburst	5	257	297	87
	10	227	236	96
	15	83	84	99

A TDWR according to the studies mentioned is by far the best radar and long range wind shear detection system out to 20 km for many airports. However there are some conditions that affect the effectiveness of the TDWR. It is susceptible to ground noise

and clutter which can hamper and affect its accuracy in detecting wind shear events. It will generally not detect very dry microbursts, gust fronts or sea breeze shears. Studies mentioned have found that the FAA's requirement of a 90% detection rate of microbursts by TDWR is very often not achieved at Las Vegas International due to clutter and also the occurrence of dry microbursts. The POD rate was also lower for Denver airport due to it being a dry site. TDWR can also fail to detect asymmetric events.

4.3.2.3 Doppler Lidar

Lidar stands for Light Detection and Ranging. Lidar systems are not a new instrument but their application and use in meteorological aviation has increased over the past 15 years with Doppler frequency technology. Lidar had mainly been used in a variety of survey and mapping applications prior to this. The Doppler Lidar operates on a similar principle to that of TDWR but with a much shorter wavelength of 2 micrometres compared to a few centimetres of the radar. The Lidar emits infrared light pulses which is transmitted at a frequency of 500 – 750 Hz. Fig 4.21 illustrates the basic operation of a Doppler Lidar system.

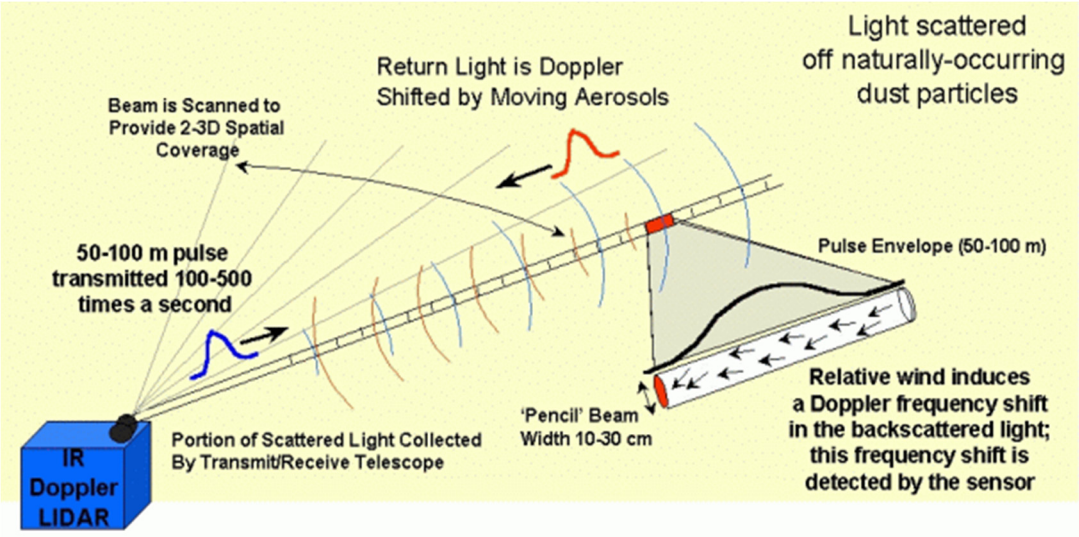

Figure 4.21: Doppler Lidar Principle of Operation (Hong Kong Observatory, 2018)

Unlike the TDWR which receives the echo from rain drops, the Lidar gets its reflection from particles of dust or aerosols in the air. The shift in frequency of the return echo or reflective signal is proportional to the movement of the aerosols. The quicker the aerosols move the larger the frequency shift will be. This enables the velocity and strength of the wind to be calculated. Lidar works best in dry conditions in the presence of aerosols that provide effective back scattering. Doppler Lidar can perform sector scans at different elevation angles along the approach and landing corridors of airport runways out to about 3 NM.

The world's first Doppler Lidar was installed at Hong Kong International Airport in 2002. The Airport then installed a second system in 2006 to enhance detection of dry microburst systems. Both systems are fully automatic with data updated every two minutes. Fig 4.22 illustrates the Lidar systems scanning of the runways at Hong Kong Airport.

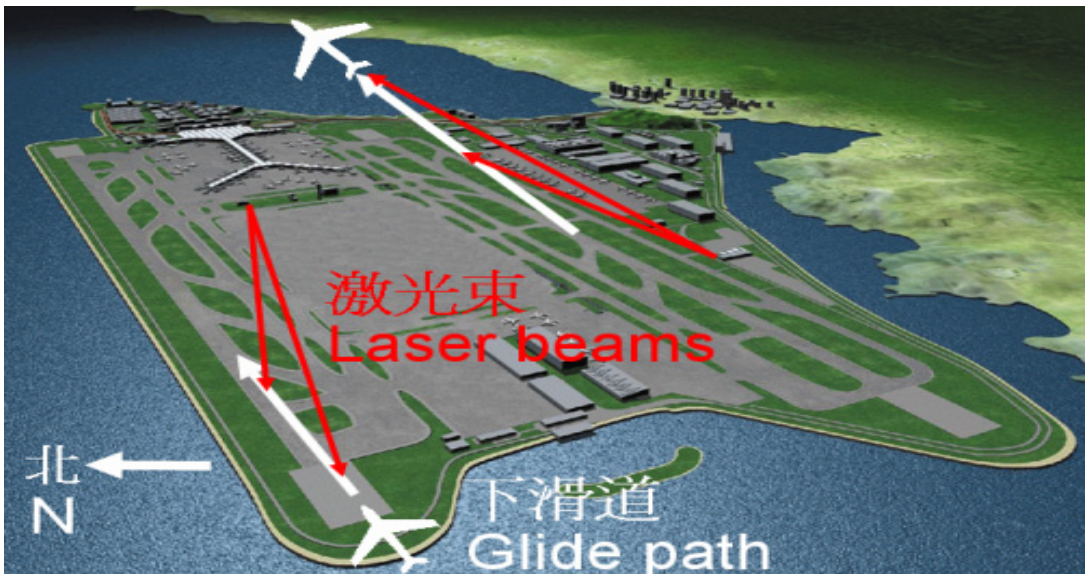

Figure 4.22: Doppler Lidar Systems Scanning Runways at Hong Kong (Hong Kong Observatory, 2018)

Doppler Lidar systems work best in dry fine weather, it is not suitable for detecting wind movement inside a thunderstorm due to the absorption of infrared light by rain drops. Lidar as a single sensor system is not suitable for microburst detection and has

a lower POD in comparison to TDWR in areas where wet conditions prevail. Lidar does not have enough range coverage in humid and rainy situations and there can be missed wind shear events between scans (Chan, 2005). Lidar is not suitable for gust front protection as it range is at best 15 km and the gust front interest area is 18 km around the airport (Cho, 2010).The 18 km extent of gust front coverage relates to the distance a gust front would travel at 15 m/s in 20 minutes which is considered an appropriate lead time for an airport operational alert. In a study carried out at Lincoln Laboratory's, it was concluded that a combination of Lidar and TDWR or weather radar is projected to form the best microburst detection probability (John Y. N. Cho, 2008). New Doppler Lidar systems now come as an off the shelf product and are increasingly being installed at airports around the world. The German Weather Service installed the WindTracer Lidar systems at Munich and Frankfurt airports where the Lidar was integrated with the X-Band weather radar. This was Europe's first integration of Lidar and radar for wind shear detection. Fig 4.23 illustrates the image map from a WindTracer LIDAR system tracking mountain turbulence approaching the runway at Hong Kong Airport.

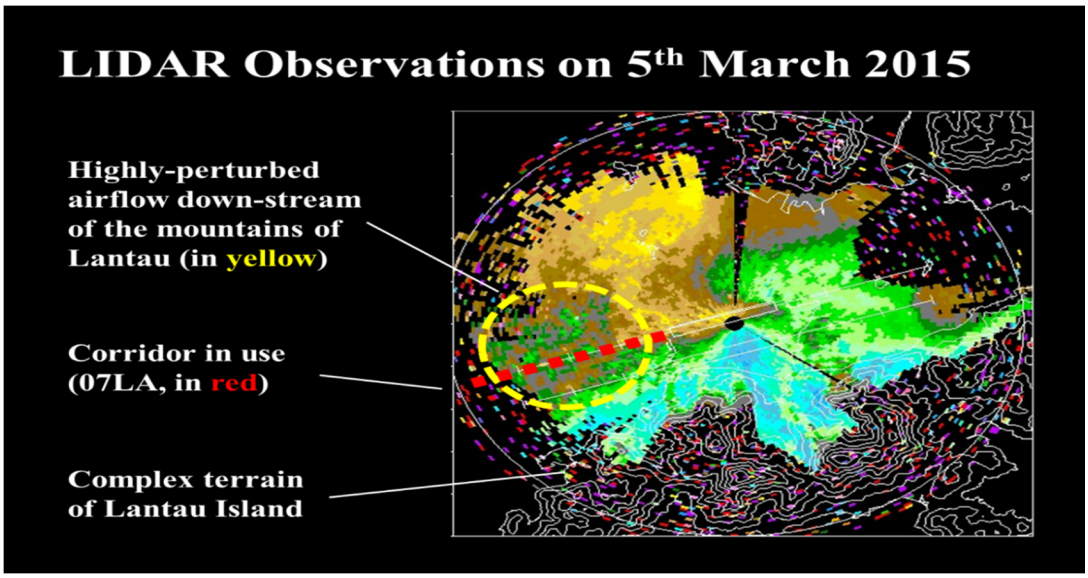

Figure 4.23: Lidar Map of Mountain Turbulence (Hong Kong Observatory, 2018)

Dubai airport recently installed a third WindTracer Doppler Lidar system from Lockheed Martin to detect wake turbulence and help reduce airport separations during arrivals thus increasing capacity at the world's busiest airport (Carey, 2015). Wake turbulence at Dubai airport is more prevalent that other international airports given the number of Super Heavy Weight Category Airbus A380 aircraft that land there each day. The WindTracer Lidar is a cost effective and affordable product and studies have shown that when combined with radar, it provides a cost effective high detection wind shear solution for airports. Lockheed Martin have stated that the WindTracer and radar integrated system provides “the highest detection rate for wind hazards, in both dry and wet environments” (Lockheed Martin, 2013).

A WindTracer Doppler Lidar and a TDWR have been fully integrated at Tokyo and Narita airports in Japan since 2003 by the Japan Meteorological Agency. This system that has been monitoring wind shear and microburst events since 2003 with a POD of between 0.97 and 0.98. The Lidar system was installed to detect low level wind shear in conditions of non-precipitation at two minute intervals out to a distance of 10 km from the flight corridors. The TDRW was installed to detect wind shear with

precipitation and microburst associated with convective currents every 1.2 minutes out to a distance of 20 km radius for microburst detection and 60 km for wind shear. Fig 4.24 depicts the benefits of the integrated operation of the TDWR/LIDAR system.

	Purpose	Measuring Method	Detection Range	Obs. Time Interval	
Lidar	To detect the sudden change region of the wind such as low level wind shears in conditions of non-precipitation	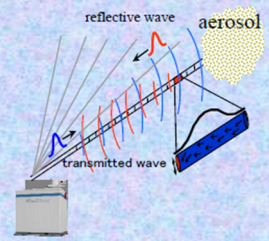	Radius: 10km	About 2 min.	In TDWR and LIDAR, the weather condition that is appropriate for the observation is different.
TDWR	To detect the low level wind shear at precipitation or the microburst generated in connection with the developed CB.	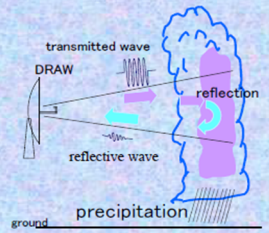	Precipitation DopplerVelocity Radius:120km Shear Line Radius:60km Microburst Radius:20km	Aerial Mode About 6 min. Airport Mode About 1.2 min.	The wind shear can be observed by on integrated operating TDWR and LIDAR in precipitation and non-precipitation conditions .

Figure 4.24: TDWR/Lidar Detection Parameters Japan (Office of Aviation Weather Observations, 2010)

The fusion of data from multiple systems has the potential to increase the wind shear detection probability. TDWR + Doppler LIDAR, Doppler LIDAR + Weather Surveillance Radar (WSR) are the best current combinations of radar systems today. Limitations in the coverage of one system due to lack of sensitivity, clutter residue or blockage can be covered by a system with better sensing capabilities in those areas of limitation. The sophisticated algorithms that allow for fuzzy logic operations allow merging on interest fields. TDWR + Doppler LIDAR, Doppler LIDAR + WSR allows for the integration of the systems which is done by computing the visible pixel by pixel for each sensor and take the greater value before summing up over the interest area (Cho, 2010). Fig 4.25 is an illustration of a block diagram of the integration of the TDWR and LIDAR systems at Tokyo and Nariata airports in Japan.

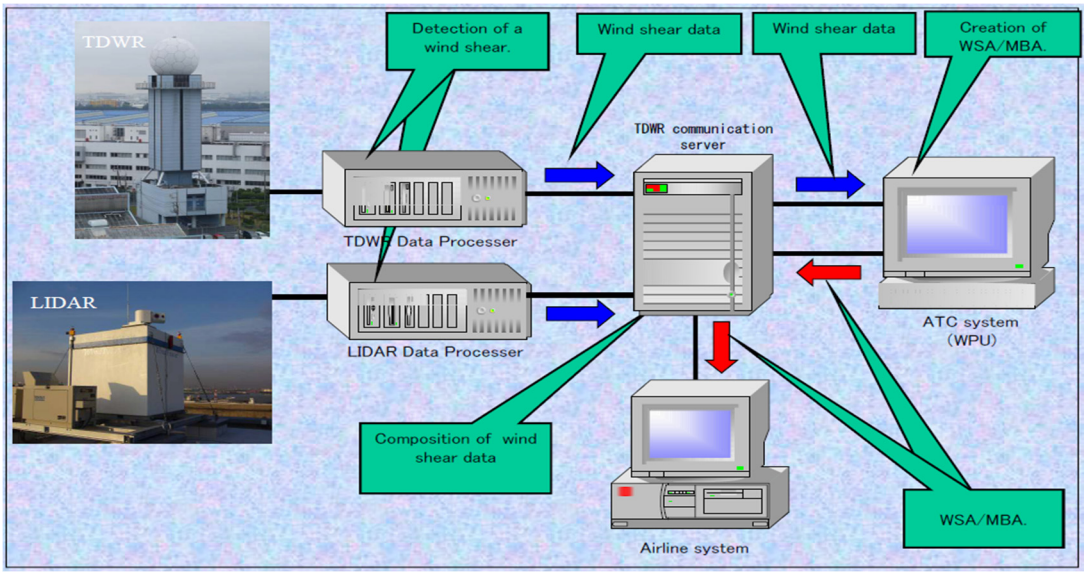

Figure 4.25: TDWR & LIDAR Integration (Office of Aviation Weather Observations, 2010)

Out to a distance of 20 km radius for microburst detection and 60 km for wind shear. Fig

4.3.2.4 Weather Surveillance Radar (WSR)

Weather Surveillance Radars have evolved and developed over the years from the earlier Airport Surveillance Radars (ASR) which were primarily developed to track aircraft to the Next Generation Radar (NEXRAD) which is known technically as WS-R-88D. As detailed previously, following a series of fatal aircraft crashes in the seventies the WISTSG group tasked with detecting LLWS and microburst occurrences instigated research on LLWAS and TDWR as previously described. The group also evaluated and researched the existing ASR-9 systems and how it could contribute to detecting microburst and wind shear events in smaller airports in the US where the air traffic volume did not justify the cost of the installation of a TDWR. In 1985 research work began on the development of a Wind Shear Processor (WSP) as an add-on to the existing ASR-9. The ASR-9 is an S-Band radar that operates at a frequency of 2.7- 2.9 GHz on an angular resolution of 1.48º x 4.8º (azimuth x elevation) with a pulse width of 1.0 µs operating at a power of 1.12MW. During 1991 field trials were conducted at Orlando International Airport to determine the detection capability of the new system

known as ASR-9 WSP. The system had a high reliability detection rate for microbursts. However, the system had a low detection rate of 0.84 when detecting wind shear associated with gust fronts. The Advanced Gust Front Algorithm (AGFA) initially developed for the TDWR was incorporated in 1991. The detection of gust fronts was less than acceptable as reduced sensitivity associated with the elevation of the fan beam of the ASR-9 significantly reduces the WSP's ability to measure the convergent wind pattern associated with low reflective gust fronts and the system produced a high level of false alarm rates. An improved Machine Intelligent Gust Front Algorithm was developed which improved gust front detection and reduced false alarms (M Weber, 1991). The WSP sweep images are updated every 4.8 seconds with a range of 15 NM. The ASR-9 WSP is an old system which can be integrated with Doppler to provide an optimal wind shear detection system for coverage areas comprising the union of the Areas Noted for Attention (ARENAs) for microbursts and an 18-km-radius circle around the airport for gust fronts. An ARENA polygon consists of the runway length plus three nautical miles final on approach and two nautical miles on departure times a width of one nautical mile. As a single sensor system, the ASR-9 WSP cannot provide the 90% microburst probability required at most airports even after upgrades to its clutter suppression capability.

The Nexrad or Weather Surveillance Radar, 1988 Doppler (WSR-88D) is one of the most advanced operational weather radar systems in the world. The WSR-88D form a network of 160 radar systems operating 24/7 in the US today (NOAA, 2018). The network is a tri-agency administered operation comprising of the National Weather Service, FAA and Defence Department. The projects function is to support weather warning and forecast missions to the three agencies as well as providing real time data for US universities and commercial weather services. The WSR-88D has been

constantly upgraded and updated since its first installation in 1992. The WSR-88D like all radar systems consists of three main modules, the Radar Data Acquisition (RDA), the Radar Product Generator and the end user display systems. The RDA provides for the detection and measurement of weather data. The RDA comprises of all the relevant hardware, firmware and software to operate and drive the antenna, transmitter, receiver and signal processor. The radar is an S- Band coherent machine operating at a frequency of 2700 – 3000 MHz, wavelength of 10.5 cm on an angular resolution of 0.925º x 0.9258º (azimuth x elevation) with a pulse width of 1.6 μs operating at a power of 750KW. In 2011 all WSR-88D units were upgraded to enable dual polarization capability. Dual polarization radar system can transmit horizontal and vertical polarized pulses simultaneously. Sampling the echoes along the horizontal and vertical plane provides far more accurate measurement of precipitation as well as hail and tornado debris detection. During normal operation the radar is constantly rotating and scanning the atmosphere using a program called Volume Coverage Pattern (VCP). The VCP rotates the beam through 360º in the azimuth through an elevation range of 0.5º to 19.5º above the horizon. In 2011 the WSR-88D had the Velocity Azimuth Display Wind Profile (VWP) product upgraded. The VWP product provides a time verses height wind profile for the volume above the radar location. Fig 4.26 illustrates a VWP for each elevation against range and height.

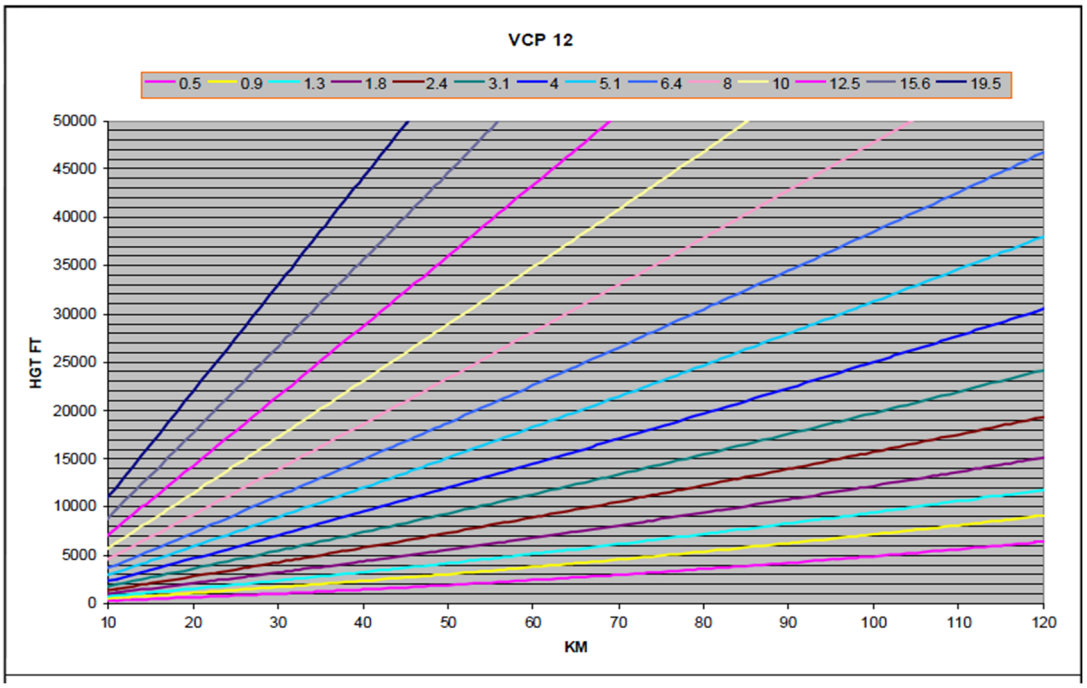

Figure 4.26: VCP Elevations Plotted on Range/Height Grid (NOAA, 2010)

A wind estimate is derived from an algorithm for each VWP height. Each VCP is designed to optimise the detection and sampling of weather data. In autumn of 2014, VCP 12 was updated to the WSR-88D systems with the first priority of the project being to reduce volume scan completion times and provide for faster low level elevation scan updates. The problem of the WSR-88D slow update rates was highlighted in a study doing a comparative analysis of terminal wind shear detection systems (John Y. N. Cho, 2008) where it was stated "NEXRADs are not suitable for microburst detection and warning, because their update rates (~5 minutes) are too slow to meet the FAA requirement." The FAA used them for Gust front detection and tracking as the update rates are adequate for this type of operation. Since the implementation of VCP 12, the volume scan completion time has been reduced to 4.1 minutes. Fig 4.27 illustrates the block diagram of the RPG Graphical User Interface of the VCP as the radar samples the atmosphere.

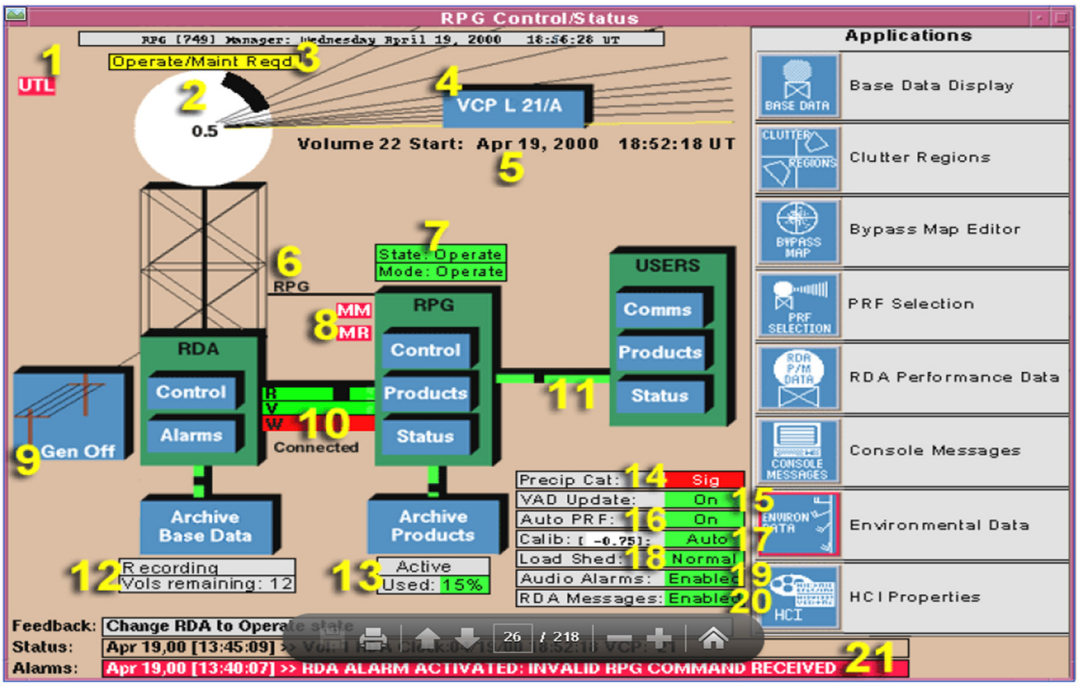

Figure 4.27: RPG Graphic User Interface for the WSR–88D (OFCM, 2006)

Despite the scan rate update time being reduced from nearly 6 minutes to 4.1 minutes, the WSR-88D radar will not detect all microburst occurrences at their maximum divergent intensity as this update time is still too slow, because microbursts in nature are short-lived entities lasting 3 to 5 minutes. Despite this fact, the VCP 12 is the coverage pattern of choice of the FAA because of because of the overlapping low-level beams in the vertical and the relatively rapid update rate of 4.1 minutes VWP for each elevation against range and height (OFCM, 2006). The WSR-88D as a single sensor system in many cases is not suitable for microburst detection at airports but combined with LIDAR would exceed the FAA requirement of a POD of 90%. For single sensor case the only radar capable of meeting microburst detection is the TDWR (John Y. N. Cho, 2008). Fig 4.28 below illustrates the image map of microburst as marked by the white cross detected by the WSR-88D system.

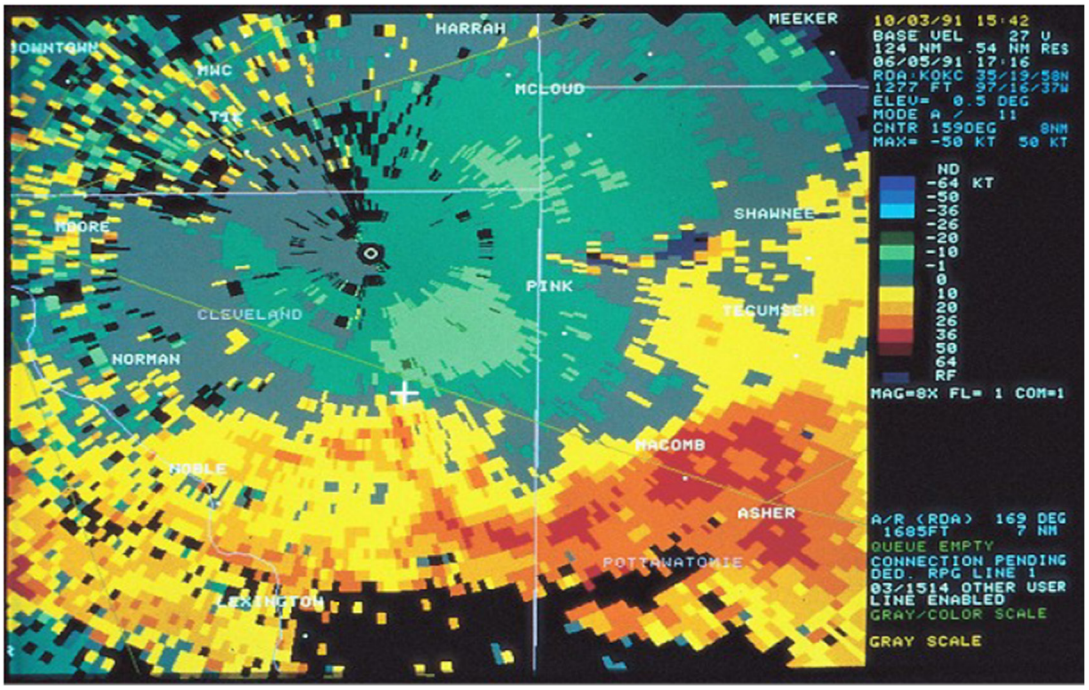

Figure 4.28: Microburst Detected by WSR-88D (NOAA, 2018)

Radar data and image maps need to communicate to the end users in the ATC. The FAA uses the Weather and Radar Processor (WARP). This is an FAA owned computer network which allows the WSR-88D data to be displayed as shown in Fig 4.27 and Fig 4.28 to air controllers in the Air Route Traffic Control Centres.

All of the systems discussed, LLWAS, TDWR, LIDAR, ASR-9, WSR-88D, Automated Surface Observing Systems (ASOS), and other NWS systems are integrated into the FAA's Integrated Terminal Weather System (ITWS). The ITWS provides the operators monitoring the system with the tools to plan safety for terminal weather events as well as being able to forecast the weather 30 minutes into the future.

4.3.3 Instruments Currently used in LLWAS in the Terminal Area

Mechanical sensors have formed the field sensing components of the LLWAS since its development over thirty years ago. The ASOS of the NWS and FAA has used rotating cup anemometers to measure wind speed and a vane to measure wind direction since the mid-1940s. Fig 4.29 illustrates the Belfort 2000 cup and vane anemometer which was used in the NWS's ASOS.

Figure 4:29 Belford Cup and Vane Anemometer

The average wind speed and direction was determined using twenty four 5 second discrete averages from the wind sensors. The highest 5 second speed value was used to determine if a gust was to be recorded. After extensive field trials of sensor performance under icing conditions, (William Benner T. C., 2002) the NWS and FAA sought a product improvement for the mechanical sensors based on the results of a 184 day test period with 3500 hours of recorded data from mechanical, ultrasonic and pressure tube sensors. The results concluded that cup and vane technology was susceptible to lock-ups in freezing precipitation conditions, it was found that when the cups and vanes became immobilized by freezing precipitation that they generally remained in that state until the temperature increased above freezing. This led to periods where wind data was not available or was inaccurate. A further problem found that when snow attached itself to the cups, this resulted in the slowing down of the rotation speed of the sensor (William Benner T. C., 2002). The FAA implemented a new gust sampling period of a running 3 seconds instead of the 5 seconds, this meant that due to their construction, the mechanical cup and vane instruments were unable to meet the new sampling criteria of the FAA (National Weather Service, 2002). In 2000, the FAA took the decision to replace all mechanical cup and vane sensors used by ASOS at the 883 NWS stations in the US with ultrasonic sensors for the reason

stated but also because of their reliability, durability and lower maintenance costs (Pattison, 2010).

The ultrasonic sensors operate with no moving parts so it is not affected by start-up torque associated with mechanical sensors and is more responsive. Ultrasonic sensors used by in LLWAS have their own in built microprocessor that captures and processes data which is then transferred over serial RS422 or RS485 interfaces. The sensors have three or four transducer arms equally spaced and mounted on the sensor base on a horizontal plane as shown in Fig 4.30 and Fig 4.31.

Figure 4:30: Vaisala Sensor (Vaisala, 2018)

Figure 4.31: Gill WindObserve Sensor (Gill , 2018)

The sensors have a North reference arm which is aligned to magnetic North during installation for aviation within the LLWAS area of the runway. The ultrasonic sensor works on the principle of measuring the time it takes for a pulse of sound to travel from point A to point B which in the case of the sensor is the transducer, this is measured by the microcontroller and the wind speed is calculated as a function of the time it takes for the sound to travel between transducers. In the case of the three arm Vaisala sensor, Wind Speed (WS) and Wind Direction (WD) are determined by

measuring the time it takes the ultrasound to travel from each transducer to the other two. The microcontroller then measures the transit time in both directions along the three paths. The transit time depends upon the wind speed along the ultrasonic path (Vaisala, 2018). The forward and reverse paths are the same for zero wind speed.

The microcontroller calculates the WS from the measured transit times using the following formula in Eq: 4.6

Eq: 4.6 $$Vw=0.5\cdot L\cdot(1/tf-1/tr)$$

The microcontroller measures the six transit times which allows Vw to be calculated for each of the three ultrasonic paths. Using the values from two of the array paths is enough to calculate and determine the WS and WD. Fig 4.32 illustrates the different measurement paths 1 – 6, distance between the transducers La, Lb, Lc and vectors provided by the Vaisala wind sensor.

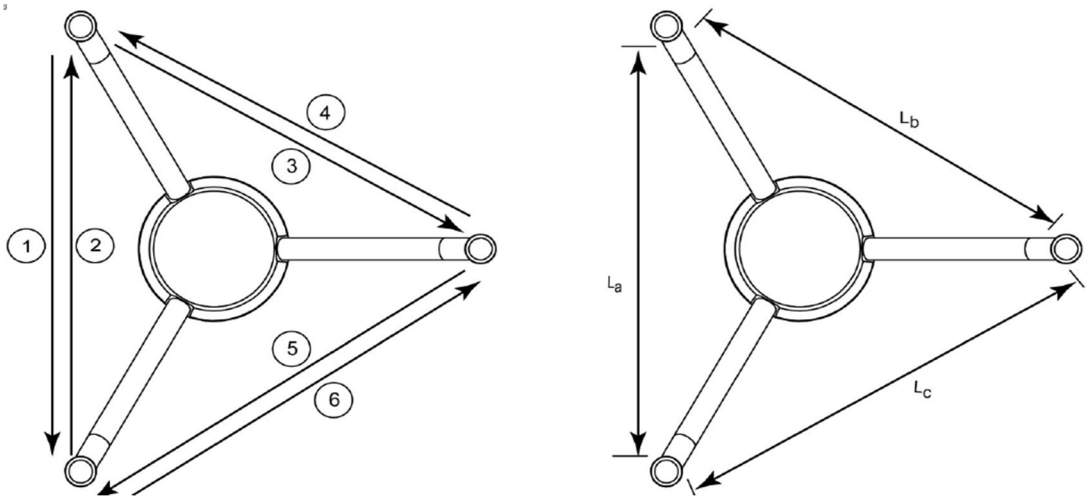

Figure 4.32: Measurement Path of Vaisala WMT700 (Vaisala, 2018)

The vectors are calculated as follows,

$Va=0.5\cdot La\cdot(1/A1-1/A2)$
$Vb=0.5\cdot Lb\cdot(1/A3-1/A4)$
$Vc=0.5\cdot Lc\cdot(1/A5-1/A6)$

The Ultrasonic sensor from Gill instruments operates with similar principles as the Vaisala but has additional message format output options using UV or Polar. The UV mode output is given as signed positive or negative speeds North-South and East-West axis, where U = South – North and V = East – West. Both message formats are output as ASCAII strings using a serial RS422 or RS485 cable to a computer system. Fig 4.33 and Fig 4.34 below illustrates the output format options that can be selected using command settings from a HyperTerminal on a pc.

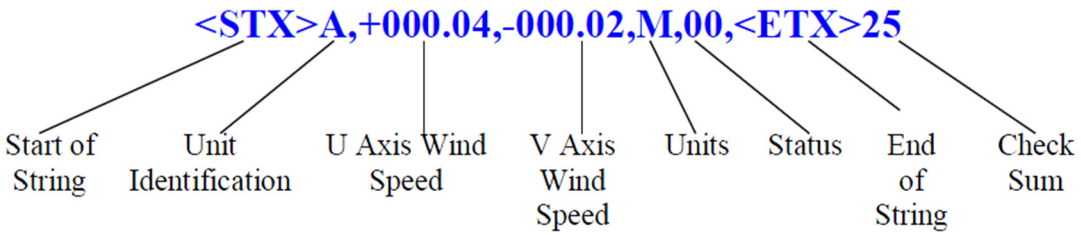

Figure 4:33: ASCII UV Format (Gill , 2018)

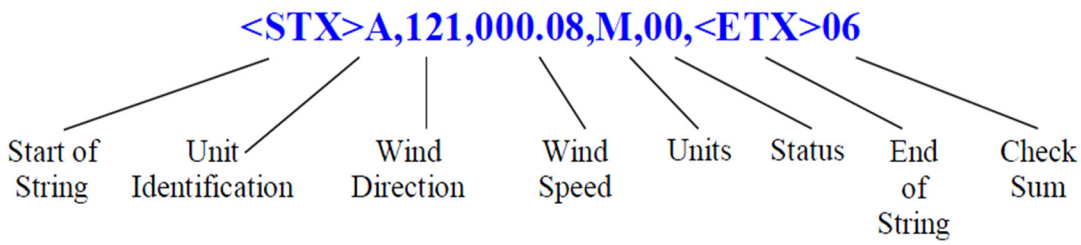

Figure 4:34: ASCII Polar Format (Gill , 2018)

The option used for LLWAS for this sensor is the Averaging Format in continuous mode. The averaging is done in accordance with WMO standards as stated. Fig 4.35 illustrates the Averaging format which includes the maximum gust speed and direction. The Maximum Gust Direction is the direction of the maximum gust measured over the short term output period. Gust is generated from a rolling 3s average of the short term output period, and reset at the end of short term output period. The short term period can be configured from 10 – 60 seconds.

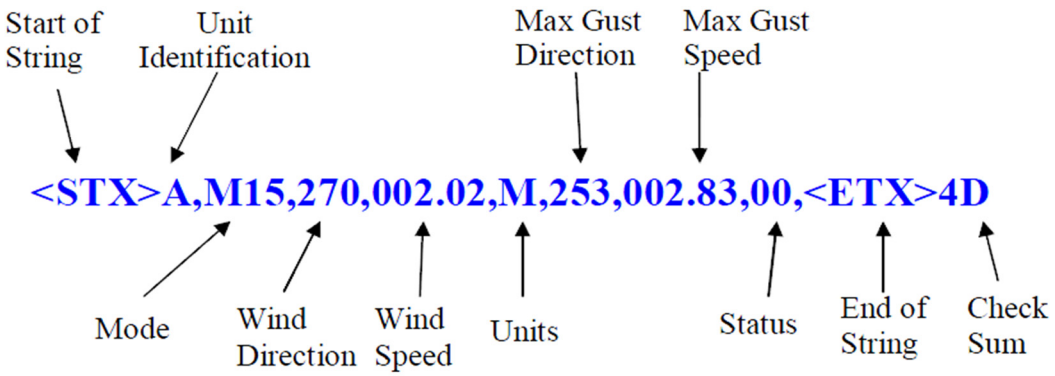

Figure 4:35: Averaging ASCII Format Output (Gill , 2018)

The maximum Gust Magnitude is the magnitude of the maximum gust measured over the short term output period. Gust is generated from a rolling 3s average of the short term output period, and reset at the end of short term output period. Fig 4.36 shows the output in textual form of the Averaging ASCII format from the sensor.

```
☻A,M15,293,000.03,M,338,000.05,51,♥47
☻A,M15,301,000.03,M,304,000.04,51,♥43
☻A,M15,299,000.03,M,285,000.02,51,♥4D
☻A,M15,303,000.02,M,336,000.02,51,♥47
☻A,M15,291,000.03,M,200,000.64,51,♥48
☻A,M15,291,000.02,M,301,000.03,51,♥48
☻A,M15,243,000.04,M,172,001.52,51,♥42
☻A,M15,236,000.03,M,090,000.08,51,♥44
☻A,M15,243,000.03,M,099,000.09,51,♥4E
☻A,M15,198,000.04,M,088,000.39,00,♥4B
☻A,M15,180,000.04,M,099,000.09,00,♥41
☻A,M15,180,000.03,M,345,000.03,00,♥4E
```

Figure 4:36: Logged Data of Averaging ASCII format from the sensor (Gill , 2018)

The principle of operation is similar to that of the Vaisala sensor as described. The Gill sensor, measures the times taken for an ultrasonic pulse of sound to travel from the North transducer to the South transducer, and compares it with the time for a pulse to travel from S to N transducer. Likewise times are compared between West and East, and E and W transducer. This is similar to the Vaisala instrument as it measures the time in the forward and reverse direction along each path. The wind speed and

direction (and the speed of sound) can then be calculated from the differences in the times of flight on each axis. Independent of factors such as temperature do not affect the calculations. Fig 4.37 illustrates the principle of operation of the Gill WindObserver sensor.

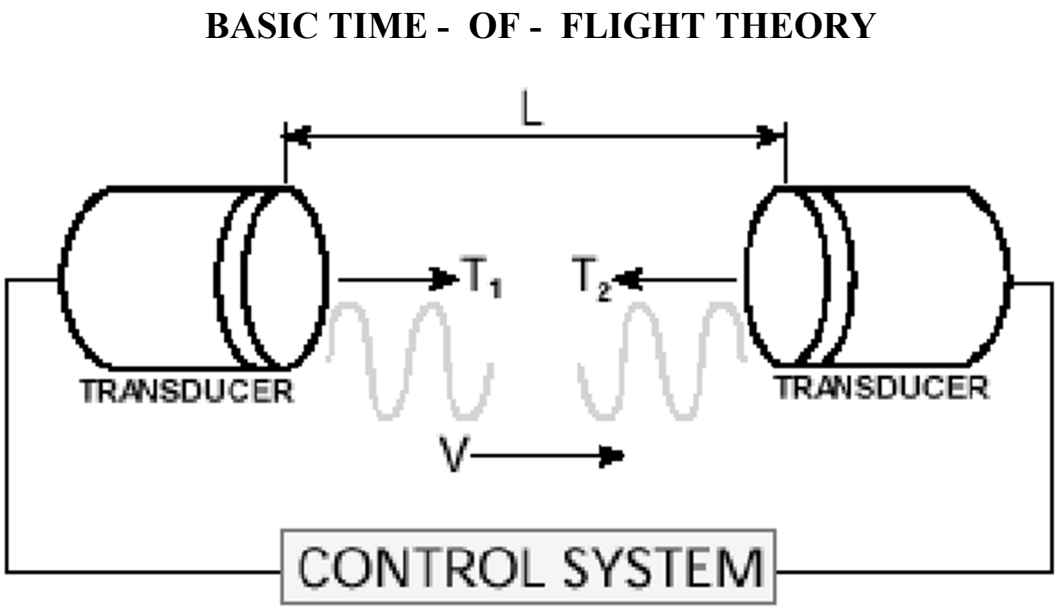

Figure 4:37: Gill Sensor Principle of Operation (Gill , 2018)

The microcontroller calculates the WS from the measured transit times using the following formula in Eq: 4.7 and Eq: 4.8.

Eq: 4.7 $T2 = \frac{L}{C-V}$ and

Eq: 4.8 $T1 = \frac{L}{C+V} \quad \therefore V = \frac{L}{2}\left\{\frac{1}{T1} - \frac{1}{T2}\right\} C = \frac{L}{2}\left\{\frac{1}{T1} + \frac{1}{T2}\right\}$

Both the Vaisala and Gill ultra-sensors are FAA and CAA accepted for airport applications and are WMO and ICAO compliant. The Vaisala sensor is currently the predominant device used by the NWS and FAA in the measurement of LLWS. Both devices have a heater option to prevent freezing but only the Vaisala sensors have analogue output range options for both wind speed and wind direction observation as

well as digital outputs. Table 4.5 below gives a comparison of both ultrasonic sensors used for aviation weather observation.

Table 4.5: Comparison of Vaisala and Gill Ultrasonic Sensors

	WS Measurement		**WD Measurement**		Measurement		Output	
VAISALA WMT 70X	Range	0-90 m/s	Range	0-359º	Output	1,2,4 Hz	Comms 1	RS-485
	Starting Threshold	0.01 m/s	Starting Threshold	0.1 m/s	Parameter	UV,Polar NMEA	Comms 2	RS-422 RS-232 RS-485 SD1-12
	Resolution	0.01 m/s	Resolution	0.01º	Units	Ms,Kt,MPH, .KPH,ft/min		
	Response Time	250 ms	Response Time	250 ms	Available Averages	Selectable 1-3600 sec	Analog WS	Frequency Push/Pull Pull/Down Pull/UP Voltage 0-10v Current 0-20ma
	Accuracy	0.1m/s or 2%	Accuracy	+/- 2%				
	Variables	Instant,Peak, Avr,Max,Min,Gust,lull	Variables	Instant,Avr, Max, Min			Analog WD	Voltage 0-10v Current 0-20ma Potentiometer
GILL 70 / 75	Range	0-75 m/s	Range	0-360º	Output	1 – 4 hz	Comms	RS-485 RS-422 RS-232
	Starting Threshold	0.01 m/s	Starting Threshold	0.01 m/s	Parameter	WMT700, NMEA,WS 425,ASCII		
	Resolution	0.01 m/s	Resolution	1º	Units	Ms,Kt,MPH, .KPH	Analog WS	N/A
	Response Time	250 m/s	Response Time	250 m/s	Available Averages	Selectable 1-3600 sec		
	Accuracy	+/- 2%	Accuracy	+/- 2%			Analog WD	N/A
	Variables	Selectable	Variables	Selectable				

5. Flight Go-arounds

A flight go-around is an aborted landing on final approach of an aircraft. It is performed by the pilot if it is believed that the correct conditions are not suitable to make a safe landing. Go-arounds as a result of Low Level wind shear and turbulence have resulted in EUROCONTROL establishing a Go-around forum in 2013. (EUROCONTROL, 2013)

5.1 Go-Around Research Data Obtained From Aviation Industry

While researching and obtaining data for this thesis, contact was established with leading stakeholders in the commercial aviation industry. Direct contact was made with Robert Graham who is the head of Airport Research at EUROCONTROL and Marco Gibillini who is the Business Case Expert. EUROCONTROL is an intergovernmental organisation with 41 Member and 2 Comprehensive Agreement States. Their purpose is to deliver a Single European Sky that will help overcome the safety, capacity and performance challenges facing European aviation in the 21st century (EUROCONTROL, 2018). Robert and his team are responsible for Runway Through Research including separation minima and reduction in approach and departure wake separation. They are extremely interested in this thesis and have asked for a copy of the finding and conclusions of the research. EUROCONTROL provided a copy of a 2011 draft report that was never finished into a study of Go-around costs in Europe. This provided some of the ground work and base data for Go-Around research investigation. Contact was made with Peter Gibson who is Corporate Communications Manager with the Civil Aviation Safety Authority in Australia and Steve Neal who is the Section Manager for Government and Corporate Relations with the Civil Aviation Safety Authority. They directed me to contact with the Australian Transport Safety Bureau. The information obtained from the Australian Transport

Safety Bureau enabled the researcher quantify the number of Go-around flights annually as a result of wind shear in Australia. Contact was made with David Hiscotte who is the Head of Operational Support with Air New Zealand, he provided information on the direct cost of a Go-around manoeuvre for an Airbus A320 at Queenstown Airport in the South Island of New Zealand. This information was benchmarked against other sources when calculating final figures. Contact was established with several people and branches of the Federal Aviation Administration in the United States. Bob Stuckert who is the Manager, Flight Inspection Support Sub-Team at Flight Program Operations provided information regarding the direct operational expense for the average commercial airline aircraft. The information provided was used in the calculation of direct costs for the Go-around procedure. Contact was established with Christine Gerencher who is Senior Program Officer - Aviation & Environment with the Transportation Research Board (TRB) in the United States was extremely helpful and engaged several members of her team and department to help with information for this research. The TRB have congratulated the researcher for this challenging work and requested a copy of the findings when completed. Further contact and communications was established with the International Civil Aviation Organisation, the International Air Transport Association and Airbus who provided additional information on Go-Arounds. Technical information relating to Low Level Wind Shear Alert Systems was sought and requested from Vaisala. Vaisala are the world's leading supplier of Low Level Wind Shear Alert Systems for airport runways. They install the majority of LLWAS for the FAA in the United States. Contact and communication was established with David Bullock in the technical support centre of Vaisala who then directed technical communications to Juhani Polvinen the Applications Manager who supplied detailed technical information about

the LLWAS that Vaisala currently install. Information regarding the technical specifications of the Wind Urchin was communicated to Juhani. Vaisala was informed about the 3D wind sampling capability of the Wind Urchin and asked if the Wind Urchin could be integrated into one of their LLWAS. Vaisala indicated that the communication protocols used by the Wind Urchin could be easily integrated into any of their weather systems. After months of ongoing communications back and forth with Vaisala, Juhani stated that "In theory it could replace 3-D ultrasonic sensors". Juhani stated that the National Centre for Atmospheric Research (NCAR) had in the past tested 3-D instruments for LLWAS but not with a modern technology such as the Wind Urchin. Juhani recommended that in order for the Wind Urchin to be considered for use by NCAR, the FAA and Vaisala that a 3-D simulation of a microburst be carried out. This process is beyond the scope of this thesis and could be done as extended PhD research. It would require funding and access to a super computer to perform a CFD modelling of a microburst and a second Wind Urchin to be constructed to monitor microburst activity from two separate points.

5.2 Cost to the Aviation Industry due to Go-arounds

A go-around procedure is performed by the pilot if it is believed that the correct conditions are not suitable to make a safe landing. In a report by the International Air Transport Association (IATA) for the Go-Around Safety Forum (IATA, 2013), it was found that out of 1050 random data samples of Aircraft Safety Reports (ASR) on go-arounds that over 39% listed environmental conditions as the reason for a go-around. 42% of those reports noted wind as the reason for a go-around. A go-around procedure has a cost implication to the airline, passengers and airport. However it should be noted that whatever the cost of a go-around in financial terms, it is insignificant compared to the failure of a pilot to initiate a go-around which results in loss of life,

loss of an aircraft and closure of an airport due to a crash. This scenario occurred at Narita Airport in Japan in 2009 (The Japan Times, 2009), when a FedEx cargo plane crashed into the runway killing the two crew while attempting to land during severe wind gusts and turbulence. The final Aircraft Accident Investigation Report recommended that studies and measures should be taken by the aircraft manufacturer to judge the necessity of a go-around (Japan Transport Safety Board, 2013). Fig 5.1 shows the fatal FEDEX crash at Tokyo – Narita airport.

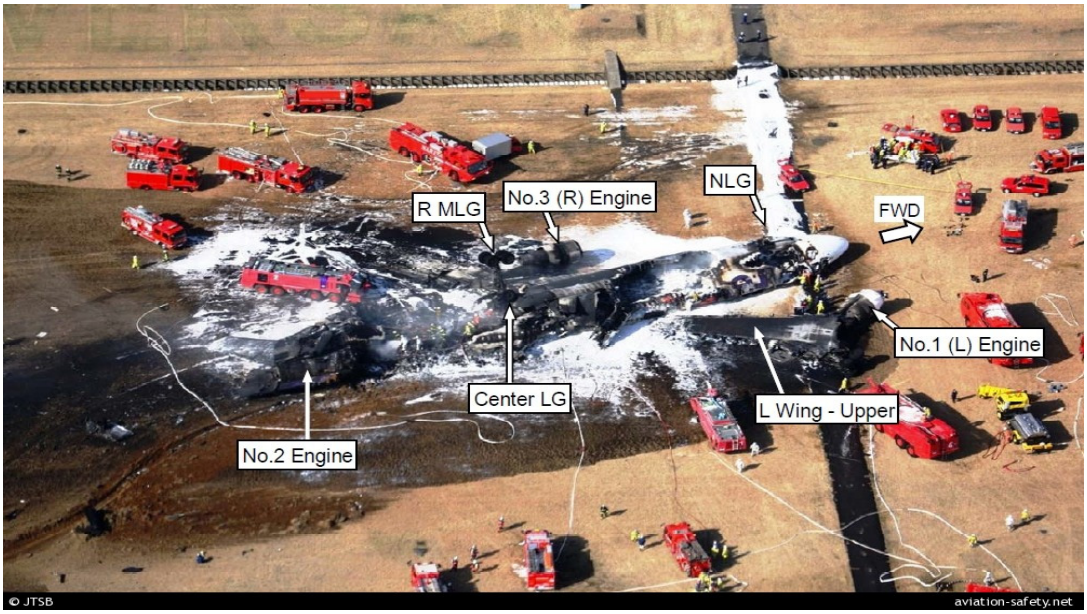

Figure 5.1: FedEx Crash Nariata Airport (Aviation Safety Network, 2009)

There are many factors that can be included to determine the total cost of a go-around, which include airport operational costs consisting of gate delays, baggage fees, knock on cost for other aircraft and passengers. This study will analyse the direct cost of a go-around and include factors such as, fuel, CO_2 emission charges, crew costs and aircraft maintenance. Go-arounds normally take between 10 to 15 minutes to complete (Australian Government, 2008). These figures are from the Australian Civil Aviation Safety Authority which records an average of 800 go-arounds in a typical year making it one of the highest in the world. A go-around time of 15 minutes has been selected

for calculation purposes. The cost of aviation fuel is based on the January 2018 figures from the US Bureau of Transportation Statistics (Bureau of Transportation Statistics, 2018). The CO_2 figures were obtained from an IATA report (IATA, 2010). The Aircraft selected for the calculations are the Airbus A320 and the Boeing 737-800 as these aircraft are the most used for airlines on short to medium haul routes around the world.

A report carried out for Airports Council International – North America which analysed aircraft operating and delay costs stated that the airline direct cost of delay per block minute was $78 per minute. This was broken down into fuel cost, crew cost, maintenance, aircraft ownership and other (Ricondo & Associates, INC., 2014). In a more recent report using the same parameters and breakdown costs, a figure of $62.55 was calculated as the airline direct cost of delay per block minute (Airlines for America, 2016). The lower figure from this report could be due to reduction of aviation fuel from $3.40 a gallon in 2014 to the January 2016 cost of $1.27 per gallon. Table 5.1 illustrates the parameters used in this calculation.

Table 5.1 (Airlines for America, 2016)

Calendar Year 2016	Direct Aircraft Operating Cost per Block Minute	Δvs.2015
Crew-Pilots/Flight Attendants	$21.34	8.7%
Fuel	18.44	-18.5%
Maintenance	12.01	3.3%
Aircraft Ownership	8.06	-8.4%
Other	2.80	-1.8%
Total Direct Operation Costs	**$62.55**	**-4.4%**

Based on todays increased fuel cost, the figure for fuel in Table 5.1 would increase to $29.50 thus increasing the airline direct cost of delay per block minute to $73.61. A go-around procedure taking 15 minutes based on this block figure would have a direct

cost of $1104.15 which at today's rate (26/03/18) equates to €887.41. In a working draft report prepared by the University of Westminster for the Performance Review Unit EUROCONTROL (Teunissen & Bernard Lacroix, Cost of a Go-around, 2011), a base figure for an Airbus A320 to complete a 10 minute go-around was calculated to be €460, the figure for a 15 minute go-around would calculate to be €690. This figure was calculated based on figures for fuel used during the go-around phase, CO_2 emitted, crew cost, maintenance cost and passenger cost. During an email correspondence with Air New Zealand Head of Operational Support (Hiscotte, 2018), it was stated that the cost of a go-around for an Airbus A320 was $1500 NZD in terms of direct costs, which at today's rate (26/03/18) equates to €878.43. During ongoing correspondence with the Manager, Flight Inspection Support Sub-Team, Flight Program Operations of the FAA, it was communicated that an 8 minute go-around was likely to be $706.53 for a Boeing 737 aircraft. This would equate to $1324 for a 15 minute go-around. This converts to €1064.69. Table 5.2 is a calculation for a 15 minute go-around procedure for an A320 and B737.

Table 5.2 Go-around Calculated Costs

Aircraft	Go-Around Flight Phase 15 Minutes								Crew	Service Maintenance	Aircraft Ownership	Total Cost
	Climb 1 Min		Holding 11 Min		Descent 3 Min		1 Kg Jet A = 3.15Kg CO_2		1 Gallon Jet A = $2.04 1 Gallon Jet A = 3.04 Kg 1 Kg = $0.67 = €0.55 $1 = €0.81			
	Fuel		Fuel		Fuel		CO2		€17.20 / Min	€9.72 /Min	€6.53 /Min	
	Kg	€	Kg	€	Kg	€	Kg	€	€	€	€	
Airbus A320	114.10	62.73	378	208	101.52	55.83	542.86	7.63	258.07	145.92	97.93	836.11
Boeing 737	120.10	66.07	398.2	219	113.76	62.57	575.18	8.34	258.07	145.92	97.93	857.90

The aircraft engine type details for the Airbus A320 was obtained from the manufacturers specifications (Airbus, 2018). The engine type for the Boeing 737-800

was obtained from the manufacturers technical specifications (Boeing, 2018) The Fuel data burn figures for each stage of the go-around phase has been obtained from the ICAO engine exhaust emissions data bank for the exact engine type used on each aircraft in Table 5.1 (ICAO, 2018). The CO_2 European emission allowance has been calculated at €14.05 t/CO_2 as at the time of research (Business Insider, 2018). The figures calculated in Table 5.2 have been computed using the latest data available for fuel, CO_2 emissions, engine fuel and emissions data from the relevant aviation sectors, authorities and aircraft manufacturers at the time of conducting this research. The go-around calculations have only taken into account the direct cost for this procedure. Other costs such as airport costs for baggage, gate costs, passenger costs and other associated costs have not been factored into to the calculations, due to the unobtainability of certain data from airport authorities. Table 5.3 is a comparison of the calculated direct cost go-around figures of this research with figures supplied by personnel in the FAA and Air New Zealand.

Table 5.3 Comparison of Go-around figures for Sampled Aircraft

Aircraft	Thesis Figures	FAA Figures	Air NZ Figures	Airlines for America	Average Figures
Airbus A320	€836.11	N/A	€878.43	€759.98	€824.84
Boeing 737	€857.90	€1065.69	N/A	€759.98	€894.52

It can be seen from Table 5.3 that a conservative figure of €800 could be taken for the purpose of calculating the total costs of go-arounds for a short to medium haul aircraft as shown. Despite exhaustive inquiries, it has been very difficult to obtain information to calculate exact figures for the Super Heavy Airbus A380. However using the engine details for the Engine Alliance GP7272 from the ICAO data bank and taking into account the four engines, additional crew numbers, additional maintenance and

ownership costs. A figure for a 15 minute go-around would be in the region of €2933 based on the same criteria used in Table 5.3.

Figures for the number of aircraft go-around manoeuvres are not recorded by every aviation authority in each country. In correspondence with the CAA in the UK, they communicated that they did not record flight go-arounds as they considered them to be a normal phase of a flight, so therefore had no go-around figures as they are not recordable (Chatfield, 2017). Despite many emails, correspondence and contacts with the FAA in the USA, it has been impossible to get any figures or data relating to go-around numbers in the US. The FAA in a reply stated that it has not put a cost on go-arounds in general but clearly they are costly and something the FAA would like to reduce (Management, 2018).

In correspondence with Alaskan Airlines, it was requested if they had information on the number of go-arounds in Alaska as this region is very prone to low level wind shear occurrences, they stated that this was not a figure that they shared publically (Alaskan Airlines, 2018). Many leading commercial companies were contacted but most companies did not to the request for go-around information. American Airlines in a reply stated that a go-around was not something that they tracked and that American Airlines has a no-fault go-around policy, recognizing that a successful approach can end in a missed approach (American Airlines, 2018). Delta Airlines stated in their reply that they are unable to accommodate any request for information on go-around costs or numbers and that it is proprietary information and which they are not able to share (Delta Airlines Inc, 2018). In a correspondence with the IATA they stated that they do not have such information on the cost of go-arounds, either generally or specific to aircraft model (Flint, 2018). The ICAO stated that they did not have any figures on go-arounds (Raillant-Clark , 2018). EUROCONTROL in Brussels

conveyed the same information that they did not have records of go-arounds for the EU but were extremely helpful in providing a copy of a unfinished draft report into the cost of a go-around (Teunissen & Bernard Lacroix, Cost of A Go-around, 2011). In Australia the Civil Aviation Safety Authority (CASA) has a web page dedicated to go-arounds which informs passengers and the public about this procedure and why it may be necessary. The CASA states that over 800 standard go-arounds are performed in a typical year (CASA, 2018). In 2017 there were 94,169 inbound international flights to Australia (The Department of Infrastructure, 2017). The Super Heavy Airbus A380 made up 7300 of these flights. This represents 7.75% of the total number of inbound flights. Base on the CASA figures of 800 go-arounds in a typical year, 7.75% would amount to 62 flights. Based on the figures calculated for the Medium haul flights and the A380, a conservative estimate cost for the 800 go-arounds each year in Australia would be €776,400 or $1.2 million Australian dollars. Given the increasing volume of airline passengers to Australia it is logical to assume that the number of go-arounds will increase unless there is better detection and forecasting of wind related events around the terminal and runway areas. The 800 Go-around flights in Australia represent 0.84% of the total incoming flights annually. There are over 106,000 flights every day taking off and landing around the world (FlightAware, 2018), if we applied the same percentage figures from Australian to these flights performing a Go-around, this would cost the aviation industry €320 million in direct costs every year based on the criteria used for the Australian model. Incorporating a system that could prevent a substantial number of Go-arounds would not only provide massive savings to airlines but increase safety to passengers and increase airport throughput and efficiency for airports, airlines and passengers.

6. Brief Overview of Wind Urchin

The Wind Urchin is a sphere shaped instrument capable of measuring wind speed and direction in 3D using sensor activated Pitot tubes mounted equally around its surface. The Wind Urchin was developed by researchers from DIT's Energy Resource Group led by Dr. Derek Kearney. The Wind Urchin was developed to estimate accurately the precise wind yield that would be available for the location and sighting of wind turbines. Research carried out by DIT identified that miscalculation of wind as a resource had resulted in lower than expected electrical energy output from wind farms resulting in investor caution for this sector. The Wind Urchin with its increased sampling and 3D measuring capability could provide greater accuracy when assessing the viability of a potential site for the construction of wind farms leading to increased investor confidence in site survey predicted figures for energy output. Fig 6.1 illustrates the Wind Urchin.

Figure 6.1: Wind Urchin (ERG, 2018)

The Wind Urchin is a multidirectional anemometer which measures wind in 3D using 64 Pitot tubes mounted and spaced equally around the surface of a sphere shaped

hardened plastic moulded design. The Wind Urchin can sample at frequencies up to 3,000 Hz providing three dimensional data on wind speed and direction. This unique design gives the Wind Urchin the ability to measure wind shear, wind veer and low level turbulence. The Wind Urchin can output in digital or analogue format enabling the device to be integrated into a LLWAS at airport runways. It has been shown and discussed in previous chapters that despite advances in LLWAS technology, there continue to be air accidents as a result of low level wind shear during the take-off and landing stages of flights. The integration of the Wind Urchin into a LLWAS will give greater accuracy of wind speed, direction and the presence of low level wind shear. The 3D capability of the Wind Urchin can measure and illustrate wind data in three dimensions. Because of the increased sampling rate of the Wind Urchin, wind data can be recorded at a frequency of 100 Hz producing 64,000 data points per second producing a greater number of samples than any other anemometer currently used in aviation for a specific timeframe. The device has a wide measuring range to measure wind speed from 0-250 m/sec. The device is made from a durable hardened plastic material, there are no moving parts ensuring that this is a low maintenance device, low cost durable instrument suitable for all environments and weather conditions.

6.1 Detailed Description of Wind Urchin Technology

The Wind Urchin is a device consisting of 64 pitot tubes orientated and positioned eqiangularly and extending radially about a sphere. The pitot tubes extend to a distance of 100.0 mm from the surface of the sphere body such that the pressure readings at the distal end or tip of each tube are taken in as close an approximation to free flow conditions as is possible. This distance has been determined as the optimum distance away from any distorted flow that is known to occur in the vicinity of the surface of any bluff body placed into a free flow stream. A pitot tube is a pressure measurement

device which works by measuring a differential pressure and is used to measure fluid flow velocity. This device was first invented in the 18th century and further modified to its present design in the late 19th century. The device is used in many industrial applications for the measurement of air, liquid and gas flow velocities. It is extensively used in the marine and aviation industries where pitot tubes are used to measure the speed of a vessel travelling through the water or to measure the airspeed of an aircraft. Fig 6.2 shows the static Pitot tube fixed to an Airbus A380 aircraft for the measurement of aircrafts airspeed, which determines the dynamic pressure of the airflow past the aircraft. Other Pitot tubes mounted on the aircraft are used to measure the aircrafts altitude or height above the ground as well as the aircrafts rate of climb and rate of descent. Fig 6.3 illustrates a diagram of a simplified pitot static system used for aircraft.

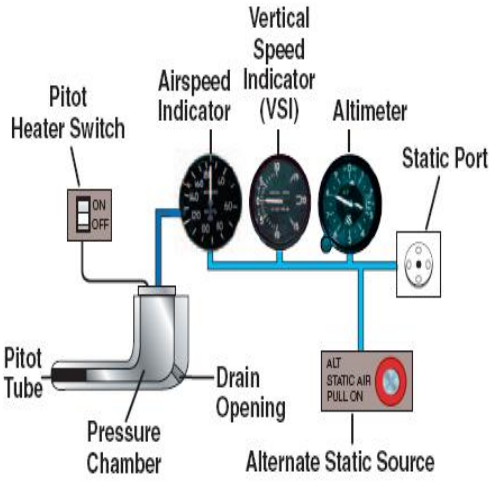

Figure 6.2: Pitot Tube on Airbus (Monniaux, 2007) **Figure 6.3: (FAA, 2018)**

The Pitot tube measures the local flow velocity at its fixed point on the sphere of the Urchin in the wind flow stream, individual pressure signals are continuously received at the distal points of each of the Pitot tubes. These pressure signals propagate at a known speed through the tubes, which are pneumatically sealed to lengths of polyurethane pressure tubing. In the case of the static Pitot tube on the Airbus aircraft,

Bernoulli's principle is used to calibrate the airspeed indicator so that it displays the indicated airspeed appropriate to the dynamic pressure. Bernoulli's principle is also used to determine the wind speed measured by the Wind Urchin. Bernoulli's principle states that an increase in the speed of a fluid occurs simultaneously with a decrease in pressure, so pressure and density are inversely related. From this principle the Bernoulli equation conceives of pressure as a point property that can vary from point to point throughout a fluid, from which a differential equation may be derived relating pressure and velocity. This in effect means that every point in a steadily flowing fluid, regardless of the fluid speed, has its own unique static pressure and dynamic pressure and the sum of these is defined to be the total pressure. Bernoulli's equation may be summarized in the following word equation: static pressure + dynamic pressure = total pressure (Princeton University, 2018). In applying this to the quantity of interest - the measurement of free air flow the total pressure is the sum of the static or atmospheric pressure plus the dynamic pressure (the pressure caused by the moving air that is sampled at the tip of the Pitot tube where the fluid flow is brought to rest – it "stagnates"). In order to determine the fluid velocity the fluid density must be known. The complete expression of Bernoulli's Equation contains the following as shown in Eq: 6.1.

Eq: 6.1

$$\frac{v_1^2}{2} + gz_1 + \frac{P_1}{\rho} = \frac{v_2^2}{2} + gz_2 + \frac{P_2}{\rho}$$

This can be used to derive a formula for converting the pressure recorded by the pressure sensors to wind speed. The overall height of the current MTP is just 3 m so any atmospheric pressure difference due to height is negligible so height: as illustrated in Eq:6.2

Eq: 6.2 $$z_1 - z_2 = 0$$

So Eq: 6.1 becomes:

Eq: 6.3 $$\frac{v_1^2}{2} + \frac{P_1}{\rho} = \frac{v_2^2}{2} + \frac{P_2}{\rho}$$

V_1 relates to the point where total pressure is equal to static pressure so v_1 equals to zero, so Eq. 6.1 becomes:

Eq: 6.4 $$\frac{P_1}{\rho} = \frac{v_2^2}{2} + \frac{P_2}{\rho}$$

Rearranging this equation we get Eq. 6.5 (Newfoundland, 2018)that relates dynamic pressure to velocity:

Eq: 6.5 $$v_2 = \sqrt{\frac{2(P_1 - P_2)}{\rho}}$$

This equation indicates that the relationship between velocity and pressure for the system is nonlinear as illustrated in Fig 6.4

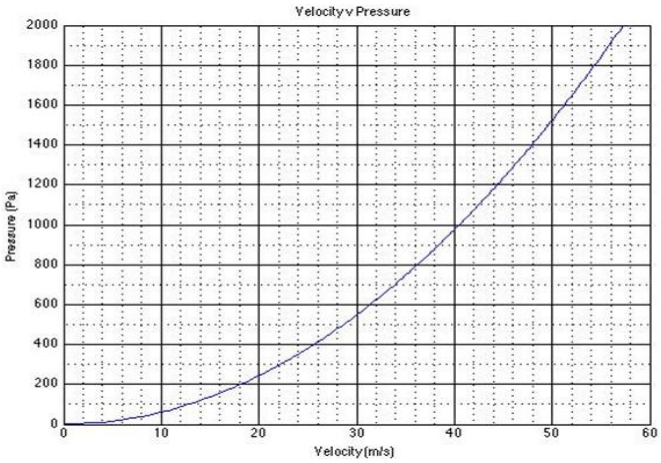

Figure 6.4 : Conversion of air pressure to wind velocity (Kearney, 2014)

Once the Wind Urchin is in a wind flow stream, the wind acting on the pressure tubing housing the Pitot tubes causes pressure signals propagate at a known speed through

the tubes. The ends of the tubes are connected to pressure sensors known as transducers. The sensors used are silicon piezo resistive pressure sensors which produce an electrical signal as a result of the pressure imposed on it. The pressure sensor used in the Urchin is an NPH series Low pressure solid state sensor that is widely used in pneumatic control systems and in the aviation industry for use in altimeters, barometers and to monitor and maintain cabin pressure. A constant current excitation to the sensor produces a voltage output that is linearly proportional to the input pressure. The dynamic pressure as a result of the wind at the tips of the tubes is transmitted to the sensors micro machined diaphragm causing a change in the value of the piezo resistors which is then amplified by a Wheatstone bridge configuration. A signal up to 100 mV is then outputted proportional to the pressure. Additional standard signal conditioning circuitry can be used to amplify the 100 mV output signal. A laser-trimmed, thick-film resistor network on a hybrid ceramic substrate within the sensor, provides temperature compensation, and a thermal accuracy full scale output (FSO) of 0.5% (Amphenol, 2018). Fig 6.5 depicts the NHP sensor and Fig 6.6 illustrates the Wheatstone configuration of the sensor.

Figure 6.5: NPH Pressure Sensor (Amphenol, 2018)

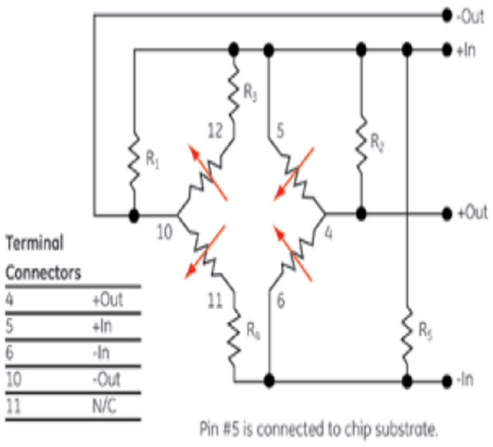

Figure 6.6: NPH Schematic Diagram

Additional amplification circuitry was installed to boost the signal and to negate interference from other devices. A Gage – 3000 general purpose transducer signal

interface board was chosen to provide the amplification and smoothing required. Fig 6.7 illustrates the Gage 3000 General Purpose Transducer Interface Board.

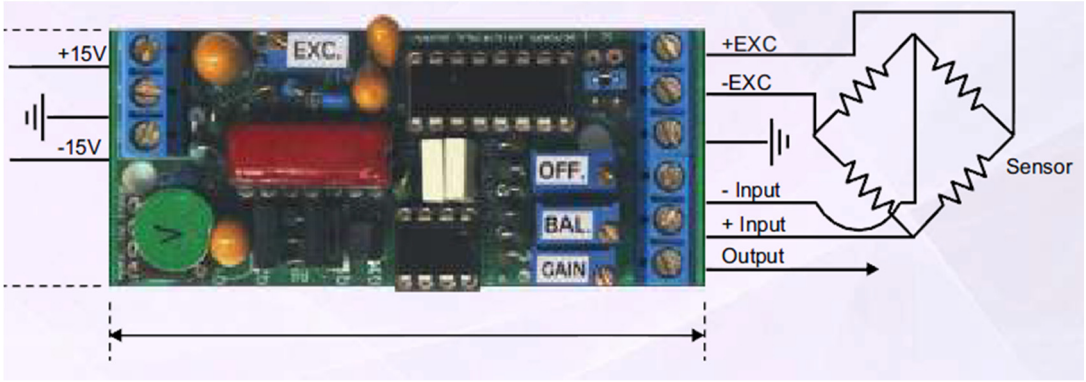

Figure 6.7: Gage 3000 General Purpose Transducer Interface Board (A.A.Lab Systems, 2018)

The NPH sensor outputs are 0 - 100mV for a range of 0 - 2.5 kPa, the pressure at the dynamic port P_2, is:

Eq: 6.6

$$P_2 = \frac{V_{GE}}{4x10^{-5}}$$

The final equation for converting the pressure at the Pitot tube to velocity (m/s) is:

Eq: 6.7

$$v_2 = \sqrt{2\left(\frac{V_{RIO}}{\frac{0.0068}{\rho}}\right)}$$

Data logging from the Wind Urchin is accomplished using the National Instruments CompactRIO Single-Board Controller. It is designed for high-volume and OEM embedded control and analysis applications that require high performance and reliability. Featuring an open embedded architecture (National Instruments, 2017). This controller is driven by a 667 MHz dual-core ARM Cortex-A9 processor. The controller is very versatile with Digital and Analogue outputs. The board has output ports for RS232, RS485, USB, CAN and Ethernet making it easily integratable with

the circuitry of the Wind Urchin. Fig 6.8 illustrates the outputs available from the controller.

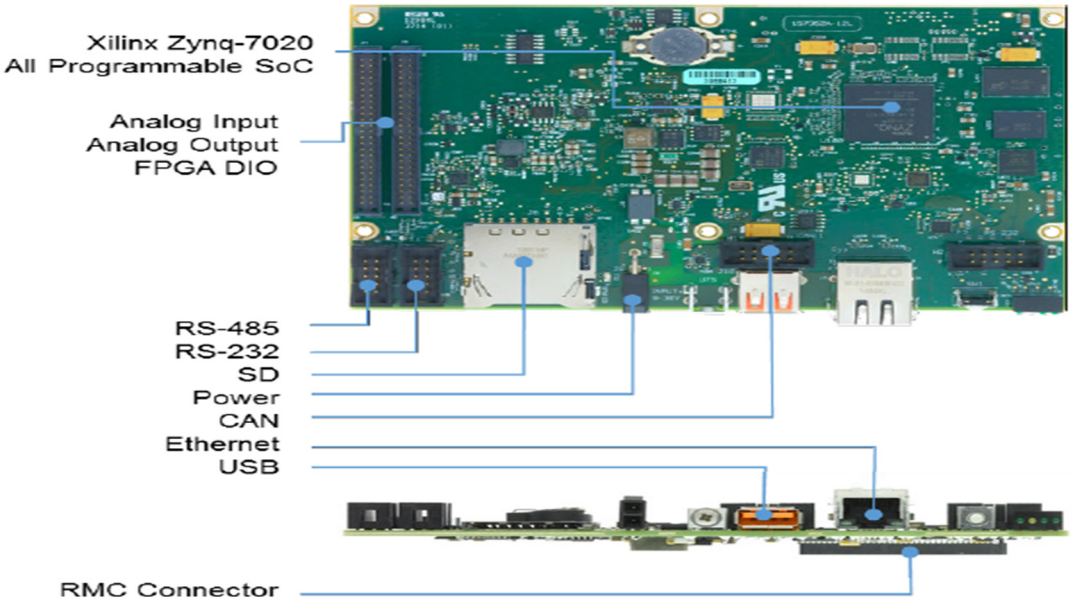

Figure 6.8: CompactRIO Single-Board Controller (National Instruments, 2017)

LabVIEW, the proprietary software for NI, was installed on a Microsoft Windows platform to record and display the logged data. LabVIEW contains 1,000 built-in signal processing, analysis, control, and mathematics functions to accelerate the development of embedded control and monitoring systems. Its high speed signal processing allows algorithms to be controlled directly in hardware to maximize reliability and determinism. A screen shot of the custom software programmes written to enable the CompactRIO to sample, and record the data from the signal conditioning boards, convert it to digital form, and transmit it to the laptop Data-logging, control, and graphical displays were required for the proto-type Multi-tube Probe. Fig 6.9 illustrates the data logging for the Urchin in LabVIEW.

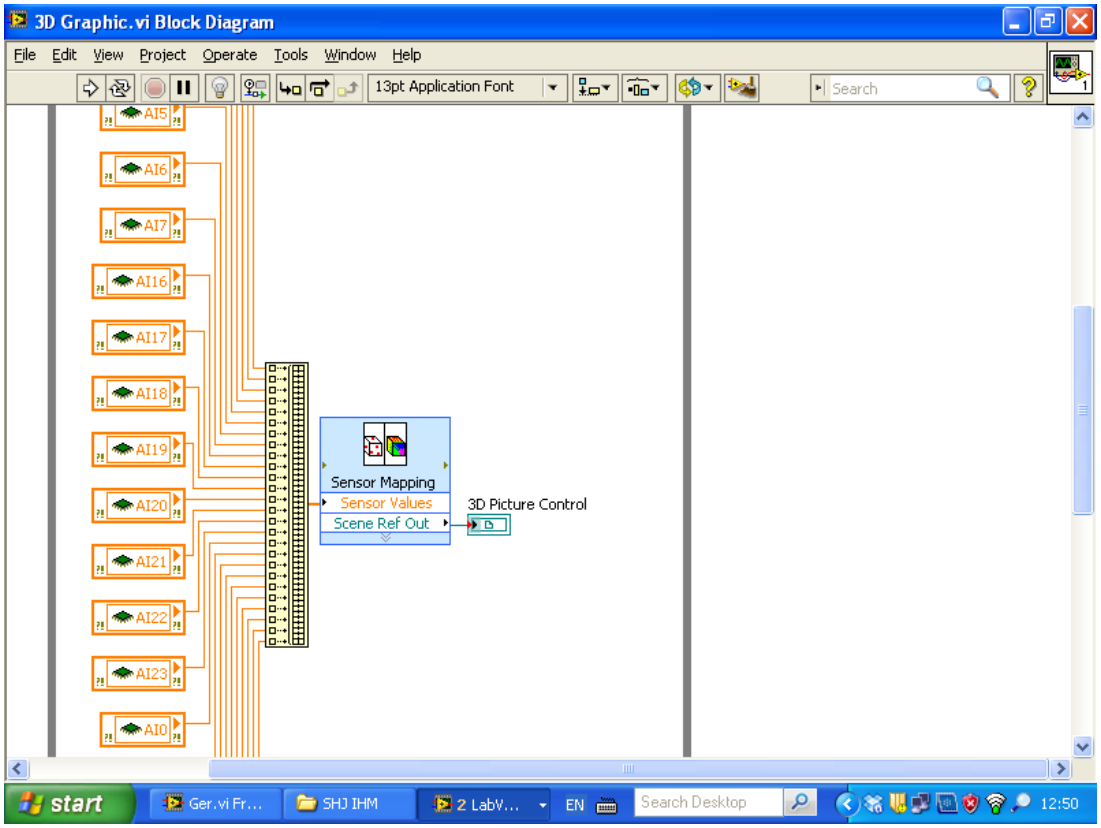

Figure 6.9: LabVIEW Screenshot for Data Logging of the Wind Urchin (Kearney, 2014)

6.2 Computer Programme to Analyse and Recorded Wind Data

The data recording, sampling and analysing for the Urchin was achieved using National Instruments LabVIEW graphical programming language and R Programming language to obtain the wind speed and direction acting on the Urchin. LabVIEW is the proprietary software designed to configure projects using the CompactRIO controller from NI. The CompactRIO stands for Compact Reconfigurable Input/output (CRIO). The CRIO is connected directly to a pc by an Ethernet cable. The CRIO is then given a unique IP address, which then allows remote login to the device. The CRIO was then formatted, identified and configured for use with the Wind Urchin and prepared for programming with the LabVIEW software. The CRIO has Analogue input modules connected to it which are plugged into a backplane, which allows the controller to read the analogue values from the Pitot sensor circuitry as illustrated in Fig 6.9. The Analogue input modules shown are AI5

to AI20 on the screen shot in Fig 6.9. The actual outputs from the Pitot tubes was stored as a TDMS file (Technical Data Management Streaming). TDMS is a NI proprietary format that is used for measuring data. It is ideally suited for the Urchin as it enables large amounts of data to be streamed at high speeds and is easily executable and exchangeable. There are two types of data contained in the TDMS file format, they are Meta data which contains names and properties and raw data which contains the measurement data in binary format. In the TDMS setup a sampling frequency of 100 Hz was selected at a sampling rate of 6400 times per second to poll the Pitot tubes. Fig 6.10 illustrates the sampling setup window in the LabVIEW software.

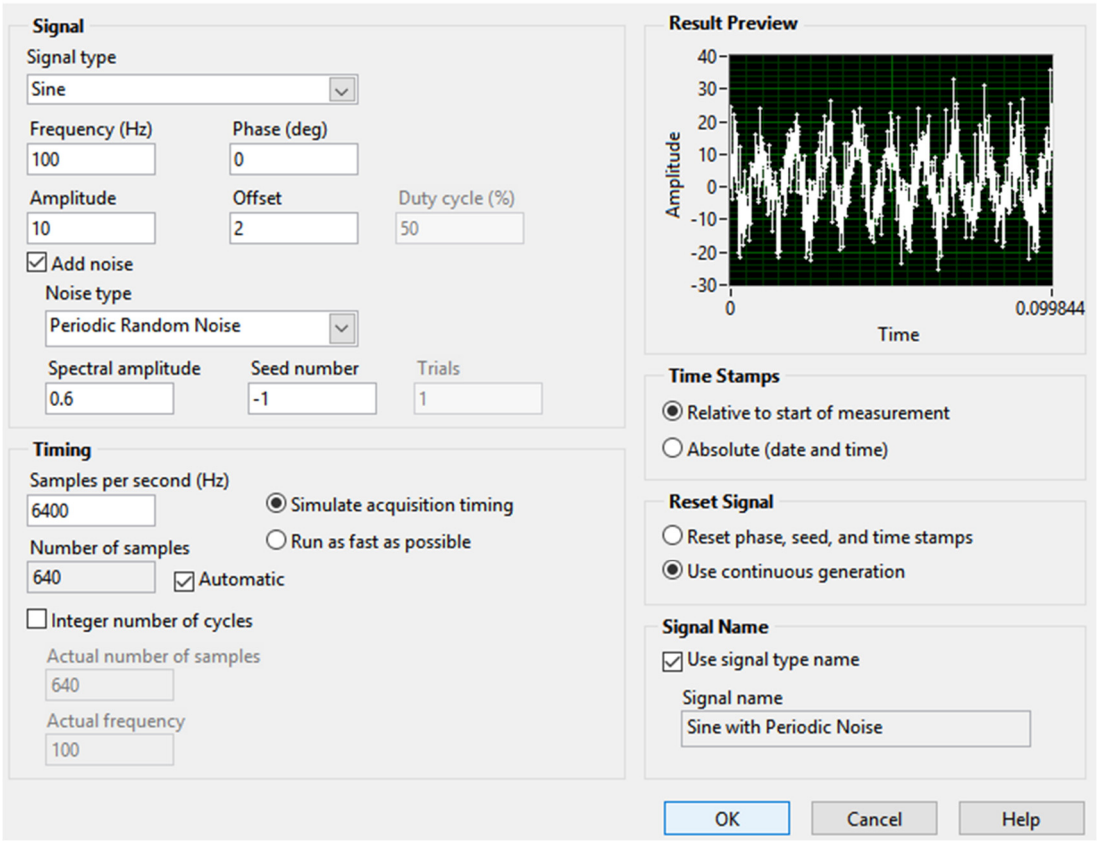

Figure 6.10: Signal Sampling for TDMS File Input

This data was streamed and logged to hard drive, where it was then converted to csv format for further manipulation. Fig 6.11 illustrates the TDMS convert to csv screen shot within the LabVIEW software.

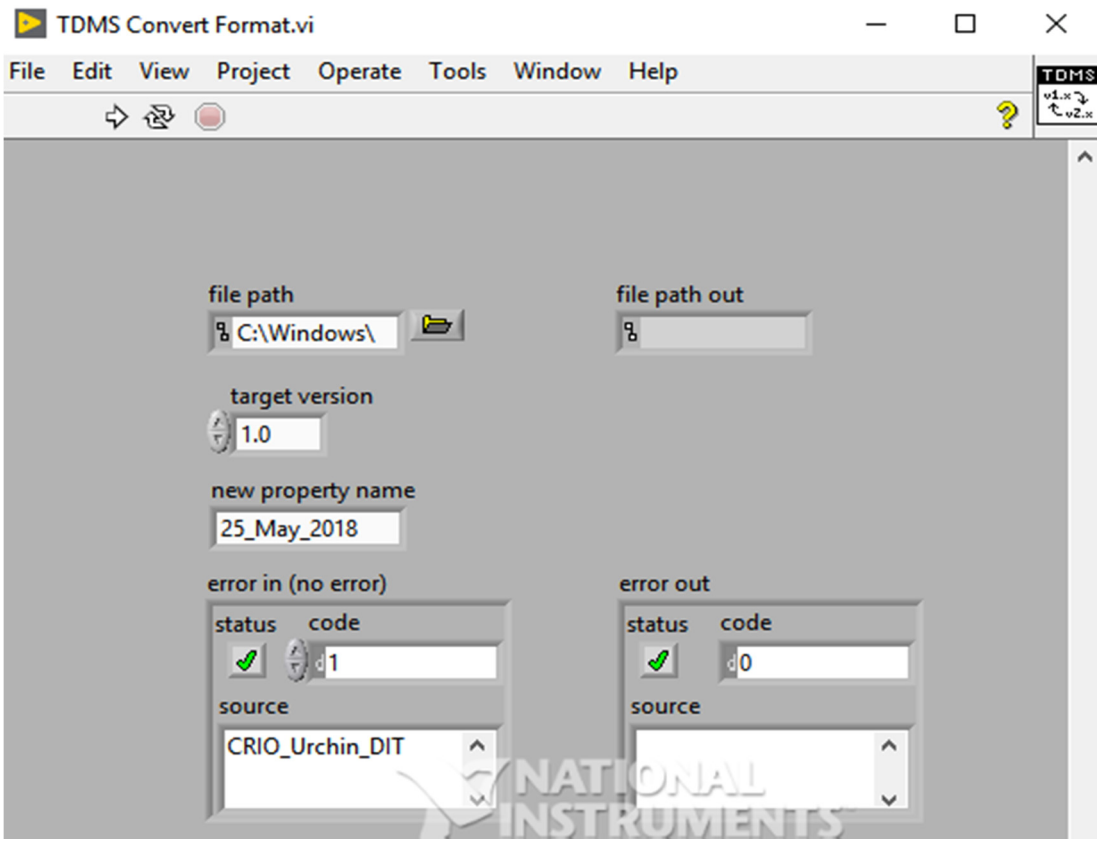

Figure 6.11: TDMS Convert to CSV file

A reference or Datum file is required to access the linear tested values of each Pitot tube. As stated, a Pitot tube is a device which has a differential pressure which is proportional to the square of the incident velocity. The pressure in each tube was recorded 100 times/sec and stored in a digital count. The pressure in each of the Pitot tubes is linearly related to the digital count. The parameters for this relationship were stored as csv values in a file known as the Baseline file. The TDMS converted file and the values of the Baseline file provide two of the component files required to determine the wind pressure being applied to each of the Pitot tubes. In order to determine the wind direction, it is necessary to know where each individual tube is located on the sphere. Each Pitot tube was referenced by its location on the sphere. This was done by creating a grid map of the sphere with the longitude and latitude co-ordinates of each tube referenced with the angles measured in radians. Fig 6.12 depicts the plan grid map layout for the Pitot tubes on the sphere.

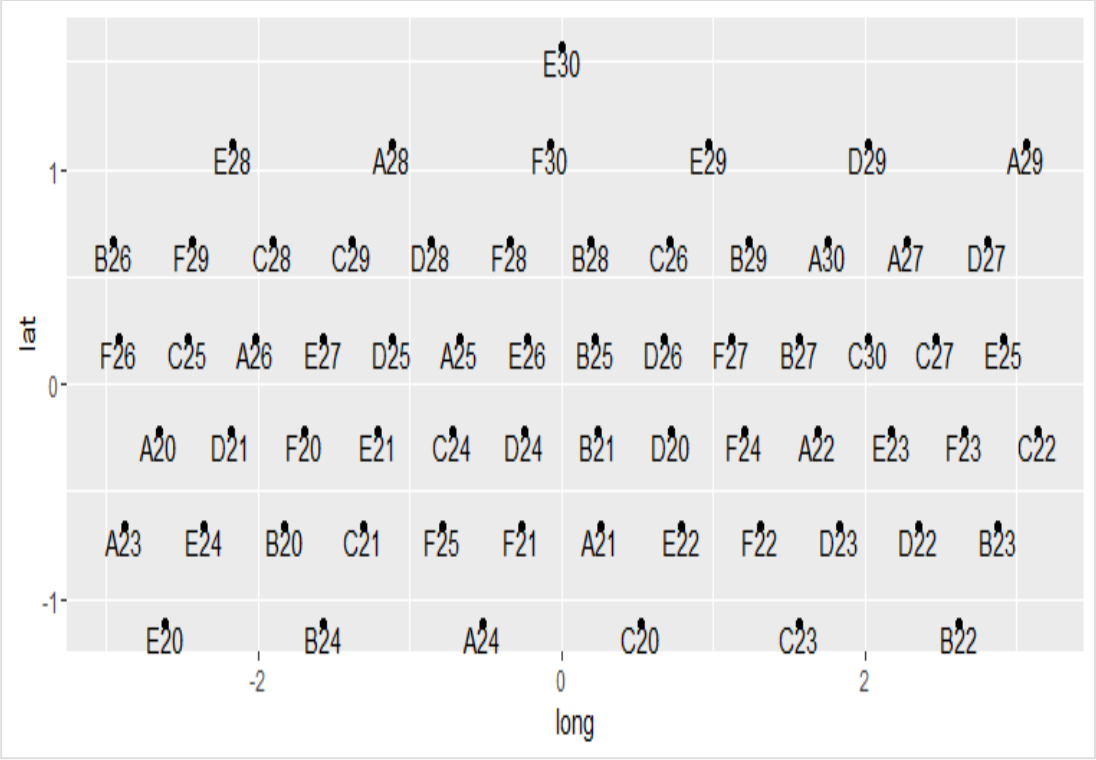

Figure 6.12: Pitot Tube Grid Map

The data for the Pitot locations on the sphere were stored in a Pitot position file and the information was saved as a CSV file. The three CSV files are then read and computed by a computer programme using the R programming language. R programming is used extensively for statistical computing and graphical techniques including linear and non-linear modelling and time series analysis making it ideal for use with the Urchin project. An R program was written and compiled to read the data from the three CSV files mentioned above, the program converts the digital counts into pressure values using the linear relationship from the parameters stored in the baseline file and calculates 1 second averages. The R program then determines the Pitot tube with the highest pressure value for each second interval in the sampled period. It must be noted that the sphere has a North referenced Pitot tube which is aligned to magnetic North for aviation applications and true North for wind turbine alignment applications. The R program designates the wind direction to the values of the Pitot tubes geographical location on the sphere using parameters in the Pitot

position file. The program designates the wind speed to the value proportional to the square root of the Pitot tubes pressure differential. The program then does a non-linear least squares optimization, centred on that designation, to determine both the velocity and direction of the wind. The program then outputs the wind speed and direction as a function of the time. Fig 6.13 depicts the Vertical wind direction and output graph from the R program for the recorded time stamp.

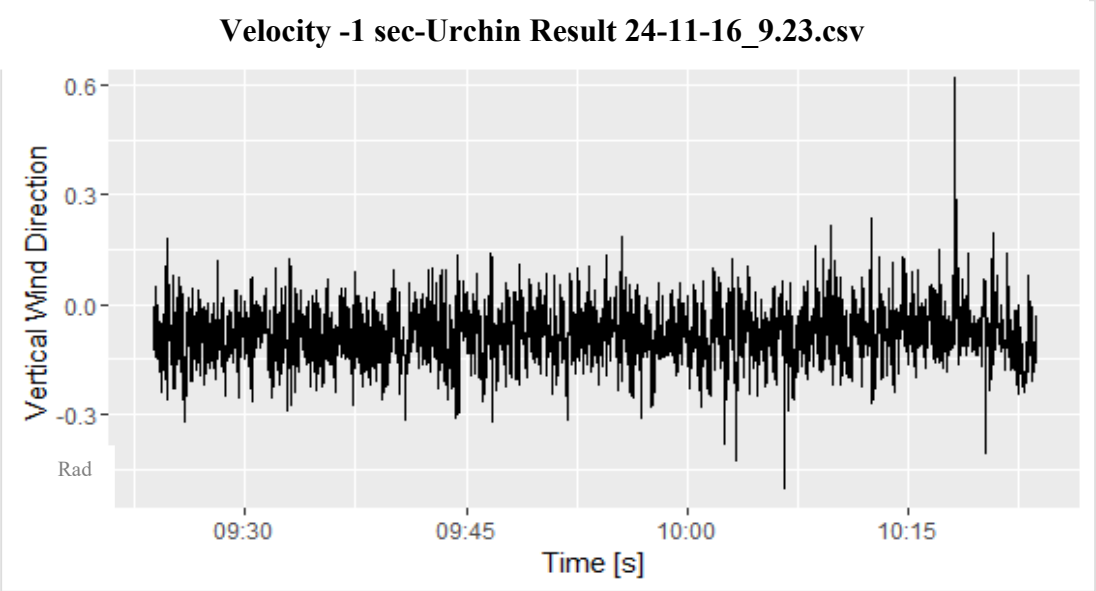

Figure 6.13: R-Code Output Vertical Wind direction Graph

Fig 6.14 depicts the Horizontal wind direction and output graph from the R program for the recorded time stamp.

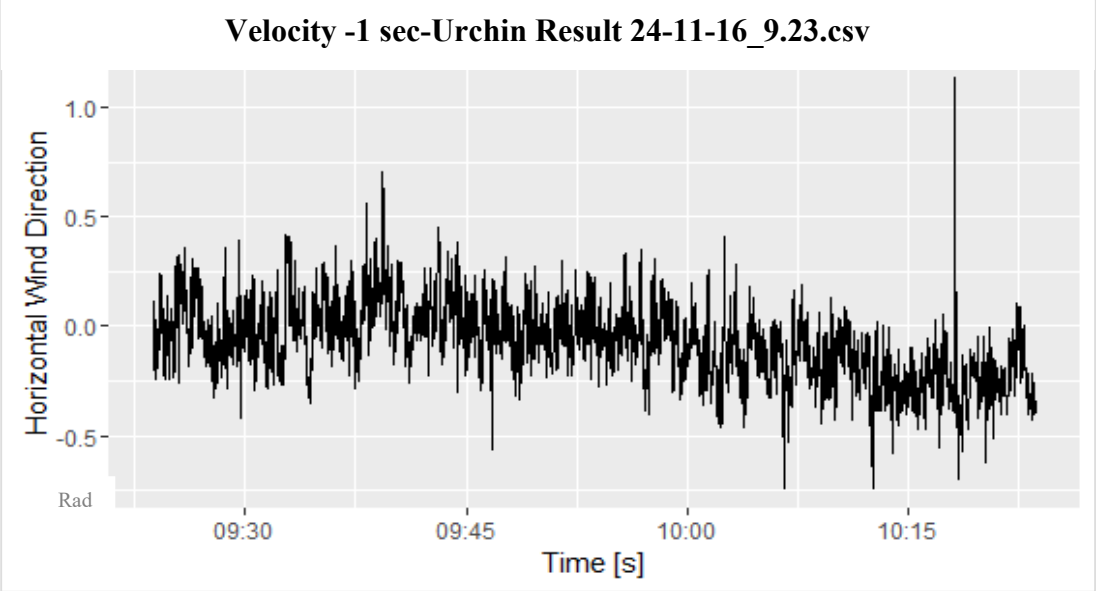

Figure 6.14: R-Code Output Horizontal Wind direction Graph

The output from the R program for the wind speed is shown in Fig 6.15 for the recorded logged data on the date and time shown below.

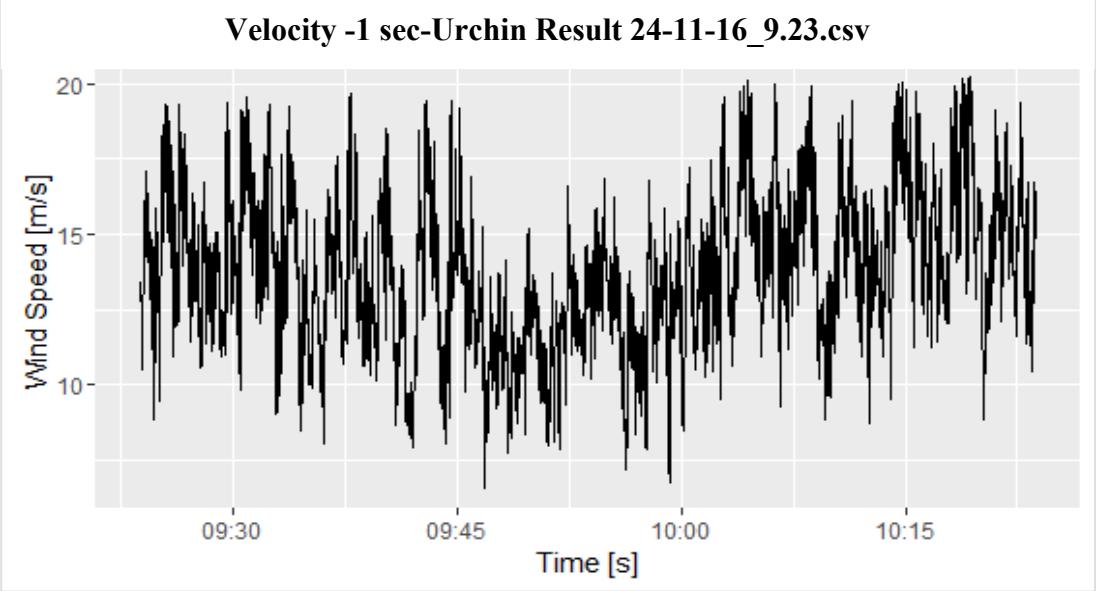

Figure 6.15: R-Code Output Wind Speed Graph

6.3 Compare Wind Urchin Data Against On site Wind Instruments

During field trials at the Baldonell aerodrome data was recorded from the runway cup anemometer and compared to that recorded from the Wind Urchin for the same time

period. Fig 6.16 shows the runway at the Casement Aerodrome in Baldonnell with the position of the mast for the runway anemometer and wind Urchin.

Figure 6.16 : Baldonnell runway and Urchin Location (sensor, 2018)

Fig 6.17 show the proximity of the Urchin to the anemometer. The Urchin was fixed at the same height as the adjacent anemometer.

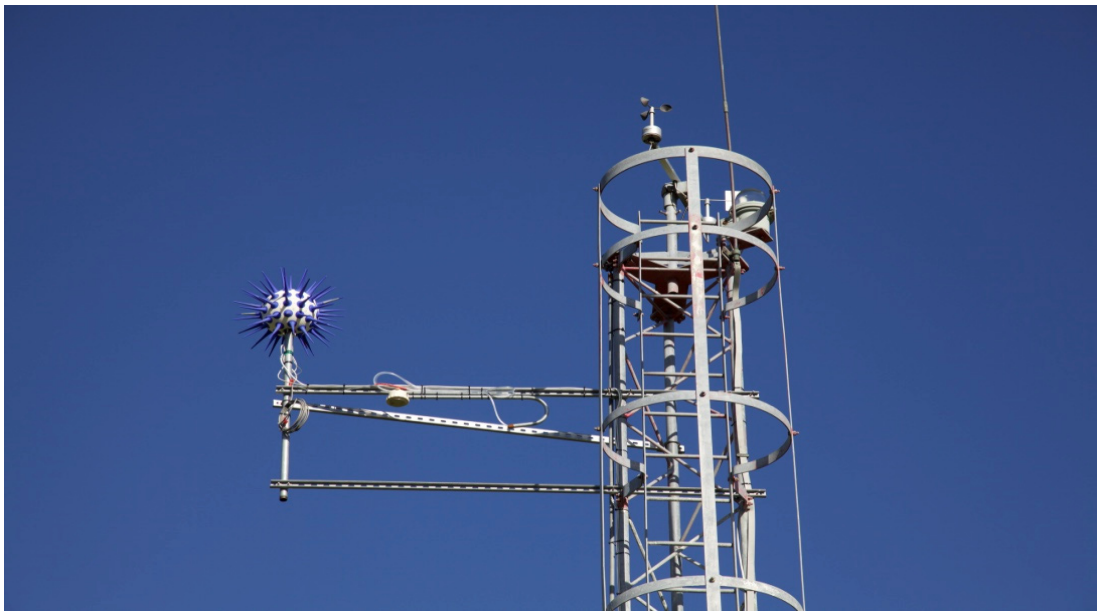

Figure 6.17: Urchin Position Baldonnell (ERG, 2018)

The cup anemometer can only measure horizontal wind speed as it only produces a singular scalar quantity and therefore does not measure total speed. The relative speed of a cup anemometer will vary with the angle of the wind as illustrated in the characteristic curve for the anemometer in Fig 6.18. Fig 6.18 illustrates the angular characteristics of the anemometer and the response of the anemometer to varying angles of wind speed attack. The wind speed to be measured is defined as the average magnitude of the horizontal component of the instantaneous wind velocity vector which means that the anemometer should not be sensitive to vertical components of wind speed and the ideal response is illustrated in Fig 6.16 by the cosine shaped wave. In Fig 6.16 it can be seen that a 10% error is shown when the anemometer is tilted at 25° to the horizontal. Fig 6.18 illustrates measurements taken at 5, 8 and 11 m/s showing errors ranging from 8 to 10%.

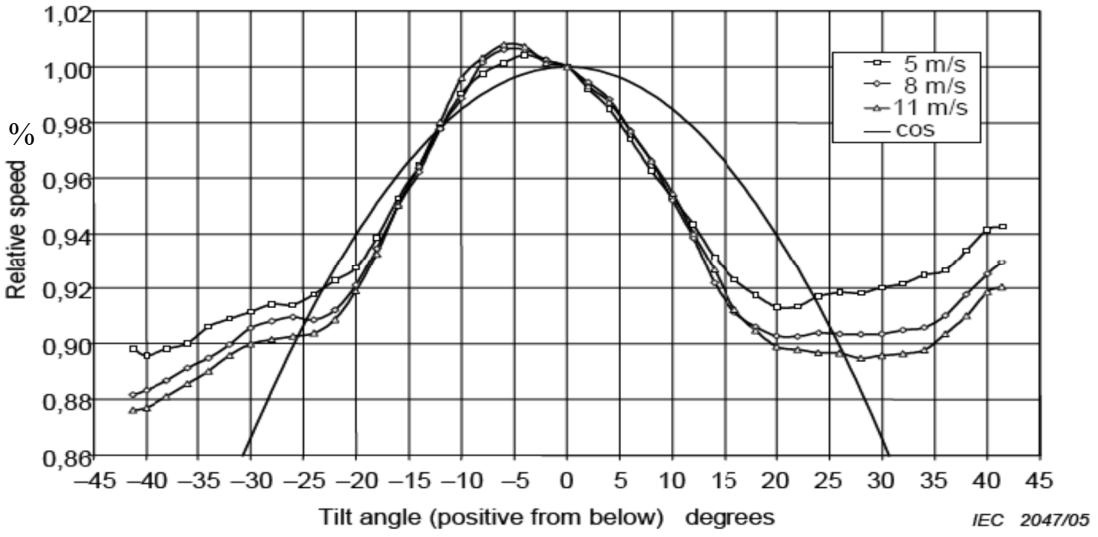

Figure 6.18: Performance Characteristics of A Cup Anemometer (J.-Å. Dahlberg, 2006)

Even today the latest cup anemometers tests in wind tunnels cannot detect the vertical wind component. In contrast the Wind Urchin measures the wind in 3D using 64 Pitot Tubes spread equally around its body with a sensor attached to each one. The Wind Urchin was positioned and orientated to magnetic North with respect to its North

referenced Pitot tube. The flat two dimensional grid reference of the Wind Urchin is illustrated in Fig 6.19.

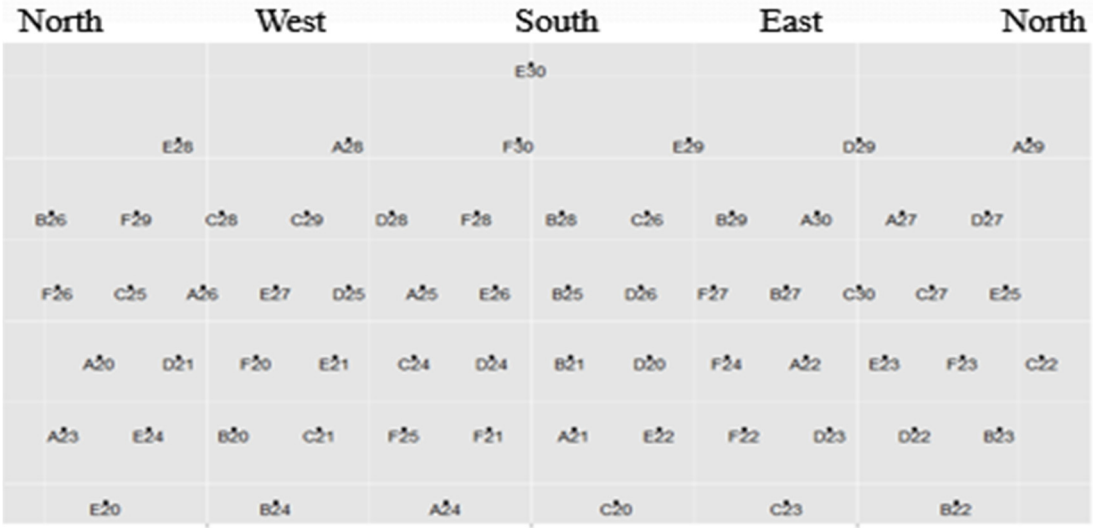

Figure 6.19: Wind Urchin Pitot Tube Grid Layout

As the wind hits the device, it maps out the direction by averaging the data from each sensor showing speed and direction but also wind shear and wind veer as illustrated by Fig 6.20.

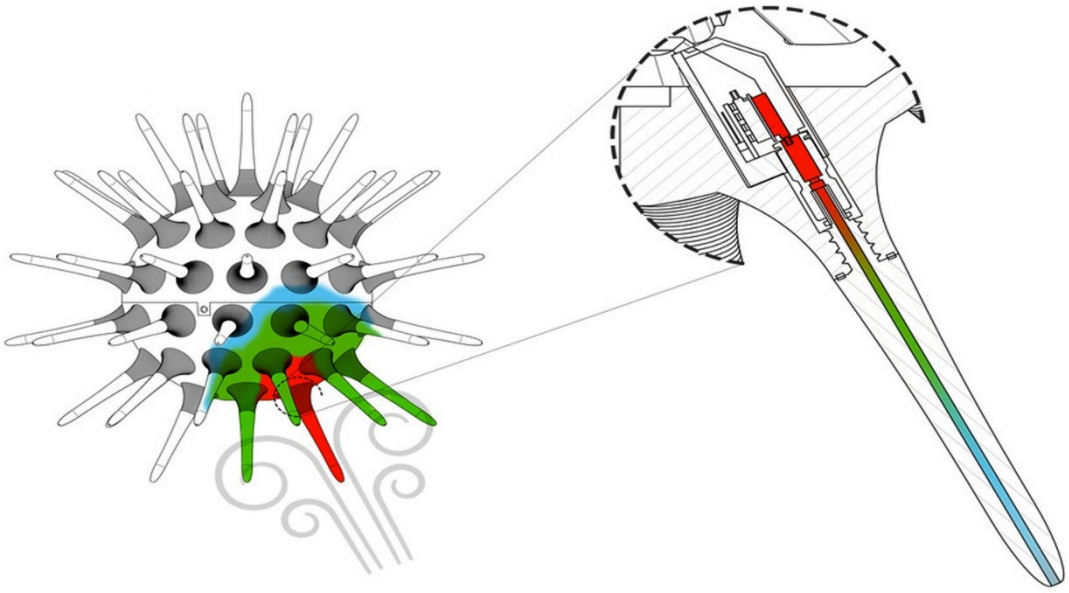

Figure 6.20: Wind Urchin Principle of Operation

Wind speed and directional data for the horizontal and vertical directions was recorded and measured for a one month period for the anemometer and Wind Urchin. This data

was analysed and graphs produced to illustrate the comparison of information from both devices. Fig 6.21 compares the raw data from the anemometer for a one month time period against the 20 second averages from the Wind Urchin.

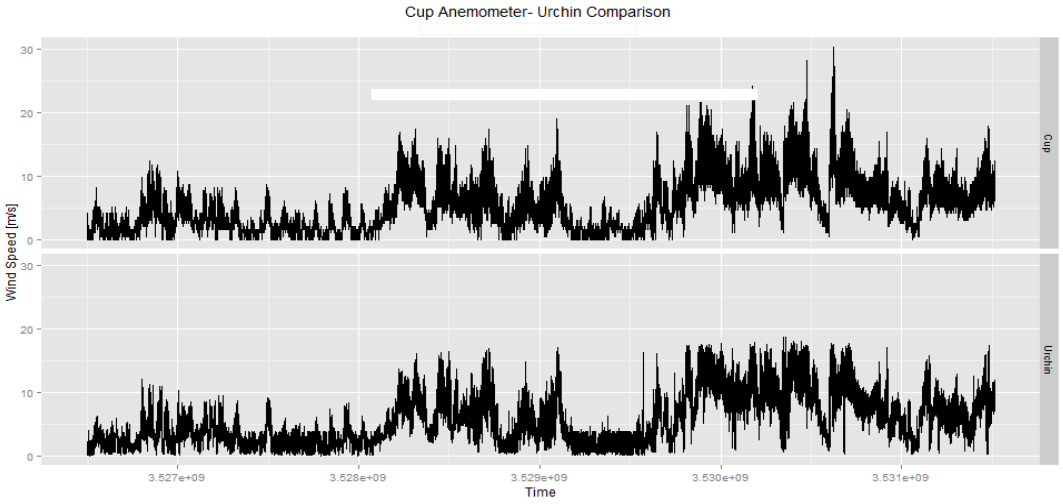

Figure 6.21: Cup Anemometer - Wind Urchin Comparison

It can be seen that the graphed data from the Wind Urchin tracks closely that of the cup anemometer for the time period analysed.

The wind speed was sampled for the same time period using 10 minute averages to analyse and compare the data from the cup anemometer and Wind Urchin. In Fig 6.22 the data from both instruments is output and superimposed onto a graphed display to illustrate more clearly how closely the data from each device correspond with respect to each device. The graphed data from the Wind Urchin is represented in blue while the data from the cup anemometer is represented in black.

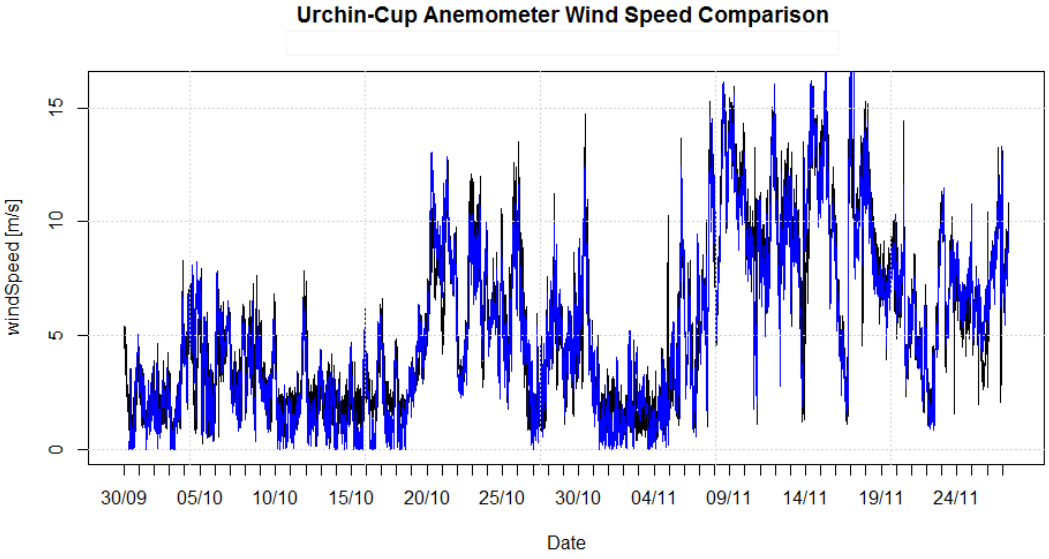

Figure 6.22: Wind Urchin - Cup Anemometer Speed Comparison for One Month / 10 Minute Averages

Fig 6.22 illustrates that the wind speed data from the Wind Urchin is measuring greater than that from the cup anemometer. This is because the Wind Urchin has recorded and averaged both the Horizontal and Vertical component of the passing wind. Fig 6.23 depicts the angular test performed in a wind tunnel at 5, 8 and 11 m/s. This test shows the anemometer significantly over reads the wind speed when subjected to high negative wind inflow angles.

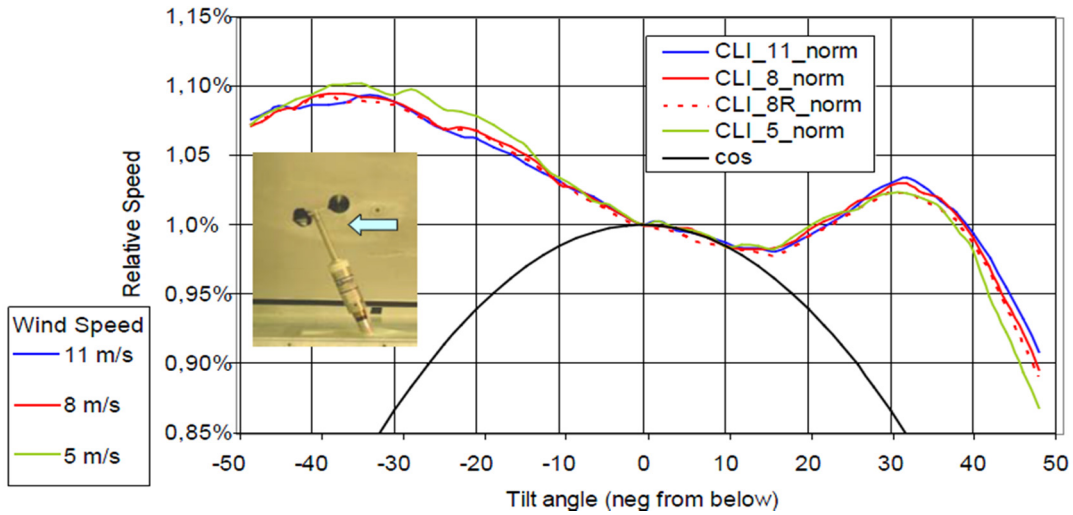

Figure 6.23: Negative From Below Tilt Angle Test (J.-Å. Dahlberg, 2006)

Fig 6.18 previously illustrated the error that occur when the anemometer is subject to positive from below winds at tilted angles from the horizontal. The cup anemometer

can only measure wind in the horizontal plane, the ideal anemometer to use is one which measures total wind speed not just horizontal wind speed, and since total wind speed represents the total power of the wind. Total wind speed is required when determining the wind resource available for wind farm analyses but in the relation to the aviation sector the vertical component of wind measure is necessary to measure wind shear and microburst activity accurately at airport runway level. In Fig 6.24 the horizontal wind speed comparison of the Wind Urchin and cup anemometer can be seen for a one week period measuring 10 minute averages of both instruments.

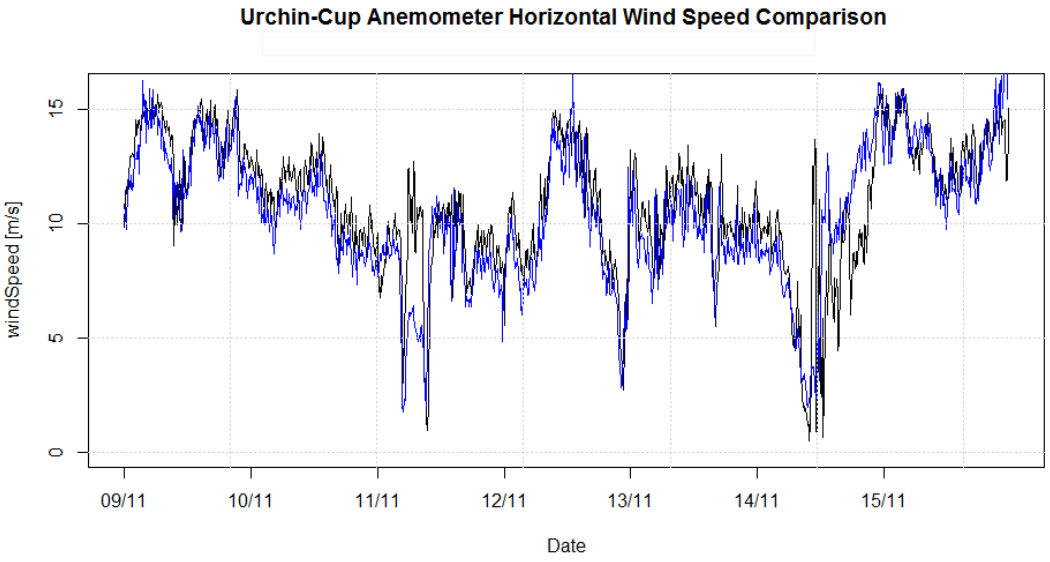

Figure 6.24: Horizontal Wind Speed Comparison for Wind Urchin - Cup Anemometer / 10 Min Avr

The graphed output from the analysed data from both instruments is very similar as this relates only to the horizontal wind speed component. The Urchin is shown in blue and the Cup in black. Fig 6.25 graphs the average horizontal wind comparison for the time period as shown in fig 6.24.

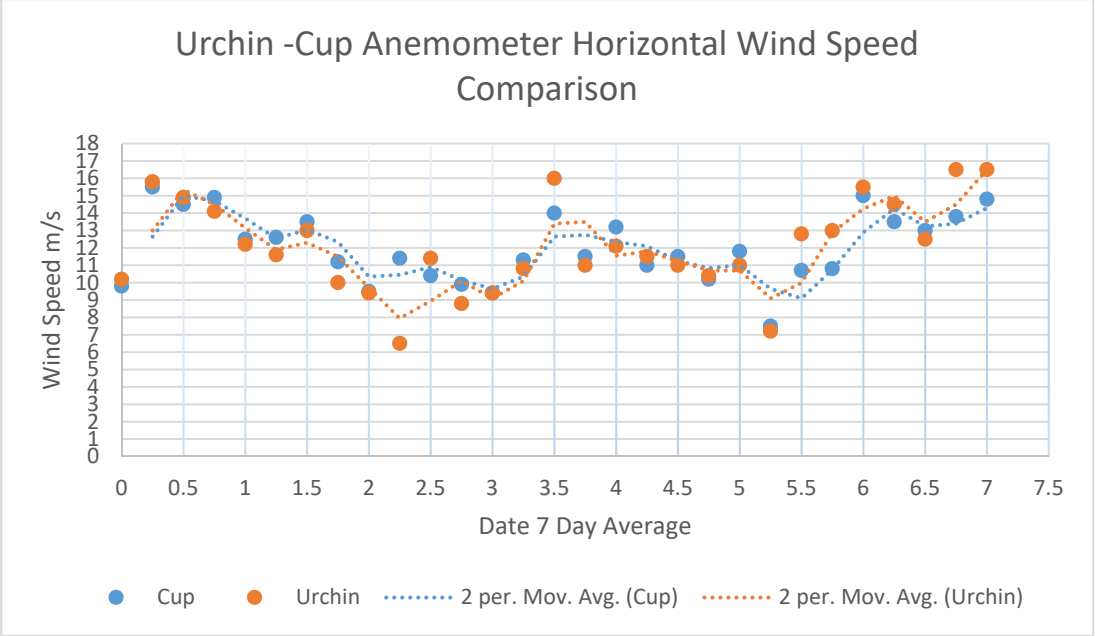

Figure 6.25: Urchin-cup Average of Fig 6 24

When the Vertical wind was analysed and graphed the results showed that the Wind Urchin recorded Vertical wind as it passed by the stimulated Pitot Tubes and as expected the cup anemometer did not record the vertical wind. The graphed data for the Vertical wind speed comparison for the same time period as used for the horizontal comparison for the Wind Urchin and cup anemometer can be seen in Fig 6.26.

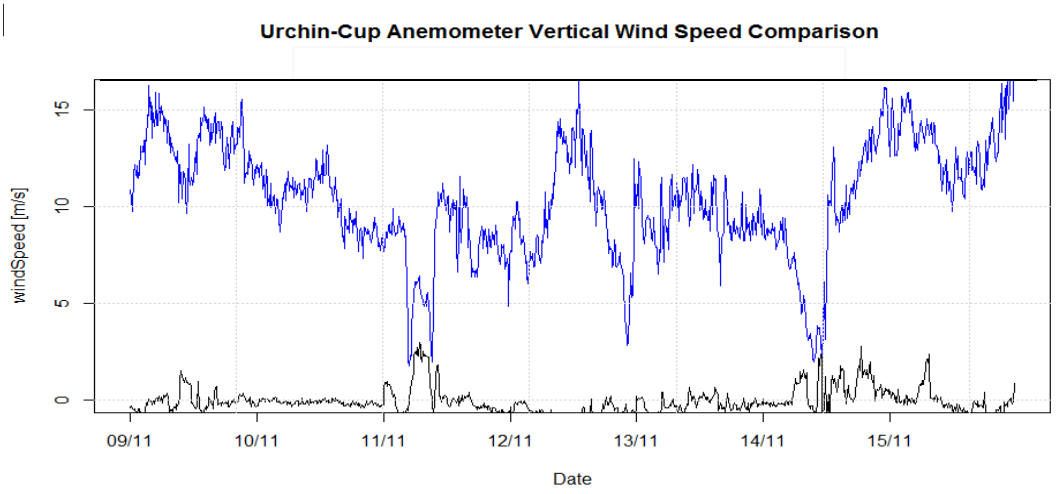

Figure 6.26: Vertical Wind Speed Comparison for Wind Urchin - Cup Anemometer / 10 Min Avr

In Fig 6.26 the Wind Urchin is represented by the blue graphed data and the cup is depicted by the black graphed data. It is very evident and clear from this illustration that the cup anemometer has not recorded any vertical wind. The cup anemometer did not record any vertical wind for the above period being analysed as it is impossible for the cup anemometer to measure vertical wind but did rotate due to a reduced level of horizontal components acting on the cup. The Urchin regularly picks up turbulent flows but only outputs the highest value at present. The Wind Urchin has recorded vertical wind in excess of 15 m/s for the same time sampled 10 minute averaged period. The Wind Urchin is a highly accurate three dimensional wind instrument with a wide measuring range to measure wind speed from 0-250 m/sec. The integration of the Wind Urchin into a Low Level Wind Shear Alert System at airport runways could significantly improve the forecasting and recording of low level wind shear and microburst activity. This as previously stated would improve safety for passengers and aircraft during the take-off and landing stages of flight. The installation and integration of the Wind Urchin into a current Low Level Wind Shear Alert System could produce significant saving for the entire aviation industry. 42% of all Go-arounds are as a result of wind conditions, the direct cost of Go-arounds have been discussed and have shown based on the researched evidence that hundreds of millions of Euro per annum could be saved if better real time wind shear data was available to pilots when on approach to landing. This could avoid wind associated Go-arounds manoeuvres. This scope of this thesis did not calculate the indirect costs to airlines, passengers, airports, travel companies, insurance companies and other stakeholders as a result of delays caused by wind associated Go-arounds. It is certain that factoring these indirect costs with the researched calculated direct costs would significantly add multiples to the current Go-Around figures shown.

7. Potential For Improved Safety In Landing And Cost Saving To The Aviation Industry

Aviation Industry Supports €2.7 Trillion of World GDP which accounts for 3.5% of Global GDP and carries over 3 billion passengers a year. The evidence gathered has shown that Go-around manoeuvre cost to Australia is €1.2 million annually in direct only costs which accounts for 0.85% of the total inbound flights. The global flight total for an average day is 102,000 Flights. Assuming a Go-around figure of 0.01%. This would conservatory cost the aviation industry €558 million annually in direct airline costs. The IATA expects passenger numbers to increase to 7.8 billion by 2036. This is a near doubling of the expected 4 billion passengers numbers for 2018 (IATA, 2018). The IATA goes on to state that the world needs to be prepared for this year on year growth. The figures calculated for this research are based on the Go-around figures for Australia. The percentage used from Australia was then applied to the current 106,000 average daily flights to obtain a costing for a global scenario. If as predicted by the IATA this number will increase to over 200,000 flights a day and applying the same criteria for Go-arounds, the cost to aviation would exceed €640 million annually for direct only costs. Given that climate change is happening with ever more increasing severe weather events, it is logical to assume that an increasing amount of flights will also be affected by wind related weather. Incorporating the Wind Urchin which is a low maintenance, low cost 3-D total wind measuring instrument into an existing LLWAS could potentially save passenger lives and save millions annually in direct costs alone.

8. Conclusion

Finding from this thesis have established that Low level wind shear and turbulence present a serious safety risk to aircraft during the approach, landing and take-off phases. Low level wind shear has been identified as one of the primary factors for aircraft go-arounds and aborted landings. Aviation reports have concluded that pilots do not always have real time up to date information about low level wind shear and turbulent conditions at runway level. Pilots need to have improved information in relation to tailwinds, wind shear and wind variations on approach and during the landing phases. The aviation industry concluded that the majority of accidents that occurred over the past 10 years have occurred during the approach, landing and go-around flight phases. At the Go-around safety forum in Brussels in 2013, it was concluded that due to rapid changing weather and runway conditions, a pilot does not always have the latest information on which to make a landing or go-around decision. Air accident reports have stated that between 2000 and 2012 there were 10 fatal accidents attributed to flight go-arounds in which 614 people died. Current methods of wind shear calculations involve data from an aircraft on descent and recording data from different anemometer spaced at different levels along a runway of mast. The limitation in this approach is that the calculation of wind shear from two winds separated by a distance gives the overall wind shear between those two points. The information does not indicate if the rate of shear is linear or not or where most of the shear occurs between the points sampled. It is wholly inadequate and does not give the maximum shear. Extreme low level wind shear and turbulence can at its worst cause aircraft to crash resulting in fatalities and injuries to passengers and crew and destruction or damage to an aircraft. At the lower end of the scale, wind shear and turbulence will result in delays to take offs and landings, aborted landings resulting in flight go-around manoeuvres or flights being diverted to another airport. We know

that according to the U.S. Department of Transport records from the National Aviation System (NAS) 33% of all delayed flights in 2016 were delayed due to weather conditions. The figure for 2017 was over 50% due to weather conditions. In the IATA report to the Go-around forum they concluded that the actual wind conditions versus the recorded and reported wind conditions given to the flight crew on final approach were an area of concern. It has been established that Low level wind shear and turbulence account for 42% of all Go-around procedures being initiated by pilots. It has been established that over 78% of all go-arounds were initiated by the flight crew and 22% were initiated by the Air Traffic Control (ATC) .This would seem to indicate the wind shear and turbulence data recorded by the ATC was not accurate or up to date for the approaching aircraft and it was the flight crew who deemed it necessary to abort the landing based on the conditions that they encountered on approach. The thesis has found that when a Go-around manoeuvre is undertaken that most commercial airline pilots, they did not have sufficient experience or training in how to handle an aircraft during a go-around caused by a wind shear event resulting in fatalities. This thesis has gathered information to calculate accurately the direct Go-around cost incurred by two of most used medium range aircraft in operation today. The thesis has found that the current conservative estimate for global Go-arounds annually is in excess of €320 million and by the year 2036 could exceed €640 million in direct costs alone. The financial cost to aviation alone would justify the installation and integration of a new 3-D wind measuring instrument into an existing Low level wind shear alert system. Beta tests from the Baldonell aerodrome have shown that the Wind Urchin recorded the vertical wind component providing the total wind speed at the airport runway while the graphs illustrated that the runway anemometers did not record any vertical wind. The ability to detect the vertical wind component accurately

is essential for tracking and recording microbursts. The research and findings of this thesis have established that despite major advances in microburst detection and Low level wind shear detection at runway level with Terminal Doppler Weather Radar, Doppler Lidar, Weather Surveillance Radar and Low Level Wind Shear Alert Systems there continue to be incidents, accidents and Go-arounds as a result of Low level wind shear and microbursts. All of the above systems are costly to install, maintain, service and upgrade. In most large commercial airports they can have at possibly two and up to three of all of the above systems installed to provide microburst and Low level wind shear alert coverage. In contrast the Wind Urchin is a low cost, low maintenance robust device. The Wind Urchin is the world's first truly three dimensional instrument that measures wind in all its aspects. It has been established that integrating the Wind Urchin into an existing LLWAS around the airfield extended boundary would not pose any technical difficulty as the protocols and interface of the Wind Urchin can be easily integrated into current systems. The Wind Urchin could theoretically replace all the current ultrasonic sensors within a LLWAS. The Wind Urchin can provide a much greater sampling rate than any other anemometer currently used in aviation for a specific timeframe. The ability of the Wind Urchin to measure both horizontal and vertical wind components would ensure that more accurate and up to date data is available to the ATC in determining if an aircraft should abort a take-off or initiate a Go-around. The Hong Kong Observatory's future development plan is for an uplink of textual and graphical wind shear and warning data directly to the cockpit. This would cut out the delay of data being transmitted to the flight crew by the ATC and provide a quicker transfer of the recorded wind data at runway level to the pilot. If the Wind Urchin was then integrated into the LLWAS, not only would the upload of data be faster but more importantly, it would be a more accurate and complete profile of

current runway wind conditions. This would provide the pilot with the latest and most accurate runway wind data enabling the pilot to determine the best course of action for any given wind situation. Fig 8.1 illustrates how the Wind Urchin could integrate into any future LLWAS.

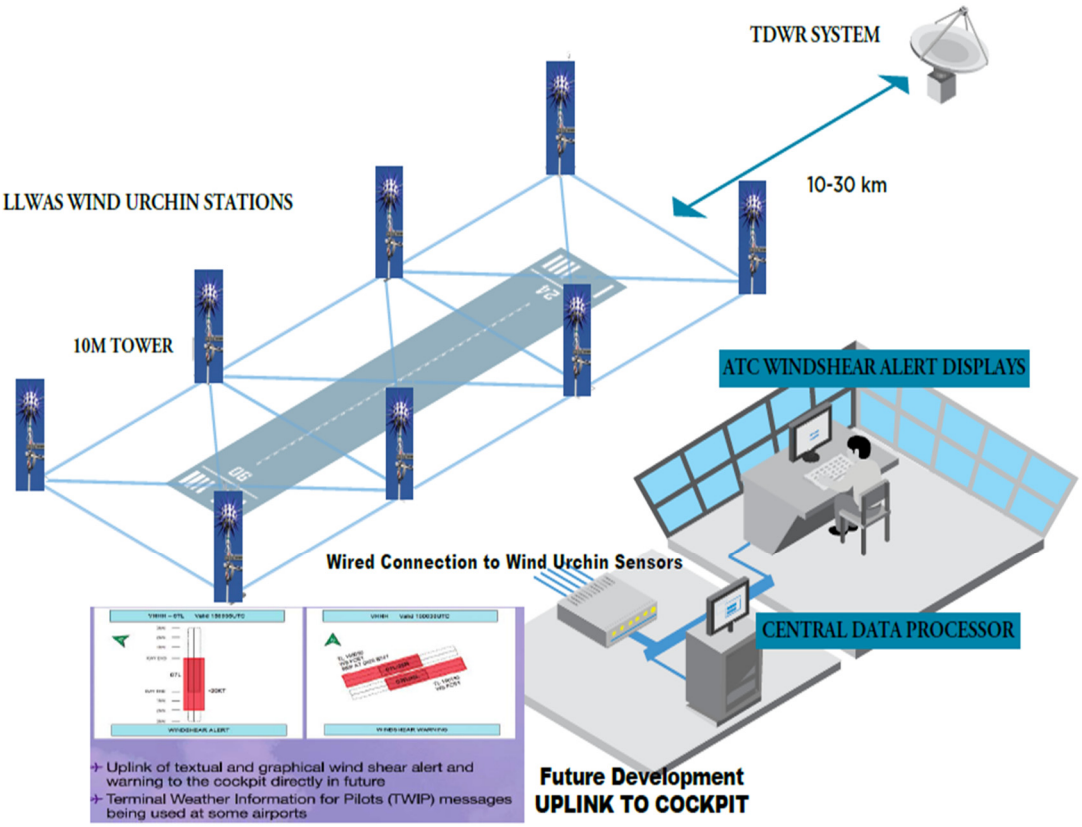

Figure 8.1: Concept of a Future LLWAS Incorporating the Wind Urchin

The benefits over existing LLWAS sensors are increased sampling rate of wind data, measurement of the total wind power at runway level, recording and measurement of horizontal and vertical wind data. Currently, LLWAS can only provide textual data to the ATC wind alert display as shown in Fig 4.14. The Wind Urchin data can produce a 3-D image map similar to those produced by TDWR and Lidar systems making it easy to interface to the airport Automated Weather Observation System (AWOS). The approach runways as shown in Fig 8.1 could be covered by an image map generated from all the runway Urchins to produce a 3-D image map of the approach and

departure runways, showing the wind intensity and wind variation as it changes across the runway area. This feature makes the Urchin unique when compared to other runway sensors currently in use today for LLWAS. Fig 8.2 illustrates the 3-D image of the wind intensity on the surface of the Wind Urchin.

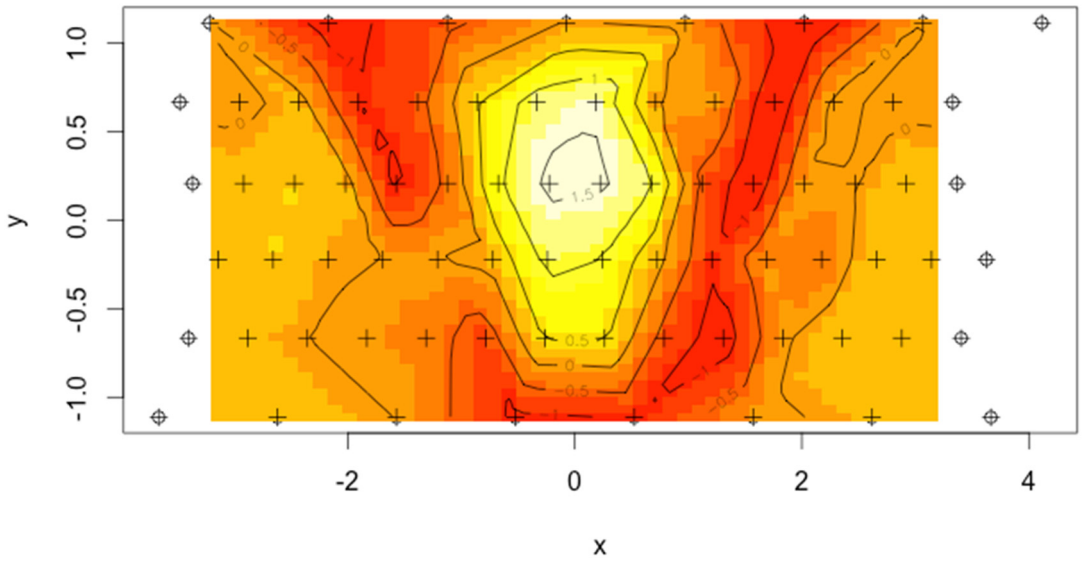

Figure 8.2: 3-D Image of Wind Intensity on the Surface of Wind Urchin (ERG, 2018)

Incorporating the Wind Urchin into current LLWAS at terminal boundary areas could improve safety for passengers and aircraft. The thesis has shown that it has the potential to save millions of Euro annually in direct cost for Go-arounds. The Wind Urchin is a commercially viable device increasing safety and reducing costs for the aviation industry. Incorporating the Wind Urchin into existing LLWAS coupled with a wind shear alert and warning uplink to the cockpit could provide the missing ingredient to existing systems to give an airport runway a Prediction of Detection Rate of close to 100%.

8.1 Further Research

The research gathered during the course of this thesis would suggest that there is a gap in the ability of current systems to provide a total Low level wind shear alert system that is corresponded in real time to pilots. The beta tests carried out at Baldonell aerodrome have shown the ability of the Wind Urchin to detect and measure wind as a 3-D entity, graphing its horizontal and vertical components. This thesis is limited in its scope due to funding. Ideally, four Wind Urchin's would need to be developed and constructed to obtain wind data from different points along an airport runway. This would give comparison data against each other and installed runway instruments. Vaisala has suggested that in order for the Wind Urchin to be considered for use in the aviation sector that a 3-D microburst simulation be carried out. This could be done as a PhD extension to this thesis but would require funding and access to a super computer to perform a CFD modelling of a microburst. The WMO has strict requirements for surface wind measurement and has set guidelines for surface weather measurements to ensure comparable measurement around the globe (WMO, 2010). The ICAO, Meteorological Service for International Air Navigation. International Civil Aviation has set requirements for instruments used to record meteorological data for use in the civil aviation industry (ICAO, 2007). The FAA and the National Aerospace System (NAS) require additional certification in addition to the WMO and ICAO for instruments used for the purpose of wind surface measurement (FAA, 2015). Further research would need to be carried out to ensure that the Wind Urchin complied with all of the above aviation organizations and standards. After a 3-D microburst simulation is completed, it would be necessary to carry out further trials at runway level with four Wind Urchins to validate all necessary information before an approach is made to industry.

Bibliography

Australian Transport Safety Bureau. (2009). *Occurrence Investigation Report AO-2007-001.* Canberra: ATSB.

Hong Kong Observatory. (2018, February 27). *(LIDAR) System*. Retrieved from Hong Kong Observatory: http://www.hko.gov.hk/aviat/lidar/page3.htm

A.A.Lab Systems. (2018, May 24). *Gage-3000.* Retrieved from A.A.Lab Systems: http://www.lab-systems.com/products/data-acq/gage3000/Gage-3000%20Brochure.pdf

Airbus. (2018, March 27). *Airbus A320neo.* Retrieved from Airbus.com: http://www.airbus.com/aircraft/passenger-aircraft/a320-family/a320neo.html#details

Airlines for America. (2016, January 26). *U.S. Passenger Carrier Delay Costs.* Retrieved from Airlines for America: http://airlines.org/dataset/per-minute-cost-of-delays-to-u-s-airlines/

Alaskan Airlines. (2018, January 24). Flight Go-arounds and aborted flight costs. *Flight Go-arounds and aborted flight costs*. Seattle, Washington, USA: Alaskan Airlines.

Albright, J. (2015, August 1). *Wind Shear: Has It Been Tamed?* Retrieved October 10, 2017, from http://aviationweek.com/bca/wind-shear-has-it-been-tamed

Allweatherinc. (2018, February 23). *Low Level Wind Shear Alert System*. Retrieved from allweatherinc: http://www.allweatherinc.com/low-level-wind-shear-alert-system/

American Airlines. (2018, January 24). Flight Go-arounds and aborted landing costs. *Flight Go-arounds and aborted landing costs*. Forth Worth, Texas, USA: American Airlines Media Relations.

Amphenol. (2018, May 24). *NovaSensor NPH Series | Solid State Low Pressure Sensor.* Retrieved from Amphenol: https://www.amphenol-sensors.com/en/novasensor/pressure-sensors/3155-novasensor-nph-series-solid-state-low-pressure-sensors

Australian Government. (2008, January 23). Retrieved from Civil Aviation Safetyn Authority: https://www.casa.gov.au/standard-page/go-arounds

Australian Transport Safety Bureau. (2002). *INVESTIGATION REPORT 200100213.* Canberra: ATSB.

Aviation Safety Network. (2009, March 23). *Photo of McDonnell Douglas MD-11F N526FE.* Retrieved from Aviation Safety Network: http://aviation-safety.net/photos/displayphoto.php?id=20090323-0&vnr=5&kind=C

Aviation Safety Network. (2018, February 13). *ASN Aviation Safety Database.* Retrieved from Flight Safety Foundation: http://aviation-safety.net/database/dblist.php?Event=WXW&lang=&page=1

Aviation Week. (2017, May 22). *German Challenger Totaled After A380 Wake Turbulence.* Retrieved from Aviation Week Network: http://aviationweek.com/ebace-2017/german-challenger-totaled-after-a380-wake-turbulence

B. A. Harper, J. D. (2010). *GUIDELINES FOR CONVERTING BETWEEN VARIOUS WIND AVERAGING PERIODS* . Geneva: WMO.

Boeing. (2018, March 27). *Boeing Next-Generation 737.* Retrieved from Boeing.com: http://www.boeing.com/commercial/737ng/

Bureau of Transportation Statistics. (2017, November 6). *Airline On-Time Statistics and Delay Causes.* Retrieved November 6, 2017, from https://www.transtats.bts.gov/OT_Delay/ot_delaycause1.asp?type=5&pn=1

Bureau of Transportation Statistics. (2018, March 23). *Airline Fuel Cost and Consumption (U.S. Carriers - Scheduled)*. Retrieved from Bureau of Transportation Statistics: https://www.transtats.bts.gov/fuel.asp

Business Insider. (2018, March 29). *CO2 European Emission Allowances PRICE COMMODITY*. Retrieved from Markets Insider: http://markets.businessinsider.com/commodities/co2-emissionsrechte

CAA New Zealand. (2008). *Wake Turbulence.* Wellington: CAA New Zealand.

Carey, B. (2015, January 29). *Lidar System Measures Wake Turbulence at Dubai Airport.* Retrieved from AINonline: https://www.ainonline.com/aviation-news/air-transport/2015-01-29/lidar-system-measures-wake-turbulence-dubai-airport

CASA. (2018, January 23). *Go-arounds*. Retrieved from Australian Government Civil Aviation Safety Authority: https://www.casa.gov.au/standard-page/go-arounds

CAWCR. (2010). *ICAO Wind Shear Systems Acquisition Workshop.* Bangkok: Centre for Australian Weather and Climate Research.

Chan, S. C. (2005). *Briefing on Windshear and Turbulence Alerting Service S.T. Chan & P.W.* Hong Kong: Hong Kong Observatory.

Chatfield, R. (2017, October 31). Flight go-around data. *Flight go-around data*. London, UK: Communications Department Civil Aviation Authority.

Cho, R. G. (2010). Wind-Shear System Cost-Benefit Analysis. *LINCOLN LABORATORY JOURNAL*, 68.

Civil Aviation Authority. (2013, June 4). *Missed Approaches in Response to Onboard Windshear Alearts.* Retrieved October 5, 2017, from https://skybrary.aero/bookshelf/books/2303.pdf

Civil Aviation Authority. (2013, June 4). *Missed Approaches in Response to Onboard Windshear Alerts.* Retrieved October 18, 2017, from https://www.skybrary.aero/bookshelf/books/2303.pdf

Daidzic, N. E. (2016). Determination of rejected landing roll runway point-of-no-return and go-around in transport category airplanes. *International Journal of Aviation, Aeronautics, and Aerospace*, 32. Retrieved from International Journal of Aviation,Aeronautics,and Aerospace.

Delta Airlines Inc. (2018, January 26). Flight Go-arounds and aborted flight costs. *Flight Go-arounds and aborted flight costs*. Atlanta, Georgia, USA: Corporate Communications Delta Airlines.

Ellis, K. &. (1978). *Development of wind shear models and determination of wind shear hazards, FAA Report No. FAA-RD-79-119.* Washington: FAA.

ERG. (2018, May 2). *Energy Resource Group.* Retrieved from Energy Resource Group: http://www.energyresourcegroup.io/

EUROCONTROL. (2013). *Go-around Safety Forum.* Brussels: Flight Safety Foundation.

Eurocontrol. (2015). *ECAT-EU.* Brussels: EUROCONTROL.

EUROCONTROL. (2018, August 30). *EUROCONTROL - Supporting European Aviation*. Retrieved from EUROCONTROL: https://www.eurocontrol.int/articles/who-we-are

FAA. (1989). *Order 6560.21A.* Washington.DC: Fedaral Aviation Administration.

FAA. (1990). *Wind Shear Training Aid.* Federal Aviation Authority.

FAA. (2001). *LOW-LEVEL WINDSHEAR ALERT SYSTEM - Network Expansion.* Washington: Department of Transport : Federal Aviation Administration.

FAA. (2015, 9 30). *Advisory Circular 150-5300-18C.* Retrieved from Federal Aviation Administration: https://www.faa.gov/documentLibrary/media/Advisory_Circular/150-5300-18C.pdf

FAA. (2016). Pilots Handbook of Aeronautical Knowledge. In FAA, *Pilots Handbook of Aeronautical Knowledge : FAA-H-8083-25B* (p. Chap 12.11). Oklahoma City: FAA.

FAA. (2018, May 21). *Aviation Hand Books and Manuals.* Retrieved from Federal Aviation Administration: https://www.faa.gov/regulations_policies/handbooks_manuals/aviation/

Federal Aviation Administration. (2012). *Wind Reporting Systems in the NAS.* Retrieved 10 10, 2017, from https://ral.ucar.edu/general/Summer2012/FPAW_2012_Summer_Presentations/Seg%204%20Surface%20Observations%20Riger%20Sultan/Armbruster%20Wind%20Reporting.pdf

Flight Safety Foundation. (1975, June 24). *Aviation Safety Network.* Retrieved from Aviation Safety.net: http://aviation-safety.net/database/record.php?id=19750624-1

Flight Safety Foundation. (2009). *fsf alar briefing note 5.4 Wind Shear.* Retrieved October 10, 2017, from https://www.skybrary.aero/bookshelf/books/812.pdf

FlightAware. (2018, September 25). *FlightAware*. Retrieved from FlightAware: https://uk.flightaware.com/

Flint, P. (2018, January 31). Cost of Go-arounds for flights. *Cost of Go-arounds for flights*. Montreal, Quebec, Canada: IATA, Head of Corporate Communications, North America.

Florescu, Ana Maria Smaranda, Georgeta Bandoc, and Mircea Degeratu. "Energy Efficiency Evaluation of Wind Energy Based on Energy Reports." Advanced Materials Research. Vol. 1008. 2014. (n.d.).

Gill . (2018, March 20). *WindObserver 70/75 User Manual.* Retrieved from Gill Instruments: meteorological technology: http://gillinstruments.com/data/manuals/1390-PS-0038%20WindObserver%2070%2075%20Manual%20Issue%205.pdf?iss=5.20170306

Gill Instruments. (2018, February 19). *WindObserver Used At Airports.* Retrieved from Gill Instruments: http://gillinstruments.com/applications/transport-travel-and-buildings/airport-aviation-wind-measurement.html

Hiscotte, D. (2018, 2 12). Go-around Cost. Auckland, New Zealand.

Hong Kong Observatory. (2018, February 21). *Windshear and Turbulence Alerts.* Retrieved from Hong Kong Observatory: http://www.hko.gov.hk/aviat/amt_e/windshear_warning_e.htm

http://en.wikipedia.org/wiki/Lidar. (n.d.).

http://www.zephirlidar.com/products/zephir-dm/. (n.d.).

IATA. (2010). *IATA Carbon Offset Program.* Montreal: IATA.

IATA. (2013). *Go-arounds.* Brussels: IATA.

IATA. (2015). *Guidance on Turbulence Management.* Montreal: IATA.

IATA. (2018, August 30). *2036 Forecast Reveals Air Passengers Will Nearly Double to 7.8 Billion*. Retrieved from IATA: https://www.iata.org/pressroom/pr/Pages/2017-10-24-01.aspx

ICAO. (1987). *Wind Shear : Circular 186-AN/122.* Montreal: ICAO.

ICAO. (2005). *Doc 9817 AN449.* Montreal: ICAO.

ICAO. (2005). *Low-level Wind Shear.* International Cival Aviation Organization.

ICAO. (2005). *Manual on Low-level Wind Shear.* Montréal: International Civil Aviation Organization.

ICAO. (2007). *Annex 3 to the Convention on International Civil Aviation: Meteorological Service for Internanational Air Navigation.* Montréal: ICAO.

ICAO. (2014). *Aircraft Volume 1 Flight Procedures.* Montreal: ICAO.

ICAO. (2016). *PROCEDURES FOR AIR NAVIGATION SERVICES.* Montreal: ICAO.

ICAO. (2018, March 27). *ICAO Aircraft Engine Emissions Databank.* Retrieved from ICAO Aircraft Engine Emissions Databank: https://www.easa.europa.eu/easa-and-you/environment/icao-aircraft-engine-emissions-databank

Insider, B. (2018, March 29). *CO2 European Emission Allowances PRICE COMMODITY*. Retrieved from Markets Insider: http://markets.businessinsider.com/commodities/co2-emissionsrechte

International Journal of Aviation, Aeronautics, and Aerospace. (2018, November 11). *Evaluate the Effect of Turbulence on Aircraft During Landing and Take-Off Phases.* Retrieved from IIJAAA: https://commons.erau.edu/ijaaa/vol5/iss4/10/

Interstate Aviation Committe. (2016). *Interim Report: Boeing 737-800 A6-FDN.* Moscow: Interstate Aviation Committe.

Interstate Aviation Committee of Russia. (2016). *Interim Report. Boeing 737-800 A6 FDN.* Moscow: Interstate Aviation Committee of Russia.

J.-Å. Dahlberg, T. P. (2006). *Methods for classification of cup anemometers.* Lyngby: Technical University of Denmark.

Japan Transport Safety Board. (2013). *AIRCRAFT ACCIDENT INVESTIGATION REPORT : FEDERAL EXPRESS CORPORATION N526FE.* Tokyo: Japan Transport Safety Board.

John Y. N. Cho, R. G. (2008). *COMPARATIVE ANALYSIS OF TERMINAL WIND-SHEAR DETECTION SYSTEMS.* Lexington, Massachusetts: American Meteorological Society.

Kearney, D. (2014). *The Development of a Three-Dimensional Wind Measurement Instrument.* Dublin: Derek Kearney.

Lockheed Martin. (2013, August 29). *Lockheed Martin WindTracer System Installed at Major Airports in Germany.* Retrieved from Lockheed Martin: https://www.lockheedmartin.com/us/news/press-releases/2013/august/0829-ss-windtracer.html

M Weber. (1991). *Airport Surveillance Radar (WSR-9) Wind Shear Processor.* Lexington: Lincoln Laboratory, MIT.

Management, F. W. (2018, February 2). Cost of flight Go-arounds. *Cost of flight Go-arounds*. Washington, DC, USA: FAA Web Management.

Mikkelsen, T. (n.d.). Remote Sensing of Wind, Technical University of Denmark Department of Wind Energy. *www.aqs.se/wordpress/wp-content/.../Lidar-and-Sodar-comparison.pdf*.

Monniaux, D. (2007, June 20). *Airspeed*. Retrieved from wikimedia: https://commons.wikimedia.org/wiki/File:Airspeed_p1230157.jpg

National Instruments. (2017, December 14). *CompactRIO Single-Board Controllers* . Retrieved from National Instruments: http://www.ni.com/pdf/product-flyers/compactrio-single-board-controllers.pdf

National Weather Service. (2002). *Replacement Wind Sensor.* Washington: Department of Transportation.

Newfoundland, U. o. (2018, June 10). *Bernoulli equation.* Retrieved from Memorial University of Newfoundland : Department of Physics and Physical Oceanography: http://www.uobabylon.edu.iq/eprints/publication_12_10196_1691.pdf

NOAA. (2010). Improving the VWP. *Nexrad Now*, 35.

NOAA. (2018, March 5). *Radar Operations Centre : Nexrad WSR-88D*. Retrieved from National Weather Service: https://www.roc.noaa.gov/wsr88d/Engineering/NEXRADTechInfo.aspx

O' Connor, A. (2018, Nov 16). *Using a Wind Urchin for Airport Wind Measurements.* Retrieved from Irish Meteorological Society: https://irishmetsociety.org/

Observatory, H. K. (2018, February 25). *Storms and Precipitation.* Retrieved from Hong Kong Observatory: http://www.hko.gov.hk/wxinfo/radars/radar_gallery/storms_e.htm#040803

OFCM. (2006). *DOPPLER RADAR METEOROLOGICAL OBSERVATIONS.* Washington: FEDERAL COORDINATOR FOR METEOROLOGICAL SERVICES AND SUPPORTING RESEARCH.

Office of Aviation Weather Observations. (2010). *Wind Shear Detection Systems in Japan.* Tokyo: Japan Meteorological Agency.

Pattison, A. (2010, October 5). A Measured Change. *Wind Systems*, p. 36.

Princeton University. (2018, may 24). *Bernoulli's Equation*. Retrieved from Princeton University: https://www.princeton.edu/~asmits/Bicycle_web/Bernoulli.html

Raillant-Clark , W. (2018, January 24). Communications Officer, ICAO. *Go-arounds*. Montreal, Quebec, Canada: ICAO.

Ricondo & Associates, INC. (2014). *Industry White Paper Aircraft Operating and Delay Cost per Enplanement.* Washington: Airports Council International.

Sharman, D. G. (2013). *NCAR In Situ Vertical winds-based EDR Estimation Algorithm.* Boulder,Colorado: UCAR.

SKYbary. (2017). *B738, Rostov-on-Don Russia, 2016*. Retrieved November 12, 2017, from https://www.skybrary.aero/index.php/B738,_Rostov-on-Don_Russia,_2016

Skybary. (2017, December 28). *Clear Air Turbulence (CAT).* Retrieved from Skybary: https://www.skybrary.aero/index.php/Clear_Air_Turbulence_(CAT)

Teunissen, D., & Bernard Lacroix, H. C. (2011). *Cost of a Go-around.* Brussels: EUROCONTROL.

Teunissen, D., & Bernard Lacroix, H. C. (2011). *Cost of A Go-around.* Brussels: EUROCONTROL.

The Department of Infrastructure, R. D. (2017). *International Airlines Operated Flights and Seats.* Canberra: Australian Government.

The Japan Times. (2009, March 24). *FedEx jet crashes at Narita; pilots die.* Retrieved from The Japan Times: http://search.japantimes.co.jp/cgi-bin/nn20090324a1.html

UCAR. (2012, August 21). *Wind Reporting in the NAS (Armbuster Wind Reporting).* Retrieved from University Corporation for Athmospheric Research: https://ral.ucar.edu/general/Summer2012/FPAW_2012_Summer_Presentations/Seg%204%20Surface%20Observations%20Riger%20Sultan/Armbruster%20Wind%20Reporting.pdf

Vaisala. (2018, March 16). *Vaisala WINDCAP® Ultrasonic Wind Sensor : User Guide.* Retrieved from Vaisala: https://www.vaisala.com/sites/default/files/documents/WMT700-User-Guide-in-English-M211095EN-H.pdf

Warit Werapuna, Y. T. (2017). Wind Shear Coefficients and their Effect on Energy Production. *ScienceDirect : Energy Procedia 138 (2017) 1061–1066*, 6.

Weber, J. Y. (2010). *Terminal Doppler Weather Radar Enhancements.* Lexington: Lincoln Laboratory, Massachusetts Institute of Technology.

William Benner, T. C. (2002). *WIND SENSOR SEVERE WEATHER PERFORMANCE TEST REPORT.* Juneau: FAA.

William Benner, T. C. (2002). *Wind Sensor Severe Weather Performance Test Report* . Juneau: FAA.

WMO. (2007). *Aviation Hazards.* Geneva: WMO.

WMO. (2010). *WMO-No-8.* Geneva: WMO.

WMO. (2016). *Technical Regulations :Volume II – Meteorological Service for International.* Montreal: WMO.

Appendices

Appendix 1: Software Programme and Urchin Baseline file

Baseline CSV file

Port#	Sensor	Baseline	sd-Base	decay -k	tau-s	slope	SE(slope)
1	E30	13725.75	28.68091	0.028255	35.39143	435.91	0.41
2	A28	13724.61	26.82052	0.074064	13.50183	430.41	0.51
3	F30	13579.51	26.50228	0.035658	28.04395	432.68	0.45
4	E29	13612.5	24.60637	0.017539	57.01498	435.19	0.76
5	D29	13656.81	27.55529	0.074059	13.50271	432	0.67
6	A29	13716.7	26.01989	0.132172	7.56592	422.36	0.93
7	E28	13811.22	26.23605	0.074124	13.49097	427.6	0.8
8	C29	13605.83	29.05472	0.015097	66.24035	436.36	0.59
9	D28	13589.32	27.70389	0.060825	16.44073	435.61	1.26
10	F28	13620.98	28.12995	0.104275	9.590062	421.92	0.86
11	B28	13687.63	26.72796	0.054369	18.39273	432.44	0.43
12	C26	13593.46	28.07689	0.036455	27.43124	435.43	0.57
13	B29	13768.67	33.83386	0.028101	35.5853	433.68	0.37
14	A30	13590.43	25.20258	0.070903	14.10378	435.41	0.7
15	A27	13760.93	27.53507	0.0436	22.93557	436.68	0.59
16	D27	13709.28	24.39025	0.125853	7.945778	430.16	0.85
17	B26	13442.41	27.03738	0.063337	15.78844	433.31	0.52
18	F29	13768.2	26.49181	0.009104	109.8423	439.56	0.24
19	C28	13748.41	28.18277	0.037381	26.75148	434.77	0.46
20	D25	13601.15	27.70256	0.035081	28.50536	432.42	0.41
21	A25	13719.38	27.39918	0.043207	23.14444	435.61	0.57
22	E26	13611.38	24.84269	0.033002	30.30134	436.62	0.35
23	B25	13615.2	29.72447	0.104112	9.605086	422.6	0.84
24	D26	13594.27	31.26198	0.01268	78.86625	438.74	0.38
25	F27	13669.99	27.36958	0.076295	13.107	430.3	0.54
26	B27	13729.22	26.9783	0.123137	8.121024	425.04	0.61
27	C30	13439.86	28.24103	0.05078	19.69275	433.64	0.47
28	C27	13538.28	26.67418	0.076623	13.05087	428.03	0.69
29	E25	13685.89	27.62253	0.098537	10.1485	424.78	0.97
30	F26	13578.82	28.31074	0.049591	20.16496	436.62	0.58
31	C25	13589.13	23.09506	0.036031	27.75389	436.78	0.38
32	A26	13632.95	27.98901	0.135121	7.400788	425.52	0.81
33	E27	13684.69	27.12994	0.082603	12.10609	430.82	0.56
34	D24	13586.19	30.22331	0.133592	7.485459	421	0.78
35	B21	13511.12	21.75534	0.067525	14.80934	426.27	1.06
36	D20	13857.25	24.96669	0.097154	10.29293	427.71	0.5
37	F24	13740.44	28.81146	0.129515	7.721092	410.87	0.58

38	A22	13525.91	28.78851	0.04447	22.48711	433.46	0.63
39	E23	13727.54	25.58494	0.025803	38.75577	435.27	0.62
40	F23	13666.45	28.21496	0.045325	22.06283	435.56	0.42
41	C22	14183.94	30.40274	0.070196	14.24573	434.36	0.64
42	A20	13740.26	23.78881	0.017074	58.56717	435.44	0.51
43	D21	13499.48	24.69591	0.066367	15.06778	433.66	0.5
44	F20	13629.23	28.24356	0.075095	13.31642	421.18	0.61
45	E21	13719.77	23.90004	0.034042	29.3756	431.76	0.32
46	C24	13588.15	26.29114	0.143149	6.985714	399.27	0.61
47	F21	13559.3	24.37475	0.043274	23.10881	434.96	0.47
48	A21	13706	26.47505	0.02537	39.41611	437.643	0.47
49	E22	13737.77	26.62485	0.080223	12.4652	420	0.64
50	F22	13601.42	27.46073	0.050791	19.68847	434.81	0.5
51	D23	13625.39	25.7325	0.032209	31.04732	433.57	0.5
52	D22	13724.64	27.19865	0.155808	6.418138	421.37	1.08
53	B23	13636.99	27.00282	0.027898	35.84467	437.04	0.44
54	A23	13637.61	27.84	0.003835	260.7505	440.08	0.61
55	E24	13661.6	26.66683	0.166074	6.021427	410.33	0.62
56	B20	13759.86	26.01688	0.065482	15.27134	425.25	0.96
57	C21	13678.21	24.05818	0.042806	23.36115	434.79	0.42
58	F25	13588.58	25.40174	0.119265	8.384672	422.25	0.82
59	C20	13572.64	24.78832	0.06616	15.11493	422.6	0.53
60	C23	13675.27	35.16709	0.041163	24.29393	430.02	0.47
61	B22	13586.11	27.24755	0.051045	19.59042	431.79	0.49
62	E20	13568.67	21.89124	0.043479	22.99941	435.16	0.38
63	B24	13659.74	24.67635	0.064098	15.60119	433.27	0.67
64	A24	13462.28	25.42742	0.063915	15.64581	428.41	0.7

R Program file for creating 1 second Average

```
Nfiles <- length(filenames)
duration <- 1/60
#filenames
timeaverage <- function(inputdf,duration){
 cn <- 60*duration # seconds averaging
 hn <- 60/duration # number of averaged bins per day
 Mu <- dim(inputdf)[1]
 ustart <- ceiling(inputdf$Time[1])
 uend <- ustart + cn*floor((inputdf$Time[Mu] - inputdf$Time[1])/cn)
 uchunks <- seq(ustart,uend,cn)
 outputmean <- aggregate(inputdf,list(cut(inputdf$Time,breaks=uchunks)),mean)
 hours <- as.numeric(outputmean$Group.1)/(hn*24)
 outputmean <- cbind(outputmean,hours)
```

```
 outputmean$windspeed <- sqrt(outputmean$Vx^2 + outputmean$Vy^2 + outputmean$Vz^2)
 outputmean$horwindspeed  <- sqrt(outputmean$Vx^2+outputmean$Vy^2)
 outputmean$direction <- 180 - outputmean$longitude/degrad
 return(outputmean)
}
kstart <- 1
kend <- Nfiles
ptm <- proc.time()
for (kk in kstart:kend){
 txt <- filenames[kk]
 data <- fread(txt,header=TRUE)
 data2 <- data.frame(data)
 data2 <- na.omit(data2)
 data2 <- data2[data2$Time !=0,]
 data2 <- data2[,-1]
 data2$Velocity1 <- ifelse(data2$Pressure > 0,sqrt(abs(200*data2$Pressure/1.225)),0)
 data2$Velocity2 <- ifelse(data2$peak > 0,sqrt(abs(200*data2$peak/1.225)),0)
 temp <- data2[,6:7]
 temp <- cbind(temp,data2[,14])
 dataxyz <- sph2car(temp,deg=FALSE)
 colnames(dataxyz) <- c("Vx","Vy","Vz")
 data2 <- cbind(data2,dataxyz)
 M <- dim(data2)[1]
 degrad <- pi/180
 rm(temp)
 data2$horvel <- sqrt(data2$Vx^2+data2$Vy^2)
 data2$direction <- 180 - data2$longitude/degrad
 data2$elevation <- 180*data2$latitude/pi
 data2$px <- data2$Vx/data2$Velocity1
 data2$py <- data2$Vy/data2$Velocity1
 data2$pz <- data2$Vz/data2$Velocity1
 meandata <- timeaverage(data2,duration)
 meandata <- meandata[,-1]
 setwd("E:/VelocityFiles-1second")
```

```
 txtlabel <- paste("Data-1s-",substr(txt,nchar(txt)-17,nchar(txt)-4),".csv",sep="")
 write.csv(meandata,txtlabel)
 setwd("E:/VelocityFiles-March18th")
 rm(data)
 rm(data2)
}
(proc.time()-ptm)
```

R Program for Calculating Urchin Velocity

```
T setwd("E:/VelocityFiles-March18th")
#setwd("Z:/urchin-P3-HuntersHill/VelocityFiles")
library("ggplot2", lib.loc="~/R/win-library/3.2")
library("rgl", lib.loc="~/R/win-library/3.2")
library("data.table", lib.loc="~/R/win-library/3.2")
library("sphereplot", lib.loc="~/R/win-library/3.2")

directoryname <- getwd()
filenames <- list.files(directoryname, pattern="*.csv", full.names=TRUE)
Nfiles <- length(filenames)
filenames

kstart <- 1104
kend <- 1129

files <- filenames[kstart:kend]
ptm <- proc.time()
DT = do.call(rbind, lapply(files, fread))
(proc.time()-ptm)

data <- data.frame(DT)
rm(DT)
data <- data[,-1]

# Averaging functions
```

```
timeaverage <- function(inputdf,duration=1){
  cn       <- duration # seconds averaging
  Mu       <- dim(inputdf)[1]
  ustart   <- ceiling(inputdf$Time[1])
  uend     <- ustart + cn*floor((inputdf$Time[Mu] - inputdf$Time[1])/cn)
  uchunks  <- seq(ustart,uend,cn)
  datamean <- aggregate(inputdf,list(cut(inputdf$Time,breaks=uchunks)),mean)
  datasd   <- aggregate(inputdf,list(cut(inputdf$Time,breaks=uchunks)),sd)
  colnames(datasd) <- paste("sd_",names(datamean),sep="")
  output   <- cbind(datamean,datasd)
  return(output)
}


cupaverage <- function(cupdf,urchinmeandf,duration=1){
  cn <- duration # seconds averaging
  Mc <- dim(urchinmeandf)[1]
  degrad <- pi/180
  cupstart <- ceiling(urchinmeandf$Time[1])
  cupend <- cupstart + cn*floor((urchinmeandf$Time[Mc] - urchinmeandf$Time[1])/cn)
  cupchunks <- seq(cupstart,cupend,cn)
  datamean <- aggregate(cupdf,list(cut(data3$UrchinTimestamp,breaks=cupchunks)),mean)
  datasd <- aggregate(cupdf,list(cut(data3$UrchinTimestamp,breaks=cupchunks)),sd)
  colnames(datasd) <- paste("sd_",names(datamean),sep="")
  output   <- cbind(datamean,datasd)
  return(output)
}

cupstdev <- function(cupdf,urchinmeandf,duration=1){
  cn <- duration # seconds averaging
  Mc <- dim(urchinmeandf)[1]
  degrad <- pi/180
  cupstart <- ceiling(urchinmeandf$Time[1])
  cupend <- cupstart + cn*floor((urchinmeandf$Time[Mc] - urchinmeandf$Time[1])/cn)
```

```
 cupchunks <- seq(cupstart,cupend,cn)
 cupdf <- cupdf[,-23]
 cupsd <- aggregate(cupdf,list(cut(data3$UrchinTimestamp,breaks=cupchunks)),sd)
 return(cupsd)
}



# http://stackoverflow.com/questions/10413678/
# how-to-assign-color-scale-to-a-variable-in-a-3d-scatter-plot
# Josh O'Brien
myColorRamp <- function(colors, values) {
 v <- (values - min(values))/diff(range(values))
 x <- colorRamp(colors)(v)
 rgb(x[,1], x[,2], x[,3], maxColorValue = 255)
}

# Keep data  when working, remove data2 as necessary
##########################################

rm(data2)
rm(data3)

data2 <- na.omit(data)
data2 <- data2[data2$Time !=0,]

data2$dateTime <- as.POSIXct(data2$Time,origin="1904-01-01")
start <- data2$dateTime[1]
end <-  data2$dateTime[dim(data2)[1]]
#start <- "2015-11-17 16:00:00"
#end <- "2015-11-17 17:10:00"
starttime <- 2082844800 + as.numeric(as.POSIXct(start,origin="1904-01-01"))
endtime <-   2082844800 + as.numeric(as.POSIXct(end,origin="1904-01-01"))
data2 <- data2[data2$Time >= starttime,]
data2 <- data2[data2$Time < endtime,]
```

```
data2$TimeStamp <- (data2$Time-data2$Time[1])
label <- substr(data2$dateTime[1],1,10)
data2 <- data2[data2$peak >0,]

data2$Velocity1 <- sqrt(200*data2$Pressure/1.225)
data2$Velocity2 <- sqrt(200*data2$peak/1.225)
temp <- data2[,6:7]
temp <- cbind(temp,data2[,16])
dataxyz <- sph2car(temp,deg=FALSE)
colnames(dataxyz) <- c("Vx","Vy","Vz")
data2 <- cbind(data2,dataxyz)
M <- dim(data2)[1]
degrad <- pi/180
rm(temp)
data2$horvel <- sqrt(data2$Vx^2+data2$Vy^2)
data2$direction <- 180 - data2$longitude/degrad
data2$elevation <- 180*data2$latitude/pi
data2$px <- data2$Vx/data2$Velocity2
data2$py <- data2$Vy/data2$Velocity2
data2$pz <- data2$Vz/data2$Velocity2

# Read Cup data
setwd("Z:/Urchin-P2-Baldonnel")
txt2 <- "BaldonnellMetMast-0110-3112-2015.csv"
data3 <- read.csv(txt2,header=TRUE,stringsAsFactors=FALSE)
data3 <- na.omit(data3)
data3 <- data3[,-2:-4]
data3$Time <- as.numeric(data3$Time)
data3$Timeh <- data3$Time/(3600*24)
data3$Velocity <- data3$InstSpeed*0.514444
data3$UrchinTimestamp <- data3$TimeStamp+2082844000
data3$dateTime <- as.POSIXct(data3$UrchinTimestamp,origin="1904-01-01")

#same limits as data 2
```

```
data3 <- data3[data3$dateTime < "2015-11-27 23:59:58 ",]
data3 <- data3[data3$dateTime > start,]
data3 <- data3[data3$dateTime < end,]



################################################
# for raw  data
################################################

maxvel <- max(data2$Velocity2)
plottitle <- paste("Urchin-Cup Anemometer Wind Speed Comparison \n From ", start," to ",end)
plot(data2$dateTime,data2$Velocity2,cex=0.1,
    main=plottitle,xlab="Date Time",sub="Urchin Blue : Cup Black",col="blue",
    ylim=c(0,maxvel),ylab="windSpeed [m/s]",frame.plot=TRUE)
lines(data3$dateTime,data3$Velocity)
grid()

plottitle <- paste("Urchin-Cup Anemometer Wind Direction Comparison \n From ", start," to ",end)
plot(data2$dateTime,data2$direction,cex=0.1,
    main=plottitle,xlab="Date Time",
    ylim=c(0,360),ylab="Direction [deg from North]",frame.plot=TRUE)
lines(data3$dateTime,data3$InstDir,col="blue")
grid()

plottitle <- paste("Urchin Wind Elevation \n From ", start," to ",end)
plot(data2$dateTime,data2$elevation,cex=0.1,
    main=plottitle,xlab="Date Time",
    ylim=c(-90,90),ylab="Direction [deg from North]",frame.plot=TRUE)
lines(data3$dateTime,data3$InstDir,col="blue")
grid()
################################
# Dont't run with full data set
################################
maxvel <- 1.1*max(data2$Velocity2)
```

```
gvel <- ggplot(data2,aes(x=TimeStamp,y=Velocity2)) + geom_point(size=0.01) + xlab("Time [h]") +
  ylab("Wind Speed [m/s]") + ggtitle(paste("Urchin Wind Speed at  Baldonnel on ",label)) +
  scale_x_continuous(breaks=c(seq(1,24,1)))
gvel


gvelHOR <- ggplot(data2,aes(x=TimeStamp,y=horvel)) + geom_point(size=0.01) + xlab("Time [h]")
+
  ylab("Wind Speed [m/s]") + ggtitle(paste("Horizontal Urchin Wind Speed at  Baldonnel on ",label))
+
  scale_x_continuous(breaks=c(seq(1,24,1)))
gvelHOR


glong <- ggplot(data2,aes(x=TimeStamp,y=longitude)) + geom_point(size=0.05) + xlab("Time [h]")
+
  ylab("Horizontal Wind Direction") + ggtitle(paste("Urchin Wind Horizontal Direction at Baldonnell
",label))
glong


glat <- ggplot(data2,aes(x=TimeStamp,y=latitude)) + geom_point(size=0.05) + xlab("Time [h]") +
  ylab("Vertical Wind Direction") + ggtitle(paste("Urchin Wind Vertical Direction at Baldonnell
",label))
glat


gsphere <- ggplot(data2,aes(x=longitude,y=latitude,colour=Velocity2)) + geom_point(size=0.1) +
  xlab("Longitude [rad]") + ylab("Latitude [rad]") +
  ggtitle(paste("Urchin Wind Direction at Baldonnell ",label))
gsphere


gvel2 <- ggplot(data2,aes(x=TimeStamp,y=Velocity2)) + geom_line() + xlab("Time [h]") +
  ylab("Wind Speed [m/s]") + ggtitle(paste("Urchin Wind Speed at  Baldonnel on ",label))
gvel2


gpress <- ggplot(data2,aes(x=TimeStamp,y=Pressure)) + geom_line() + xlab("Time [h]") +
  ylab("Pressure [mbar]") + ggtitle(paste("Urchin Differential Pressure at  Baldonnel on ",label))
gpress
```

```
#################################
#split plots
#################################

temp <- approx(data2$Time,data2$Velocity2,xout=data3$UrchinTimestamp)
data3$urchin <- temp$y
newdata <- data.frame(data3$UrchinTimestamp,data3$Velocity,data3$urchin)
colnames(newdata) <- c("Time","Cup","Urchin")
newdata$datetime <- as.POSIXct(newdata$Time,origin="1904-01-01")
newdata$Time <- newdata$datetime
newdata <- newdata[,-4]
melteddata <- melt(newdata, id="Time")
gp
 <- ggplot(melteddata,aes(x=Time,y=value))+geom_line()+
  ggtitle(paste("Urchin-Cup Anemometer Wind Speed Comparison \n  From ", start," to ",end))+
  xlab("Time") +ylab("Wind Speed [m/s]")
gp + facet_grid(variable ~ .)

temp <- approx(data2$Time,data2$direction,xout=data3$UrchinTimestamp)
data3$urchin <- temp$y
newdata <- data.frame(data3$UrchinTimestamp,data3$InstDir,data3$urchin)
colnames(newdata) <- c("Time","Cup","Urchin")
newdata$datetime <- as.POSIXct(newdata$Time,origin="1904-01-01")
newdata$Time <- newdata$datetime
newdata <- newdata[,-4]
melteddata <- melt(newdata, id="Time")
gp <- ggplot(melteddata,aes(x=Time,y=value))+geom_line()+
  ggtitle(paste("Urchin-Cup Anemometer Wind Direction Comparison \n  From ", start," to ",end))+
  xlab("Time") +ylab("Degrees from North")
gp + facet_grid(variable ~ .)

temp <- approx(data2$Time,data2$elevation,xout=data3$UrchinTimestamp)
data3$urchin <- temp$y
newdata <- data.frame(data3$UrchinTimestamp,data3$InstDir,data3$urchin)
```

```
colnames(newdata) <- c("Time","Cup","Urchin")

newdata$datetime <- as.POSIXct(newdata$Time,origin="1904-01-01")

newdata$Time <- newdata$datetime

newdata <- newdata[,-4]

melteddata <- melt(newdata, id="Time")

gp <- ggplot(melteddata,aes(x=Time,y=value))+geom_line()+

  ggtitle(paste("Urchin Elevation versus Cup Anemometer Wind Direction \n  From ", start," to
",end))+

  xlab("Time") +ylab("Urchin Elevation [deg]                Degrees from North")

gp + facet_grid(variable ~ .,scales="free_y")


################################

# 3-D plotting of raw data

################################


cols <- myColorRamp(c("black","red","green", "blue"), data2$Velocity2)

plot3d(data2$TimeStamp,data2$longitude,data2$latitude,ylim=c(-pi,pi),

      zlim=c(-pi/2,pi/2),size=0.05,col=cols,

      main ="Wind Direction")


maxvel <- max(data2$Velocity2)

plot3d(data2$Velocity2,data2$longitude,data2$latitude,xlim=c(0,maxvel),ylim=c(-pi,pi),

      zlim=c(-pi/2,pi/2),size=0.05,col=cols)



################################

# 2-D histograms of raw data

################################


##### Addendum: 2D Histogram + 1D on sides (from Computational ActSci w R) #######

#http://books.google.ca/books?id=YWcLBAAAQBAJ&pg=PA60&lpg=PA60&dq=kde2d+log&sour
ce=

#bl&ots=7AB-RAoMqY&sig=gFaHSoQCoGMXrR9BTaLOdCs198U&hl=en&sa=X&ei=

#8mQDVPqtMsi4ggSRnILQDw&redir_esc=y#v=onepage&q=kde2d%20log&f=false
```

```
library("MASS", lib.loc="C:/Program Files/R/R-3.1.1/library")
library(RColorBrewer)
rf <- colorRampPalette(rev(brewer.pal(11,'Spectral')))
r <- rf(32)
ngrid <- 50
h1 <- hist(data2$longitude, breaks=ngrid, plot=F)
h2 <- hist(data2$latitude, breaks=ngrid, plot=F)
top <- max(h1$counts, h2$counts)
k <- kde2d(data2$longitude, data2$latitude, n=ngrid)

# margins
dev.off()
oldpar <- par()
par(mar=c(3,3,1,1))
layout(matrix(c(2,0,1,3),2,2,byrow=T),c(3,1), c(1,3))
image(k, col=r,main="Longitude") #plot the image
par(mar=c(0,2,1,0))
barplot(h1$counts, axes=F, ylim=c(0, top), space=0, col='red',
      main="Distribution of angles  ")
par(mar=c(2,0,0.5,1))
barplot(h2$counts, axes=F, xlim=c(0, top), space=0, col='red',
      horiz=T,main="Latitude")
par(oldpar)



##################################################
# for averaged data
##################################################
tn <- 120 # Seconds for averaging
urchinmean <- timeaverage(data2,tn)
cupmean <- cupaverage(data3,urchinmean,tn)
cols <- myColorRamp(c("black","blue","green", "red"), urchinmean$Velocity2)

maxvel <- max(max(urchinmean$Velocity2),max(urchinmean$horvel))
```

```
plottitle <- paste("Urchin-Cup Anemometer Wind Speed Comparison \n","Both",tn,"second averages: From ", start," to ",end)

len <- dim(urchinmean)[1]

plot(urchinmean$dateTime,urchinmean$Velocity2,type="l",

    main =plottitle,sub="Urchin Black : Cup Blue",

    xlab="Date Time",ylim=c(0,maxvel),ylab="windSpeed [m/s]",frame.plot=TRUE)

#axis.POSIXct(1, at=seq(urchinmean$dateTime[1], urchinmean$dateTime[len], by="hour"), format="%H")

axis(side=2)

lines(cupmean$dateTime,cupmean$Velocity,col="blue")

grid()


plottitle <- paste("Urchin-Cup Anemometer Horizontal Wind Speed Comparison \n","Both",tn,"second averages:  From ", start," to ",end)

plot(urchinmean$dateTime,urchinmean$horvel,type="l",

    main =plottitle,sub="Urchin Black : Cup Blue",

    xlab="Date Time",ylim=c(0,maxvel),ylab="windSpeed [m/s]",frame.plot=TRUE)

#axis.POSIXct(1, at=seq(urchinmean$dateTime[1], urchinmean$dateTime[len], by="hour"), format="%H")

axis(side=2)

lines(cupmean$dateTime,cupmean$Velocity,col="blue")

grid()



plottitle <- paste("Urchin-Cup Anemometer Wind Direction Comparison \n","Both ",tn,"second averages:  From ", start," to ",end)

len <- dim(urchinmean)[1]

plot(urchinmean$dateTime,urchinmean$direction,type="l",

    main=plottitle,xlab="Date Time",sub = "Urchin Black      Cup Blue",

    ylim=c(0,360),ylab="wind direction [deg from North]",frame.plot=TRUE)

#axis.POSIXct(1, at=seq(urchinmean$dateTime[1], urchinmean$dateTime[len], by="hour"), format="%H")

#axis(side=2,at=seq(0,360,30))

lines(cupmean$dateTime,cupmean$InstDir,col="blue")

grid()
```

```
plottitle <- paste("Urchin-Elevation \n",tn,"second average:  From ", start," to ",end)
len <- dim(urchinmean)[1]
plot(urchinmean$dateTime,urchinmean$elevation,cex=0.5,
    main=plottitle,xlab="Date Time",sub = "Colour coded for velocity",
    ylim=c(-90,90),ylab="wind direction [deg from North]",frame.plot=TRUE,col=cols)
#axis.POSIXct(1, at=seq(urchinmean$dateTime[1], urchinmean$dateTime[len], by="hour"),
format="%H")
#axis(side=2,at=seq(0,360,30))
grid()



plottitle <- paste("Urchin-Elevation \n",tn,"second averages:  From ", start," to ",end)
len <- dim(urchinmean)[1]
plot(urchinmean$direction,urchinmean$elevation,cex=0.5,
    main=plottitle,xlab="Wind direction [deg from North]",sub = "Colour coded for velocity",
    ylim=c(-90,90),ylab="Wind elevation",frame.plot=TRUE,col=cols)
grid()

###################################
#Split plots
###################################

temp <- approx(urchinmean$Time,urchinmean$Velocity2,xout=cupmean$UrchinTimestamp)
cupmean$urchin <- temp$y
newdata <- data.frame(cupmean$UrchinTimestamp,cupmean$Velocity,cupmean$urchin)
colnames(newdata) <- c("Time","Cup","Urchin")
newdata$datetime <- as.POSIXct(newdata$Time,origin="1904-01-01")
newdata$Time <- newdata$datetime
newdata <- newdata[,-4]
melteddata <- melt(newdata, id="Time")
gp <- ggplot(melteddata,aes(x=Time,y=value))+geom_line()+
  ggtitle(paste("Urchin-Cup Anemometer Wind Speed Comparison \n",tn,"second averages:  From ",
start," to ",end))+
  xlab("Time") +ylab("Wind Speed [m/s]")
gp + facet_grid(variable ~ .)
```

```
newdata <- data.frame(urchinmean$dateTime,urchinmean$Vx,urchinmean$Vy,urchinmean$Vz)
colnames(newdata) <- c("Time","Vx","Vy","Vz")
melteddata <- melt(newdata, id="Time")
gp <- ggplot(melteddata,aes(x=Time,y=value))+geom_line()+
  ggtitle(paste("Urchin Velocity Components \n",tn,"second averages:  From ", start," to ",end))+
  xlab("Time") + ylab("Degrees from North")
gp + facet_grid(variable ~ .)



newdata <- data.frame(cupmean$UrchinTimestamp,cupmean$InstDir,cupmean$urchin)
colnames(newdata) <- c("Time","Cup","Urchin")
newdata$datetime <- as.POSIXct(newdata$Time,origin="1904-01-01")
newdata$Time <- newdata$datetime
newdata <- newdata[,-4]
melteddata <- melt(newdata, id="Time")
gp <- ggplot(melteddata,aes(x=Time,y=value))+geom_line()+
  ggtitle(paste("Urchin Elevation versus Cup Anemometer Wind Direction \n  From ",tn,"second
averages:  From ", start," to ",end))+
  xlab("Time") + ylab("Urchin Elevation [deg]                Degrees from North")
gp + facet_grid(variable ~ .,scales="free_y")

################################
# 3-D plotting of averaged data
################################

cols <- myColorRamp(c("black","blue","green", "red"), urchinmean$Velocity2)
maxvel <- max(urchinmean$Velocity2)

plot3d(urchinmean$Velocity2,urchinmean$longitude,urchinmean$latitude,xlim=c(0,maxvel),ylim=c(
-pi,pi),
      zlim=c(-pi/2,pi/2),size=3,col=cols)

plot3d(urchinmean$TimeStamp,urchinmean$longitude,urchinmean$latitude,ylim=c(-pi,pi),
```

```
    zlim=c(-pi/2,pi/2),size=3,col=cols,
    main = paste("Wind Directions from ",start," to ",end))


plot3d(urchinmean$px,urchinmean$py,urchinmean$pz,xlim=c(-1,1),ylim=c(-1,1),zlim=c(-
1,1),col=cols)

plot3d(urchinmean$TimeStamp,urchinmean$Velocity2,urchinmean$sd_Velocity2,size=3,col=cols)

plot3d(urchinmean$TimeStamp,urchinmean$direction,urchinmean$sd_direction,size=3,col=cols)



turbvel <- data.frame(urchinmean$dateTime,urchinmean$Velocity2,urchinmean$sd_Velocity2)

colnames(turbvel) <- c("DateTime","mean_velocity","sigma_velocity")

turbvel$Index <- turbvel$sigma_velocity/turbvel$mean_velocity

melteddata <- melt(turbvel,id="DateTime")

gp <- ggplot(melteddata,aes(x=DateTime,y=value)) + geom_line() +

 ggtitle(paste("Urchin Velocity : Mean Standard Deviation, and Turbulence Index \n  From
",tn,"second averages:  From ", start," to ",end))+

 xlab("Time")

gp + facet_grid(variable ~ .,scales="free_y")


turbang <-
data.frame(urchinmean$dateTime,urchinmean$direction,urchinmean$elevation,urchinmean$sd_direct
ion,urchinmean$sd_elevation)

colnames(turbang) <-
c("DateTime","mean_direction","mean_elevation","sigma_direction","sigma_elevation")

turbang$deltaA <-
((degrad**2)/(4*pi))*turbang$sigma_direction*turbang$sigma_elevation*cos(turbang$mean_elevatio
n*degrad)

turbdir <-
data.frame(turbang$DateTime,turbang$mean_direction,turbang$mean_elevation,turbang$deltaA)

colnames(turbdir) <- c("DateTime","mean_direction","mean_elevation","deltaA")

melteddata <- melt(turbang,id="DateTime")

gp <- ggplot(melteddata,aes(x=DateTime,y=value)) + geom_line() +

 ggtitle(paste("Urchin : Mean Direction, Mean Elevation, Stdev Direction, Stdev Elevatiion,and
Turbulence Index \n  From ",tn,"second averages:  From ", start," to ",end))+

 xlab("Time")

gp + facet_grid(variable ~ .,scales="free_y")
```

```
turbulence <-
data.frame(urchinmean$dateTime,urchinmean$Velocity2,urchinmean$direction,urchinmean$elevatio
n,
                    urchinmean$sd_Velocity2,urchinmean$sd_direction,urchinmean$sd_elevation)

colnames(turbulence) <- c("DateTime","mean_velocity","mean_direction","mean_elevation",

                  "sigma_velocity","sigma_direction","sigma_elevation")

turbulence$Index <- turbulence$sigma_velocity/turbulence$mean_velocity

turbulence$deltaA <-
((degrad**2)/(4*pi))*turbulence$sigma_direction*turbulence$sigma_elevation*

  cos(turbulence$mean_elevation*degrad)

turbulence$deltaV <- 2*turbulence$deltaA*turbulence$mean_velocity^2*turbulence$sigma_velocity

turbulence$xyz <- 8*urchinmean$sd_Vx*urchinmean$sd_Vy*urchinmean$sd_Vz

turbdir <- data.frame(turbulence$DateTime,turbulence$mean_velocity,turbulence$mean_direction,


turbulence$mean_elevation,turbulence$Index,turbulence$deltaA,turbulence$deltaV,turbulence$xyz)

colnames(turbdir) <-
c("DateTime","mean_velocity","mean_direction","mean_elevation","turbulence_index","deltaA","del
taV","deltaXYZ")

melteddata <- melt(turbdir,id="DateTime")

gp <- ggplot(melteddata,aes(x=DateTime,y=value)) + geom_line() +

  ggtitle(paste("Urchin : Mean velocity, Mean Direction, Mean Elevation, Turbulence Index and
delta_Area \n  From ",tn,"second averages:  From ", start," to ",end))+

  xlab("Time")

gp + facet_grid(variable ~ .,scales="free_y")


#urchinmean <- urchinmean[urchinmean$sd_direction < 20,]


temp1 <- diff(urchinmean$direction)

temp2 <- diff(urchinmean$elevation)

hist(temp1,breaks=50)

hist(temp2,breaks=50)
```

Link to Recorded Data Files from Wind Urchin and Anemometers

https://drive.google.com/open?id=1JZBnt186XQFC8JXX0Sln0nLwcVlaonmj

Publish Papers with Recommendations and Results

Paper published in the International journal of Aviation, Aeronautics and Aerospace (IJAAA) (International Journal of Aviation, Aeronautics, and Aerospace, 2018) "Evaluate The Effect of Turbulence on Aircraft During Landing and Take-Off Phases". A second paper has been published in the IJAAA (International Journal of Aviation, Aeronautics, and Aerospace, 2018) "Low Level Turbulence Detection For Airports"

Oral presentation delivered to Irish Meteorological Society on 15 November 2018 where I was the main speaker in Dublin's custom house, (O' Connor, 2018) titled "Using a Wind Urchin for Airport Wind Measurements".